MEASUREMENT OF THE OSCILLATORY FLOW BIREFRINGENCE OF POLYSTYRENE SOLUTIONS

By

JOHN LINDBLAD SCHRAG II

Bachelor of Arts
University of Omaha
Omaha, Nebraska
1959

Master of Science
Oklahoma State University
Stillwater, Oklahoma
1961

Submitted to the Faculty of the Graduate School
of the Oklahoma State University
in partial fulfillment of the requirements
for the degree of
DOCTOR OF PHILOSOPHY
May, 1967

MEASUREMENT OF THE OSCILLATORY FLOW BIREFRINGENCE OF POLYSTYRENE SOLUTIONS

Thesis Approved:

G B Thurston
Thesis Adviser

H Harrington

George Gavis

E C Kerker

D D Durham
Dean of the Graduate College

ACKNOWLEDGMENTS

The author wishes to take this opportunity to express his gratitude to Dr. G. B. Thurston for his many helpful suggestions and invaluable guidance throughout the course of this investigation; to his wife, Beverly, for her constant encouragement and her assistance with the manuscript; to Mr. and Mrs. John Wyhof for their assistance in proofreading the manuscript; to the U.S. Army Research Office, Durham, and the Office of Naval Research, U.S. Navy, for grants awarded to Dr. G. B. Thurston for the financial support of this work; and to the Physics Shop personnel for their excellent work in the construction of apparatus.

TABLE OF CONTENTS

LIST OF TABLES

LIST OE FIGURES

Figure Page

Figure Page

CHAPTER I

INTRODUCTION

The geometrical shape of most molecules is sufficiently elongated or asymmetric for the distribution of electrons within the molecule to give rise to an anisotropic electrical polarizability at optical frequencies. In crystalline solids the ordering of such molecules within the solid gives rise to the birefringence of the solid. In liquids not subject to any force fields there is a random orientation of the molecules of the liquid. Thus although the individual molecules may be anisotropic, there is no net anisotropy for the liquid. However, if these anisotropic molecules can be given a preferential orientation by some means, the liquid will exhibit a net anisotropy. Many molecules may be oriented to some degree by electric, magnetic or hydrodynamic fields, or combinations thereof. The optical anisotropy produced by the partial orientation of molecules subject to hydrodynamic forces gives rise to the anisotropy of the index refraction of the fluid known as the Maxwell effect or flow birefringence.

The optical and mechanical properties of macromolecules can be readily examined by means of flow birefringence, since most macromolecules are either elongated rigid structures for which hydrodynamic flow of the solvent medium around the molecule will exert relatively large orienting forces on the molecule, or elongated flexible or semi-flexible structures for which the hydrodynamic flow will not only produce

orientation of the molecule but will also deform it.

In 1866 Maxwell noted that the state of strain in a fluid might be detectable by the modification of polarized light passed through the liquid. In 1873 (59) he published a description of the flow birefringence exhibited by Canada balsam when subjected to the shearing forces produced by the motion of a spatula moving up and down in its own plane. The same year Mach (58) recorded observations of flow birefringence in metaphosphoric acid as well as Canada balsam. The following year Maxwell (60) described a concentric cylinder apparatus in which steady two-dimensional laminar flow could be obtained so that flow birefringence in liquids could be produced more readily. During the next few years many investigators measured the flow birefringence of various materials and sought for an adequate theoretical analysis of the effect. Kundt (56) published one of the first theories of flow birefringence. In his treatment the birefringence was related to the stresses in the liquid. Many theories followed, but it was not until 1928 when Raman and Krishnan (74) published a theory based on the molecular orientations produced by flow that significant agreement between theory and experiment was obtained. They assumed that the stress produced by flow in a liquid in which rigid macromolecules are suspended exerts orienting forces on these molecules. The result of this assumption is that the birefringence should be proportional to solvent viscosity and the gradient of the flow velocity in the liquid, as had been observed experimentally. By the early 1930's enough experimental evidence had been collected to indicate that there were differences between the flow birefringence exhibited by solutions containing suspended rigid particles and that exhibited by solutions of flexible or

partially flexible macromolecules. Rigid particle theories have since been developed that describe the experimental flow birefringence of dilute solutions containing special shapes of such particles subject to steady flow (15). For example, Boeder (2) treated the case of ellipsoids of revolution with high axial ratio, a treatment later modified by Sadron (78), while Peterlin and Stuart (65, 68) and Kuhn (48) treated the general case of rigid ellipsoids of revolution. Scheraga, Edsall and Gadd (79) extended the work of Peterlin and Stuart to high velocity gradients. Cerf and Thurston (16) have considered the extension of the treatment of Peterlin and Stuart to the case of oscillatory flow.

Description of the flow birefringence exhibited by solutions containing flexible macromolecules has proved to be more difficult than for the rigid particle case since the macromolecule in solution will not only orient when the solution flows but will also deform, the amount and character of the deformation depending on the flexibility of the molecule being examined. Further, the dimensions of most polymer chains are such that the effective diameter of such a chain is comparable to the diameter of the solvent molecules, so that consideration of the interaction of the solvent and chain in terms of frictional forces may not apply. Hence the hydrodynamic equations for continuous media may not apply. Further, the statistical problem to be solved is complicated by the character of the deformation. Thus only simplified models of flexible macromolecules in solution have been studied in which the solvent is assumed to be a continuous medium.

The first attempts at the description of the flow birefringence exhibited by dilute solutions of flexible chain macromolecules were

those of Haller (31) and Kuhn (48). Haller considered a model of the chain consisting of a deformable sphere. In flow the sphere is distorted into an ellipsoidal shape due to the external stresses acting on the sphere. He incorporated an internal viscosity in the sphere that gives rise to additional internal stresses. The birefringence exhibited by the deformed sphere is assumed to be proportional to the deformation of the sphere. Kuhn treated deformable elongated particles as well as the deformable sphere.

Kuhn and Kuhn (51, 52) presented the first quantitative treatments for dilute solutions of unbranched polymer chains that began with a two-dimensional treatment for a free-draining molecule, i.e., one in which the velocity of the solvent near a given region of the chain is unmodified by the other segments of the chain, using as a model of the polymer chain a dumbbell model consisting of two beads connected by a Hookean spring. The hydrodynamic interaction between the solvent and the model is assumed to occur at the beads. The viscosity and flow birefringence of the solution is determined by the end-to-end vector for the dumbbell model. The most probable value of the end-to-end distance for the model is determined by analyzing the configurations of the chain using a subchain concept. The molecule is considered to be made up of N subchains, each subchain being sufficiently large that the end-to-end vectors of the subchains are randomly oriented with respect to each other. Thus the end-to-end vectors of the subchains for a freely flexing chain will obey random walk statistics. Kuhn and Kuhn (53, 54, 55) later incorporated internal viscosity to account for energy losses in the chain itself, as well as a variable draining condition. The birefringence properties were obtained using the segmental

polarizability concept of Kuhn and Grün (50). The dumbbell model is not applicable to oscillatory flow since only two relaxation times would be exhibited by the model, the relaxation time corresponding to the rotary diffusion constant for the dumbbell and the relaxation time for the spring subjected to viscous forces at its end points. Since a polymer molecule will interact hydrodynamically with the solvent throughout the molecule, it can exhibit many relaxation times, a fact which is evident from oscillatory flow birefringence and viscosity data (22, 29, 38, 92).

Kramers (47) proposed and treated the so-called pearl necklace model of a flexible macromolecule in which the molecule is replaced by a number of beads connected by massless linking rods, assuming that the hydrodynamic forces exerted on the chain are exerted on the beads only. He treated three cases in which the rods were assumed to have complete freedom of rotation at the bead joints, the rods were restricted to free rotation in a cone corresponding to the valence angle of the bonds in the polymer chain being modeled, and the rods were assumed to be restricted in their rotational freedom in the cone corresponding to rotation at the valence angle of the bonds. He also included interaction between adjacent links in the chain.

Hermans (33, 35) carried out a three-dimensional treatment of the Kuhn and Kuhn theory applicable to small velocity gradients and free-draining molecules. He concluded that the hydrodynamic interaction between elements of the chain would have to be included in the various theories before a valid comparison of theories could be made. Copic (19, 20) treated the elastic dumbbell model of Kuhn and Kuhn incorporating the form birefringence as well as the intrinsic birefringence

of the chain and found that for steady flow the form effect can be significant if the solvent index of refraction is different from that of the polymer, and it would increase with increasing molecular weight.

Tsvetkov (96, 97, 100) treated a model of the polymer chain consisting of a deformable ellipsoid of revolution with trapped solvent within the ellipsoid. The optical treatment is more complete than most others in that form birefringence and "microform" birefringence, originating in the interaction among neighboring chain elements, are included as well as the intrinsic birefringence of the chain.

The various theories for flexible macromolecules mentioned thus far are applicable only to steady flow since the models do not predict a spectrum of relaxation times as has been observed experimentally. Peterlin (66, 67) proposed a model of the linear polymer chain consisting of a chain of elastic dumbbells joined together to form a chain of beads and connecting Hookean springs. The treatment is a two-dimensional analysis incorporating variable hydrodynamic interaction as well as a simplified treatment of concentration dependence in which the shape of the molecules is assumed to be independent of concentration. All of the previous theories mentioned assume sufficiently dilute solutions that the chain molecules do not interact with each other.

Cerf (6, 7, 8, 9, 10, 11) treated a deformable sphere model of chain molecules assuming the sphere to be both permeable and impermeable to the flowing solvent, incorporating internal viscosity and Brownian motions of the chain. The optical birefringence is treated following the method of Boeder. He later noted that his treatment of the deformable sphere would lead to a spectrum of relaxation times (13).

Several review articles dealing with flow birefringence are to be found in the literature which review the theoretical treatments of steady flow birefringence and present typical steady flow birefringence data for various rigid and flexible particles (15, 24, 41, 98).

More recently the flow birefringence and viscosity exhibited by dilute solutions of flexible macromolecules have been treated utilizing more sophisticated models of the macromolecule and more detailed treatments of the role of Brownian motions. These treatments predict spectrums of relaxation times for the various models and thus permit a description of oscillatory flow behavior corresponding more nearly to the observed oscillatory flow birefringence and viscosity than the models described previously. Kirkwood and Riseman (46) treated a model chain consisting of a chain of rigid links joined together at an angle corresponding to the valence angle of the molecule being modeled. They assume hindered rotation between links similar to the hindered rotation of the bonds in the actual molecule. The entire link is assumed to interact with the solvent, much as a rigid body being forced through a continuous liquid medium, with the force exerted by the chain link on the fluid being characterizable by a friction coefficient dependent on the character of the macromolecule being modeled. Hydrodynamic interaction between links of the model is also incorporated. Kirkwood (44, 45) treated the same model in more detail, obtaining expressions describing the diffusion of the model chain and the viscosity increment due to the presence of the chain for both steady and oscillatory flow. He also discussed the application of the theory to flow birefringence problems.

Rouse (75) adopted a model of the flexible macromolecule in which

the molecule is replaced by a chain of identical beads connected by Hookean springs, assuming complete flexibility at the bead joints. Each bead-spring-bead segment of the model is assumed to correspond to a subchain of the molecule, the spring being connected between the beads located at the end points of the subchain. Thus the description of the subchain corresponds to that of an entire chain as given by Kuhn and Kuhn (51, 52). The beads are assumed to interact with the solvent much as a macroscopic sphere being forced through a flowing liquid interacts with that liquid. The behavior of the chain is analyzed for oscillatory as well as steady flow by a determination of the normal modes of the chain. The theory as given did not evaluate the flow birefringence of a solution of such chains, but did evaluate the viscosity of the solution for both steady and oscillatory flow, assuming no hydrodynamic interaction between the chain segments (free-draining chain). The chain is assumed to have N subchains.

Cerf (12, 13, 14) adopted a model for the flexible macromolecule identical to that of Rouse except that he incorporated an internal viscosity for the chain to describe energy losses in the chain itself. The retarding force due to the internal viscosity was first introduced as being proportional to the difference in velocities of the end points of the subchain. Later, however, a specification of the internal viscosity was given in which an internal viscosity coefficient was associated with each of the normal modes of vibration of the chain. The flow birefringence for steady flow was evaluated using the optical treatment of Kuhn and Grün to describe the optical polarizability of the subchain.

Zimm (103, 104) adopted the same model as that of Rouse and Cerf

except that he included hydrodynamic interaction between the beads in the model chain which Rouse did not, but did not include an internal viscosity as did Cerf. The mathematical treatment of the model is similar to that of Cerf. From the analysis of the normal modes of vibration of the chain, a differential equation of the distribution function is obtained that is applicable for oscillatory as well as steady flow. The birefringence is incorporated using the treatment of Kuhn and Grűn to describe the optical properties of the subchain. Expressions are given for the flow birefringence and viscosity for oscillatory or steady flow, and the relaxation time spectrum is evaluated for a chain having a large number of subchains N using the limiting hydrodynamic interaction conditions of free-draining and non-free-draining chains. The viscosity expression obtained by Zimm for the free-draining molecule agrees with that of Rouse if the latter is specialized to the case of large N . The Zimm approach has also been applied to branched or closed ring polymer chains (3). Tschoegl (94, 95) has evaluated the viscosity expressions given by the Zimm theory for intermediate degrees of hydrodynamic interaction, and later incorporated excluded volume effects as well. Again, the number of segments N is assumed to be large.

Oscillatory flow birefringence and viscoelasticity measurements for flexible macromolecules in solution have been carried out by various experimenters and compared with the Zimm and Rouse theories. Viscoelasticity measurements have been performed on solutions of polyisobutylene, polystyrene, polymethyl styrene and other linear chain polymer molecules by Ferry and co-workers and compared against the Zimm, Rouse and Tschoegl theories (22, 27, 29, 30, 38, 81). Some steady

flow birefringence and viscosity measurements on identical solutions have been carried out by Philippoff (71, 72). Lamb and Matheson (57) have studied the viscoelastic properties of polystyrene in various solvents and compared the data with the predictions of the Rouse and Zimm theories. Cerf and Thurston examined the theoretical relationship between viscoelasticity and oscillatory flow birefringence as given by the Zimm theory and applied their results to measurements made on a solution of polystyrene (16). Recently oscillatory flow birefringence measurements for a polystyrene solution have been compared against the Zimm theory using the number of beads in the chain model as a theoretical parameter (92). The results obtained demonstrated that the assumption of a large number of segments for the chain was not applicable for the polystyrene studied. Oscillatory flow birefringence has also been used as an indicator for the analysis of plane shear wave propagation and plane shear wave interference (80, 89, 91).

The measurements presented in this study are measurements of the steady and oscillatory flow birefringence and steady flow viscosity of three solutions of polystyrenes of differing molecular weights in a viscous solvent. A reduction technique was applied to the data to permit an examination of the frequency dependence of the oscillatory flow birefringence corresponding to a range in frequency of up to 10^5 cps. These measurements were performed on a thin fluid layer apparatus described previously (90).

The purposes of the study were first, to obtain measurements of the frequency dependence of the polystyrene solutions at various temperatures covering a sufficiently wide range in temperature and frequency to be able to examine the relaxation curves of the oscillatory

flow birefringence for these samples. Second, to compare the measured oscillatory flow birefringence against the theoretical birefringence given by the Zimm theory, using the number of chain segments and limiting degrees of hydrodynamic interaction as the variable parameters, as well as to compare the measurements with viscoelastic data for comparable solutions (29). It is felt that these comparisons will be useful for an examination of the validity of certain aspects of the Zimm theory when applied to these polystyrene solutions.

The oscillatory flow birefringence is a sensitive means for examination of the dynamics of the motions of the polymer chains in solution. The effective frequency range covered for the measurements contained herein is sufficient to examine most of the relaxation curve for the oscillatory flow birefringence for the polystyrene-Aroclor solutions studied. Comparison of the Zimm theory and the flow birefringence data indicates that the Zimm theory does describe the character of the oscillatory flow birefringence and that it is essential to consider the number of chain segments as a parameter for an adequate description of the oscillatory flow birefringence.

CHAPTER II

THEORY

1. Optical Properties of Dilute Solutions of Unbranched Chain Molecules as Given by Kuhn and Grün

The anisotropic character of the optical properties of a suspension of macromolecules in flow may be conveniently examined by measuring the optical birefringence in flow exhibited by the suspension. The corresponding theoretical treatment of the optical properties of such a medium is usually based on a theoretical calculation of the electric moment per unit volume $\vec{P}$ or the polarizability per unit volume γ. The birefringence Δn is then obtained from the calculated $\vec{P}$ or γ using the relation between the index of refraction n and the mean polarizability per molecule α of a medium consisting of randomly oriented molecules given by the Lorentz-Lorenz formula (4).

Consider the electric field in a liquid medium in which a molecule i is surrounded by identical molecules, assuming an electromagnetic wave to be incident upon the medium. If the surrounding molecules are evenly distributed around the molecule i, and if each molecule is assumed to react to an electromagnetic field as though it were an ideal dipole, then the electromagnetic field seen by any one molecule i is that due to the incident electromagnetic wave plus that due to the other molecules (dipoles) in the solution. Since the molecules are assumed to have essentially random orientations, the

molecules contained in a small sphere surrounding a given molecule may be considered to approximate a homogeneous, isotropic medium. Thus if $\vec{p}$ denotes the average electric dipole moment of one of these molecules, then for n_v such molecules per unit volume the average electric dipole moment per unit volume $\vec{P}$ of the medium is given by

$$\vec{P} = n_v \vec{p} = \eta \vec{E} \tag{II-1}$$

where η is the dielectric susceptibility of the medium and $\vec{E}$ is the incident electromagnetic wave. If the medium is assumed to be non-magnetic so that the external and internal magnetic fields are the same, the propagation of the electromagnetic wave through the medium may be described by considering only the electric moment of the medium given by equation (II-1). If also the average electric dipole moment $\vec{p}$ of a molecule is assumed to be proportional to the internal field $\vec{E}'$ acting on the molecule according to

$$\vec{p} = \alpha \vec{E}' \tag{II-2}$$

where α is the mean polarizability of the molecule, then the average electric moment per unit volume $\vec{P}$ is given by

$$\vec{P} = n_v \vec{p} = n_v \alpha \vec{E}'. \tag{II-3}$$

Note that for any individual molecule the polarizability in equation (II-2) will be a tensor quantity since the molecule itself is not isotropic. However, since these molecules are assumed to have a random orientation, the mean polarizability α is used. Thus α will be a scalar quantity for random orientations of the molecules (4). The internal electric field acting on any given molecule may be

divided into two components, the incident electric field $\vec{E}$ and the contributions arising from the dipole fields of the other molecules in the medium. Thus the internal field $\vec{E}_j'$ acting on the molecule is given by

$$\vec{E}_j' = \vec{E} + \sum_{\substack{l \\ l \neq j}} \vec{E}_{jl} \qquad \text{(II-4)}$$

where $\vec{E}_{jl}$ denotes the field of the l^{th} molecule (or dipole) at the site of j, and the summation is carried out over all molecules in the medium. For a linear electric dipole, the field is given by

$$\vec{E}_{jl} = \text{curl curl } \frac{\vec{p}_l(t - R_{jl}/c)}{R_{jl}} \qquad \text{(II-5)}$$

where $\vec{p}_l$ denotes the moment of the l^{th} dipole, t denotes time and R_{jl} is given by

$$R_{jl} = |\vec{r}_j - \vec{r}_l| \qquad \text{(II-6)}$$

where $\vec{r}_j$ and $\vec{r}_l$ denote the locations of the j^{th} and l^{th} dipoles (4). If the moment $\vec{p}$ of a molecule may be considered to approximate a continuous function of position and time, and the number of molecules per unit volume may be considered to approximate a continuous function of position, then it can be shown from equations (II-4), (II-5) and (II-6) that

$$\vec{P} = n_v \alpha (\vec{E} + \vec{E}_d) \qquad \text{(II-7)}$$

where $\vec{E}_d$ denotes the contribution of the dipoles (4). If $\vec{E}$ is assumed to be a plane wave of wavelength sufficiently large to subject

the volume under consideration to a field that is approximately constant spatially, then for the volume element under consideration $\vec{E}$ will be of the form

$$\vec{E} = \vec{A} e^{i\omega t} \tag{II-8}$$

and it can be shown that

$$\vec{E}' = \vec{E} + \frac{4\pi}{3}\vec{P} \tag{II-9}$$

for the volume element considered (4). Assuming further that at optical frequencies the dielectric constant ϵ of the medium will be related to the index of refraction n by the Maxwell relation

$$\epsilon = n^2, \tag{II-10}$$

since ϵ is related to η by

$$\eta = \frac{\epsilon - 1}{4\pi}, \tag{II-11}$$

then from equations (II-1), (II-9), (II-10) and (II-11) the following important result can be obtained:

$$\frac{4\pi}{3} n_N \alpha = \frac{n^2 - 1}{n^2 + 2}, \tag{II-12}$$

the Lorentz-Lorenz relation. A rigorous development of equation (II-12) is presented in Chapter 2, section 2.4.2 of reference (4). From equations (II-3) and (II-12) $\vec{E}'$ may be written as

$$\vec{E}' = \frac{\vec{P}}{n_N \alpha} = \vec{P} \cdot \frac{(n^2+2)}{(n^2-1)} \cdot \left(\frac{4\pi}{3}\right). \tag{II-13}$$

If the polarizability per unit volume γ of the medium is defined by

$$\vec{P} = \gamma \vec{E}' \tag{II-14}$$

then from equations (II-13) and (II-14) γ will be given by

$$\gamma = \frac{\vec{P}}{\vec{E}'} = \frac{(n^2-1)}{(n^2+2)} \cdot \left(\frac{3}{4\pi}\right) = n_N \alpha . \tag{II-15}$$

Equation (II-15) holds for randomly oriented anisotropic molecules subject to the additional assumptions regarding replacement of a molecule by an ideal dipole, etc., as noted. To obtain an equation relating a small change in n to a small change in γ, equation (II-14) may be differentiated with respect to n.

$$\frac{d\gamma}{dn} = \left(\frac{3}{4\pi}\right) \frac{6n}{(n^2+2)^2} = \frac{9n}{2\pi(n^2+2)^2} . \tag{II-16}$$

So, for $\Delta\gamma$ small,

$$\Delta n \simeq \frac{2\pi(n^2+2)^2}{9n} \Delta\gamma . \tag{II-17}$$

Thus if $\Delta\gamma$ may be calculated based on some theoretical model of a suspension of partially oriented macromolecules, the birefringence Δn of the suspension may be approximated by equation (II-17) provided that $\Delta\gamma$ is sufficiently small. For dilute solutions containing macromolecules, n is usually replaced by n_s, the solvent index of refraction, since $n \simeq n_s$ for dilute solutions.

Consider the optical anisotropy exhibited by a long chain macromolecule suspended in a solvent with randomly oriented molecules so

that the solvent can be considered to approximate a continuous medium. The optical anisotropy of the macromolecule will have two major contributors, the intrinsic anisotropy and the form anisotropy. The intrinsic anisotropy arises from the electron distributions in the constituent elements of the molecule while the form anisotropy results from the modification of the electric field at a given point on the molecule by the other segments of the molecule (19). Thus the form effect contribution can be appreciable when the molecule has a mean index of refraction that is different from that of the solvent.

The long chain molecule is replaced by a suitable model for ease of calculation. The model used herein is that of Kuhn and Grün (50). The molecular chain is divided into N equal length segments or subchains, each subchain containing enough monomer units that the vectors joining the end points of individual subchains are randomly oriented with respect to each other. Thus a freely flexing chain consisting of N subchains is formed, to which random walk statistics may be applied to analyze the configurations of the chain. The subchain concept thus permits an approximate determination of the configurations of chain molecules which are not freely flexing at the individual bonds of the chain, since the inclusion of enough of the partially flexible bonds in a subchain will cause the end-to-end vectors for neighboring subchains to assume random orientations with respect to each other. It is assumed that the subchains have no permanent dipole moment and that the macromolecule is sufficiently small with respect to the wavelength of the incident light that the isotropic field of the solvent seen by the molecular segments is essentially the same for all segments at any given instant of time. Also, the intrinsic polarizability of the

subchain is considered to be describable by an ellipsoid of revolution having its principal axes along and normal to the vector joining the endpoints of the subchain. The principal values of the polarizability for the subchain are denoted by α_1 , α_2 and α_3 , where α_1 is the polarizability corresponding to the direction of $\vec{A}_i$ and $\alpha_2 = \alpha_3$ is the polarizability corresponding to directions normal to $\vec{A}_i$. The values of α_1 , α_2 and $|\vec{A}_i|$ are assumed to be constant and independent of the orienting forces acting on the chain to produce the net optical anisotropy of the chain. Such an assumption is probably not valid for force fields exerting large forces on such a chain, since the chain would tend to stretch out to its maximum extension and thus to alter considerably the configurations of the subchains as well.

The electric field $\vec{E}_i$ acting on the segment i will be given by

$$\vec{E}_i = \vec{E}_o + \sum_{\substack{j=1 \\ j \neq i}}^{N} \vec{E}_{ij} \qquad \text{(II-18)}$$

where $\vec{E}_o$ is the isotropic internal field due to the presence of the solvent and $\vec{E}_{ij}$ is the field at the site of i due to the segment j (19). The fields $\vec{E}_{ij}$ are responsible for the so-called form birefringence, a birefringence that may exist when no intrinsic birefringence is present. If the segment j has the same average polarizability as that of the solvent, then the field $\vec{E}_{ij}$ is essentially that given by a substitution of solvent molecules at the location j in the chain, plus a very small perturbing field due to the anisotropy of the polarizability of the chain segment j .

Since the field produced by the randomly oriented solvent molecules surrounding the chain has been given by the term $\vec{E}_o$ and the average polarizability is proportional to n^2 from equation (II-15), whenever the chain has the same average index of refraction as that of the solvent, the form birefringence will be negligible (19, 20, 98). The component $\vec{E}_{ij}$ is related to the dipole moment $\vec{p}_j$ of the j^{th} segment by the interaction tensor T_{ij}.

$$\vec{E}_{ij} = T_{ij}\,\vec{p}_j \tag{II-19}$$

Thus the field at i may be written as

$$\vec{E}_i = \vec{E}_o + \sum_{\substack{j=1 \\ j\neq i}}^{N} T_{ij}\,\vec{p}_j \tag{II-20}$$

from equations (II-18) and (II-19). If electrical saturation effects are negligible so that

$$\alpha_i\,\vec{E}_i = \vec{p}_i \tag{II-21}$$

where α_i is the polarizability tensor for the segment i, then from equations (II-20) and (II-21) the dipole moment $\vec{p}_i$ of segment i will be given by

$$\begin{aligned}\vec{p}_i &= \alpha_i\vec{E}_o + \sum_{\substack{j=1 \\ j\neq i}}^{N} \alpha_i\,\vec{E}_{ij} \\ &= \alpha_i\vec{E}_o + \sum_{\substack{j=1 \\ j\neq i}}^{N} \alpha_i\,T_{ij}\,\vec{p}_j .\end{aligned} \tag{II-22}$$

Equation (II-22) is a system of 3 N equations for the components of $\vec{p}_i$ which could be evaluated at any instant of time if the location and orientation of all segments of the chain were known.

Since such information cannot be obtained, it is necessary to employ averaging techniques to obtain useful values for $\vec{p}_i$. Since $\vec{E}_o$ is regarded as being constant throughout the volume enclosing the macromolecule at any instant of time,

$$\langle \vec{p}_i \rangle_{av} = \langle \alpha_i \rangle_{av} \vec{E}_o + \sum_{\substack{j=1 \\ j \neq i}}^{N} \langle \alpha_i T_{ij} \vec{p}_j \rangle_{av} \qquad \text{(II-23)}$$

where the averaging is done over the possible configurations of the chain. Consider a function $\vec{f}_i$ defined by

$$\vec{f}_i = \sum_{\substack{j=1 \\ j \neq i}}^{N} \left[\langle \alpha_i T_{ij} \vec{p}_j \rangle_{av} - \langle \alpha_i T_{ij} \rangle_{av} \langle \vec{p}_j \rangle_{av} \right] . \qquad \text{(II-24)}$$

The addition and subtraction of equations (II-23) and (II-24) yields

$$\langle \vec{p}_i \rangle_{av} = \langle \alpha_i \rangle_{av} \vec{E}_o + \sum_{\substack{j=1 \\ j \neq i}}^{N} \langle \alpha_i T_{ij} \rangle_{av} \langle p_j \rangle_{av} + \vec{f}_i . \qquad \text{(II-25)}$$

Equation (II-24) may be rewritten by noting that

$$\langle A \langle B \rangle \rangle = \langle A \rangle \langle B \rangle . \qquad \text{(II-26)}$$

Thus

$$\vec{f}_i = \sum_{\substack{j=1 \\ j \neq i}}^{N} \left[\langle \alpha_i T_{ij} \vec{p}_j \rangle_{av} - \langle \alpha_i T_{ij} \langle \vec{p}_j \rangle_{av} \rangle_{av} \right] . \qquad \text{(II-27)}$$

Or,

$$\vec{f}_i = \sum_{\substack{j=1 \\ j \neq i}}^{N} \langle \alpha_i T_{ij} \{ \vec{p}_j - \langle \vec{p}_j \rangle_{av} \} \rangle_{av} . \qquad \text{(II-28)}$$

Thus if $\vec{p}_j$ is sufficiently near to its average value throughout the vagaries of chain motion that occur, the function $\vec{f}_i$ will be negligible. It is usually assumed that $\vec{f}_i$ is negligible, although this may not be a good approximation for liquids (43). Thus the average dipole moment for the subchain is assumed to be given by

$$\langle \vec{p}_i \rangle_{av} \simeq \langle \alpha_i \rangle_{av} \vec{E}_o + \sum_{\substack{j=1 \\ j \neq i}}^{N} \langle \alpha_i T_{ij} \rangle_{av} \langle \vec{p}_j \rangle_{av} . \qquad \text{(II-29)}$$

For the freely flexing chain under equilibrium conditions where the chain may be described in terms of random walk statistics, the following approximation has been used (19)

$$\langle \alpha_i T_{ij} \rangle_{av} \simeq \langle \alpha_i \rangle_{av} \langle T_{ij} \rangle_{av} . \qquad \text{(II-30)}$$

Combining equations (II-29) and (II-30) one obtains

$$\langle \vec{p}_i \rangle_{av} \simeq \langle \alpha_i \rangle_{av} \vec{E}_o + \sum_{\substack{j=1 \\ j \neq i}}^{N} \langle \alpha_i \rangle_{av} \langle T_{ij} \rangle_{av} \langle \vec{p}_j \rangle_{av} \qquad \text{(II-31)}$$

where the first term is the intrinsic anisotropy contribution and the second term the form effect contribution to $\langle \vec{p}_i \rangle_{av}$.

Consider the field at the site of subchain i due to segment j. If i is sufficiently far from j, the field of j at the site of i will approximate that of an ideal dipole located at the site of j. The field of an ideal dipole immersed in a medium of index of refraction n_s is given by

$$\vec{E}(\vec{r}) = \frac{1}{n_s^2} \cdot \frac{[3\vec{n}(\vec{p}\cdot\vec{n}) - \vec{p}]}{r^3} , \qquad \text{(II-32)}$$

where $\vec{r}$ is the vector joining the dipole and the point of observation, $\vec{m}$ is a unit vector directed along $\vec{r}$ and $\vec{p}$ is the dipole moment of the dipole (39). Thus from equation (II-19) the interaction tensor T_{ij} will be given by

$$T_{ij} = \left[\frac{3\vec{r}_{ij}\vec{r}_{ij}}{r_{ij}^2} - 1 \right] \left(\frac{1}{n_s^2 r_{ij}^3} \right) \qquad \text{(II-33)}$$

assuming the subchains of the chain can be considered to radiate as ideal dipoles.

From equations (II-33) and (II-31) it is seen that an evaluation of the second term of equation (II-31) depends upon the knowledge of the distribution function of the chain. Such distribution functions are available for dilute suspensions of chains subjected to small non-time varying flows (42, 50), or to no flow. However, apparently no distribution functions for such chain molecules subject to small oscillatory flows are available, although Zimm (109) has evaluated integrals involving such a distribution function. Since the case of particular interest for the work presented herein is that of oscillatory flow in a solvent having an index of refraction within 0.1 of that of the polymer being studied, the form effect given by the second term of equation (II-31) is assumed negligible in the work to follow. Thus the optical anisotropy of the chain molecule is assumed to be due to only the intrinsic anisotropy α_i characteristic of the subchain of the molecule.

Neglecting the form effect, the average intrinsic polarizability of the whole molecule can be obtained by adding the appropriate components of the intrinsic polarizability tensors for each of the

subchains in the molecule to obtain the polarizability for the entire chain and then computing an average value. Or, one can compute the components of the average polarizability tensor for one subchain and multiply it by the number of subchains. The latter approach, that of Kuhn and Grün (50) is presented here. Figure 1 shows the coordinate system chosen, in which the Z direction coincides with the end-to-end vector $\vec{h}$ for the entire chain. The subchains characterized by the vectors $\vec{A}_i$ are not parallel to $\vec{h}$, but have random orientations with respect to $\vec{h}$ and each other. One such subchain vector $\vec{A}_i$ is shown in Figure 2.

Consider the 1, 2, 3 principal axis coordinate system for the vector $\vec{A}_i$ and its associated polarizability tensor α_i given by

$$\alpha_i = \begin{pmatrix} \alpha_1 & 0 & 0 \\ 0 & \alpha_2 & 0 \\ 0 & 0 & \alpha_3 \end{pmatrix} . \qquad \text{(II-34)}$$

The polarizability tensor α_i corresponding to the X_i, Y_i, Z_i or the X, Y, Z coordinate systems may be obtained from equation (II-34) as follows. Since α_i is symmetric in the 2, 3 plane, the orientation of the 2 and 3 axes are arbitrary so long as the 1, 2, 3 axes remain orthogonal. If axis 2 is chosen so that it lies in the plane of the Z_i and the 1 axis, then the 3 axis is in the X_i, Y_i plane, forming an angle of $(90° - \phi)$ with the X_i axis. Thus the direction cosines g_{ij} relating the coordinate systems, expressed in terms of the spherical coordinates θ and ϕ are as follows:

$$\begin{array}{lll} g_{1X} = \sin\theta\cos\phi & g_{1Y} = \sin\theta\sin\phi & g_{1Z} = \cos\theta \\ g_{2X} = \cos\theta\cos\phi & g_{2Y} = \cos\theta\sin\phi & g_{2Z} = -\sin\theta \\ g_{3X} = \sin\phi & g_{3Y} = -\cos\phi & g_{3Z} = 0 \end{array} \qquad \text{(II-35)}$$

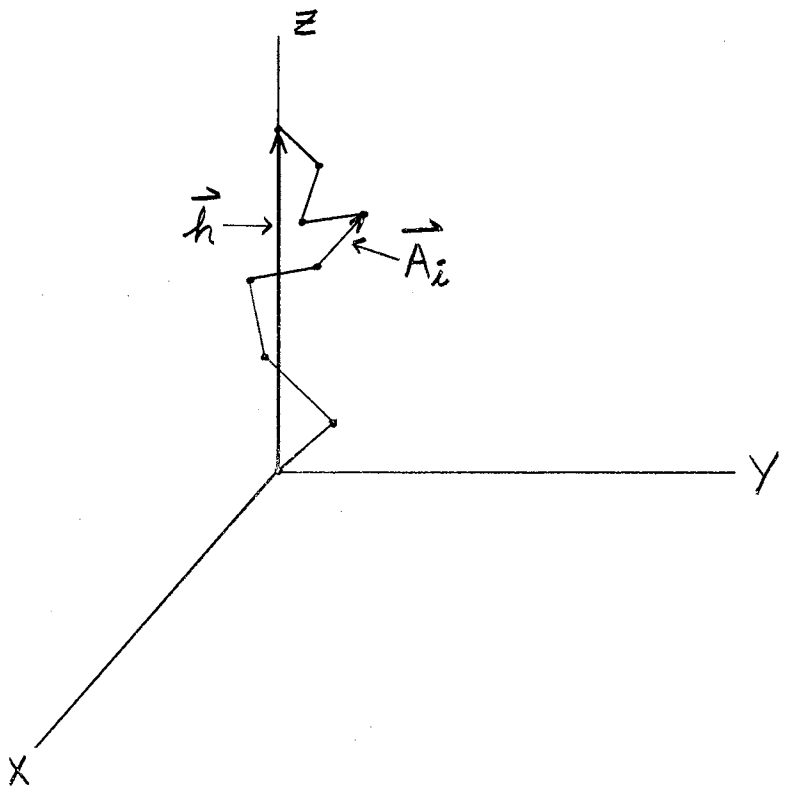

Figure 1. Coordinate System for the Specification of the Spatial Configurations of the Chain Model of Kuhn and Grün.

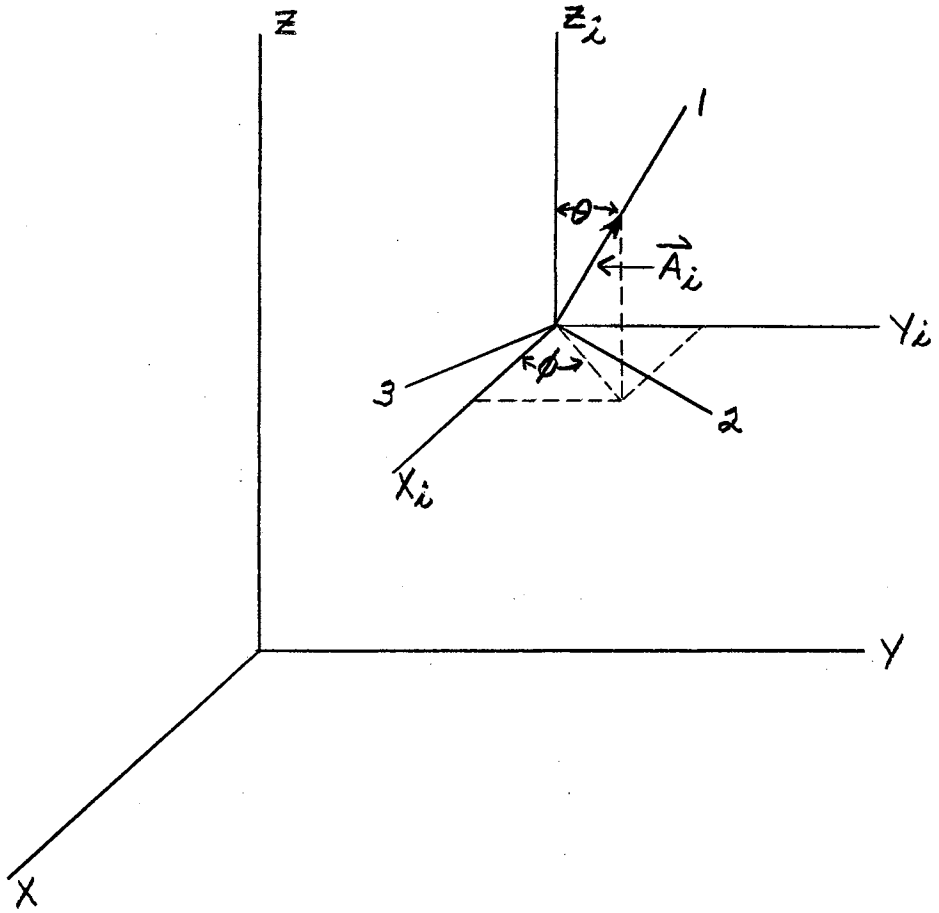

Figure 2. Coordinate Systems for the Specification of the Orientation of the i^{th} Subchain of the Chain Model of Kuhn and Grün.

Thus the components of the polarizability tensor α_i corresponding to the X , Y , Z coordinate system are given by

$$(\alpha_{XX})_i = \alpha_1 g_{1X} g_{1X} + \alpha_2 g_{2X} g_{2X} + \alpha_2 g_{3X} g_{3X}$$
$$= (\alpha_1 - \alpha_2) \sin^2\theta \cos^2\phi + \alpha_2$$

$$(\alpha_{YY})_i = \alpha_1 g_{1Y} g_{1Y} + \alpha_2 g_{2Y} g_{2Y} + \alpha_2 g_{3Y} g_{3Y}$$
$$= (\alpha_1 - \alpha_2) \sin^2\theta \sin^2\phi + \alpha_2$$

$$(\alpha_{ZZ})_i = \alpha_1 \cos^2\theta + \alpha_2 \sin^2\theta \qquad \text{(II-36)}$$

$$(\alpha_{XY})_i = (\alpha_{YX})_i = \alpha_1 g_{1X} g_{1Y} + \alpha_2 g_{2X} g_{2Y} + \alpha_2 g_{3X} g_{3Y}$$
$$= (\alpha_1 - \alpha_2) \sin^2\theta \cos\phi \sin\phi$$

$$(\alpha_{XZ})_i = (\alpha_{ZX})_i = (\alpha_1 - \alpha_2) \sin\theta \cos\theta \cos\phi$$

$$(\alpha_{YZ})_i = (\alpha_{ZY})_i = (\alpha_1 - \alpha_2) \sin\theta \cos\theta \sin\phi \,.$$

Average values of the $(\alpha_{ij})_i$ are now obtained by evaluating $(\overline{\alpha_{ij}})_i$, averaging over the orientations of the segments of the chain according to

$$(\overline{\alpha_{ij}})_i = \frac{\int_\phi \int_\theta (\alpha_{ij})_i \, dN}{\int_\phi \int_\theta dN} \qquad \text{(II-37)}$$

where dN , the incremental number of chain elements, is to be expressed in terms of θ and ϕ . Since the end-to-end vector $\vec{h}$ for the chain coincides with the Z axis, the rotational symmetry in the X , Y plane yielding identical values of $\vec{h}$ means that the

number of subchains oriented at an angle ϕ is independent of ϕ. However, it is obvious that a variation in the magnitude of $\vec{h}$ will alter the distribution of the values of θ. For example, if the chain is stretched so that $\vec{h}$ approaches the maximum value attainable, then the angles θ will approach zero degrees. Hence the incremental number of chain elements is related to the angles θ and ϕ by

$$dN = \frac{N}{2\pi} F(\theta)\, d\theta\, d\phi \qquad \text{(II-38)}$$

where $F(\theta)$ is a function of θ only. Combining equations (II-37) and (II-38), one obtains

$$(\overline{\alpha_{ij}})_i = \frac{1}{2\pi} \int_{\phi=0}^{2\pi} \int_{\theta=0}^{\pi} (\alpha_{ij})_i F(\theta)\, d\theta\, d\phi. \qquad \text{(II-39)}$$

The application of equation (II-39) to equations (II-36) yields

$$(\overline{\alpha_{xx}})_i = (\overline{\alpha_{yy}})_i = \int_{\theta=0}^{\pi} \left[\frac{(\alpha_1 - \alpha_2)\sin^2\theta}{2} + \alpha_2 \right] F(\theta)\, d\theta \qquad \text{(II-40)}$$

$$(\overline{\alpha_{zz}})_i = \int_{\theta=0}^{\pi} \left[\alpha_1 \cos^2\theta + \alpha_2 \sin^2\theta \right] F(\theta)\, d\theta \qquad \text{(II-41)}$$

and

$$(\overline{\alpha_{xy}})_i = (\overline{\alpha_{xz}})_i = (\overline{\alpha_{yz}})_i = 0. \qquad \text{(II-42)}$$

Note that from equation (II-42) the average polarizability tensor for the i^{th} segment is diagonal in the X, Y, Z coordinate system. Kuhn and Grün evaluated the function $F(\theta)$ of equation (II-39) assuming N large. They obtained

$$F(\theta) = \frac{1}{2} \cdot \frac{\beta}{\sinh\beta} \cdot \sin\theta \cdot e^{-\beta\cos\theta}, \tag{II-43}$$

where β is the inverse Langevin function of $(h/N|\vec{A}|)$. Equation (II-40) may thus be evaluated as follows:

$$(\overline{\alpha_{xx}})_i = (\overline{\alpha_{yy}})_i = \frac{1}{2}\int_{\theta=0}^{\pi} \left[\frac{(\alpha_1-\alpha_2)\sin^2\theta}{2} + \alpha_2\right] \cdot \frac{\beta}{\sinh\beta} e^{-\beta\cos\theta} \sin\theta \, d\theta \tag{II-44}$$

$$= (\alpha_1-\alpha_2)\left[\frac{1}{\beta^2} - \frac{1}{\beta}\coth\beta\right] + \alpha_2. \tag{II-45}$$

Similarly, equation (II-41) yields

$$(\alpha_{zz})_i = \frac{1}{2}\frac{\beta}{\sinh\beta}\left[\int_{\theta=0}^{\pi} \alpha_1 \cos^2\theta \, e^{-\beta\cos\theta} \sin\theta \, d\theta + \int_{\theta=0}^{\pi} \alpha_2 \sin^2\theta \, e^{-\beta\cos\theta} \sin\theta \, d\theta\right] \tag{II-46}$$

$$= (\alpha_1-\alpha_2)\left[1 + \frac{2}{\beta}\left(\frac{1}{\beta} - \coth\beta\right)\right] + \alpha_2.$$

Equations (II-45) and (II-46) may be simplified by the introduction of the Langevin function $L(\beta)$ defined by

$$L(\beta) = \coth\beta - \frac{1}{\beta} = \frac{h}{N|\vec{A}|}. \tag{II-47}$$

The function $L(\beta)$ may be expanded in series form as

$$L(\beta) = \frac{\beta}{3} - \frac{\beta^3}{45} + \frac{2\beta^5}{945} - \frac{\beta^7}{4725} + \cdots . \quad \text{(II-48)}$$

If β is sufficiently small, $L(\beta)$ may be approximated by the first two terms of the series expansion. Applying equations (II-47) and (II-48) to equations (II-45) and (II-46) assuming $\beta < 0.6$ yields the following:

$$(\overline{\alpha_{xx}})_i = (\overline{\alpha_{yy}})_i = \frac{(\alpha_1 - \alpha_2)}{\beta} L(\beta) + \alpha_2 \quad \text{(II-49)}$$

$$\simeq \frac{\alpha_1 + 2\alpha_2}{3} - (\alpha_1 - \alpha_2)\beta^2/45$$

and

$$(\overline{\alpha_{zz}})_i = (\alpha_1 - \alpha_2)\left[1 - \frac{2}{\beta} L(\beta)\right] + \alpha_2 \quad \text{(II-50)}$$

$$\simeq \frac{\alpha_1 + 2\alpha_2}{3} + 2(\alpha_1 - \alpha_2)\beta/45 .$$

The polarizability of the whole chain is equal to the product of the average segmental polarizability times the number of segments N. Hence if the polarizability of the chain along $\vec{h}$ is designated by γ_1 and the polarizability normal to $\vec{h}$ is designated by γ_2, then from equations (II-49) and (II-50) for $\beta < 0.6$ one obtains

$$\gamma_1 = N(\overline{\alpha_{zz}})_i \simeq \frac{N(\alpha_1 + 2\alpha_2)}{3} + 2N(\alpha_1 - \alpha_2)\beta^2/45 \quad \text{(II-51)}$$

and

$$\gamma_2 = N(\overline{\alpha_{xx}})_i \simeq \frac{N(\alpha_1 + 2\alpha_2)}{3} - N(\alpha_1 - \alpha_2)\beta^2/45. \quad \text{(II-52)}$$

Thus the difference of the principal polarizabilities for small β is given by

$$\Delta\gamma \equiv \gamma_1 - \gamma_2 \simeq 3N(\alpha_1 - \alpha_2)\beta^2/45 \,. \tag{II-53}$$

Equations (II-51), (II-52) and (II-53) may be written in terms of h, N and $|\vec{A}|$ using equations (II-47) and (II-48) assuming β to be sufficiently small that

$$\frac{\beta}{3} \gg \frac{\beta^3}{45} \,. \tag{II-54}$$

For β such that equation (II-54) holds, equation (II-53) becomes

$$\Delta\gamma \simeq \frac{3}{5}(\alpha_1 - \alpha_2)\frac{h^2}{N|\vec{A}|^2} \,. \tag{II-55}$$

Since equation (II-54) implies that $h << N|\vec{A}|$, the value of $\overline{h^2}$ obtained for the average end-to-end distance of the chain for small h may be used (50). Thus

$$\overline{h^2} = NA^2 \tag{II-56}$$

so that for $h << N|\vec{A}|$, $\Delta\gamma$ for the entire chain is given by

$$\Delta\gamma \simeq \frac{3}{5}(\alpha_1 - \alpha_2)\frac{h^2}{\overline{h^2}} \tag{II-57}$$

assuming the number of subchains N to be large.

2. The Viscoelasticity and Oscillatory Flow Birefringence of Unbranched Chain Molecules in Dilute Solution as Given by the Zimm Theory

The behavior of flexible, linear polymer molecules suspended in a viscous medium has been analyzed by Zimm for dilute solutions which are subjected to sinusoidally time varying velocity gradients, using as a model for the polymer a chain of identical beads joined by identical Hookean springs (103). The treatment includes forces on the beads due to Brownian motion, as well as those due to hydrodynamic interactions among the beads of the chain. The differential equation describing the motions of the chain is converted to a solvable form by a coordinate transformation to an appropriate set of normal coordinates. The complex viscosity and flow birefringence expressions are obtained for the model for the case in which the solution is subjected to a sinusoidally time varying velocity gradient, assuming a model chain in which hydrodynamic interaction is either vanishingly small or very large. It should be noted that internal viscosity in the joints of the model and intermediate degrees of hydrodynamic interaction are not considered.

The model of the linear polymer chain adopted by Zimm consists of N identical segments joining $N+1$ identical beads with complete flexibility at each bead (no internal viscosity) so that adjacent segments have a random angular distribution with respect to each other. Thus random walk statistics may be applied to the model unless the chain is subjected to large orienting forces (70). Thus, if the distance between any two adjacent beads in the chain is denoted by l, the probability function $W(l)$ for the distribution of the length of the segment is assumed to be gaussian in character. That is,

$$W(\ell) = a e^{-\frac{3\ell^2}{2b^2}} = a e^{\left[-\frac{3(\ell_x^2+\ell_y^2+\ell_z^2)}{2b^2}\right]} \qquad \text{(II-58)}$$

where b^2 is the average value of ℓ^2, ℓ_x, ℓ_y and ℓ_z are the X, Y and Z components of ℓ, and a is a constant. The probability function of equation (II-58) implies that the segments in the chain model are equivalent to Hookean springs, so that the chain model becomes one of identical beads and identical connecting springs as shown in Figure 3.

Kuhn has shown that the replacement of a section of a linear polymer molecule by a Hookean spring is probably a fairly accurate representation of the behavior of the molecule when sufficiently small external forces are applied (50, 51, 55). Since a real polymer chain does not have complete freedom between monomer units, but is restricted to certain bond angles, etc., random walk statistics can be applied only to sections (or subchains) of the chain which contain a sufficiently large number of monomer units that neighboring sections will have random angular distributions with respect to each other (51, 55). For a molecule made up of a large number of subchains having such random orientations, Kuhn obtained a distribution function for the end-to-end distance $W(h)$ of the chain of the form

$$W(h) = a' e^{-\frac{3h^2}{2\overline{h^2}}} \qquad \text{(II-59)}$$

where a' is a constant and $\overline{h^2}$ is the average value of h^2. If one assumes that the polymer molecule is replaced by a Hookean

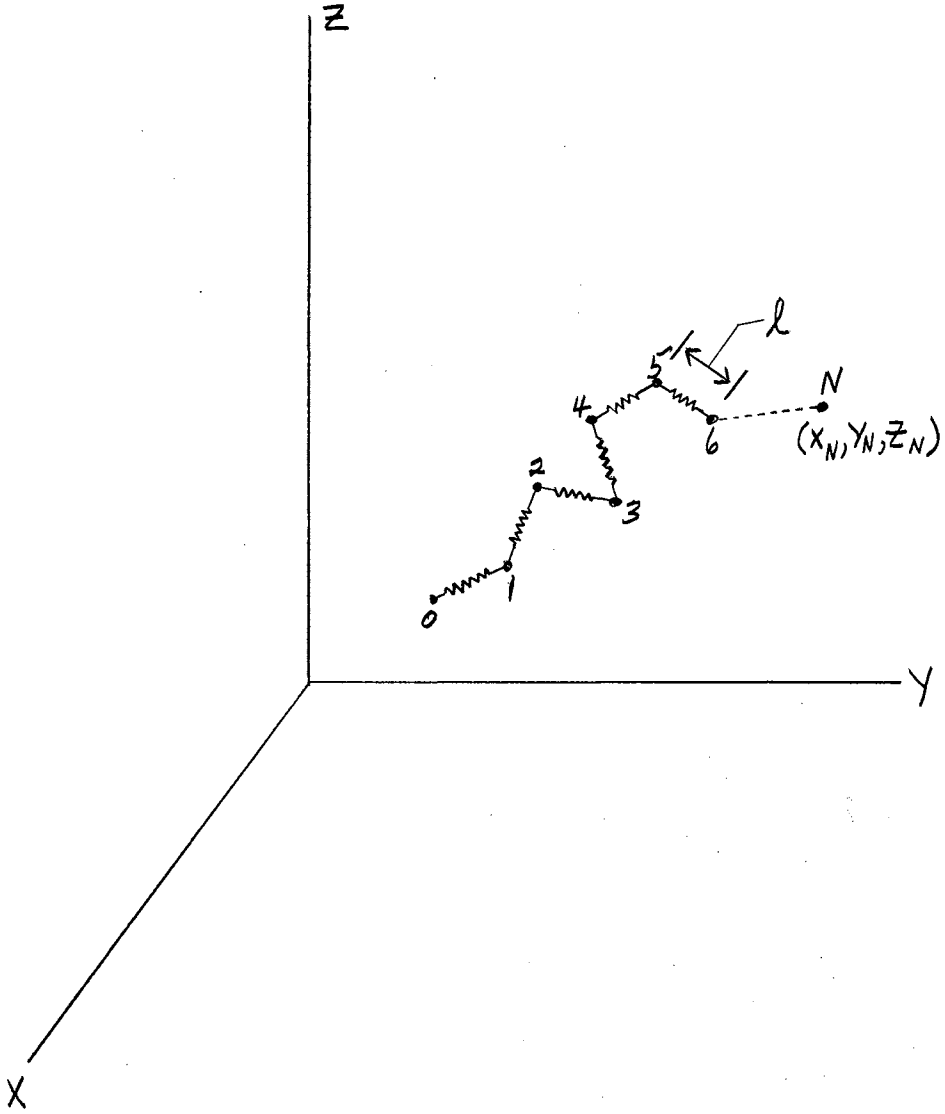

Figure 3. Coordinate System for the Specification of the Spatial Configurations of the Bead and Spring Chain Model of Zimm.

spring of force constant K with endpoints coinciding with the endpoints of the polymer, the potential energy of the spring will be given by

$$V = \frac{K h^2}{2} . \tag{II-60}$$

Thus if Boltzmann statistics are applicable, the Boltzmann probability function

$$W = a' e^{-\frac{V}{kT}} \tag{II-61}$$

when combined with equation (II-3) yields

$$W(h) = a' e^{-\frac{K h^2}{2kT}} \tag{II-62}$$

where k is Boltzmann's constant and T is the absolute temperature. Thus if K is given by

$$K = \frac{3kT}{h^2} \tag{II-63}$$

equation (II-5) and equation (II-2) are identical. If one further assumes that the molecule may be subdivided into submolecules that likewise obey random walk statistics, then the submolecule of length l may likewise be replaced by a spring of mean force constant

$$K = \frac{3kT}{l^2} \tag{II-64}$$

so that the probability function for the submolecule length l will be

$$W(l) = a' e^{-\frac{K l^2}{2kT}} = a' e^{-\frac{3 l^2}{2 l^2}} \tag{II-65}$$

which is identical in form to equation (II-58). Thus the submolecule of the polymer molecule behaves as though there were a Hookean spring joining its end points, having a mean force constant given by equation (II-64), so that the entire molecule consisting of N submolecules may be approximated by considering the N submolecules to be replaced by N such springs.

The analysis of the behavior of the spring and bead model of Figure 3 can be simplified by noting that if the springs are assumed to have zero length when no stretching force is applied, then the spring of force constant K joining the i^{th} and the j^{th} beads is equivalent to three separate Hookean springs oriented along the X , Y and Z coordinate axes, having the same force constant K . Thus the single segment of the model or the entire model may be analyzed by considering its projections upon the axes of the chosen coordinate system. Thus the complicated 3-dimensional array of springs and beads may be simplified by reducing it to three 1-dimensional arrays lying along the coordinate axes.

For mathematical simplicity, the chain model is assumed to be suspended in a continuous viscous liquid which can interact with the chain through the beads only, although such an assumption obviously does not correspond to the behavior of a real polymer molecule for which all regions of the molecule can interact with the liquid. The interaction of the bead and the fluid is assumed to be such that a force $\vec{F}_j$ having components F_{xj} , F_{yj} , F_{zj} is exerted on the liquid by the bead when the bead is moving with a velocity $\vec{v}$ having components v_x , v_y , v_z which is different from the velocity which the fluid would have at j if the

bead were absent. Thus

$$F_{xj} = \zeta(\dot{x}_j - v'_{xj})$$
$$F_{yj} = \zeta(\dot{y}_j - v'_{yj}) \qquad \text{(II-66)}$$
$$F_{zj} = \zeta(\dot{z}_j - v'_{zj})$$

where ζ is a friction constant and v'_{xj}, v'_{yj}, v'_{zj} are the components of the velocity that the fluid would have if the j^{th} bead were absent. Thus the force that the bead exerts on the fluid is assumed to be proportional to the velocity of the bead relative to the surrounding fluid much like the Stokes law force exerted on a viscous fluid when a macroscopic sphere is forced through the fluid. From Stokes law, the force exerted on a fluid by a moving sphere has components

$$F_u = 6\pi\eta_s r(\dot{u}_j - v'_{uj}), \quad u = x, y, z, \qquad \text{(II-67)}$$

where r is the radius of the sphere and η_s is the fluid viscosity. Thus to a first approximation the friction factor ζ characteristic of a polymer chain segment might be expected to be directly proportional to the solvent viscosity, and to have essentially the same variation with temperature that η_s would have, although its magnitude would not be expected to be given by equation (II-67).

There are two separate forces which are assumed to act on the beads, the restoring forces of the spring elements in the chain model and the forces due to Brownian motion in the solution. From equation (II-64), the restoring force $\vec{F}_R$ acting on the j^{th} bead due to the springs from $(j-1)$ to j and j to $(j+1)$ will have

components given by

$$F_{Ru_j} = \frac{3kT}{b^2}(u_j - u_{j-1}) + \frac{3kT}{b^2}(u_{j+1} - u_j) \qquad \text{(II-68)}$$
$$= -\frac{3kT}{b^2}(-u_{j-1} + 2u_j - u_{j+1}) .$$

The forces associated with the Brownian motion of the chain are introduced by noting that the average Brownian motion for a random walk process has been shown to obey the standard differential equation for diffusion (17). Thus if the distribution function $\psi(X_0, Y_0, Z_0, X_1, \ldots, Z_N)dX_j dY_j dZ_j$ gives the probability of finding each bead j between X_j and $X_j + dX_j$, Y_j and $Y_j + dY_j$ and Z_j and $Z_j + dZ_j$, then since probability is directly proportional to concentration, the application of Fick's law to ψ yields an average Brownian force $\vec{F}_{Bj}$ acting on the bead j having components F_{Bjx}, F_{BjY}, F_{Bjz} given by

$$F_{Bju} = -kT\frac{\partial(\ln\psi)}{\partial u_j}, \quad u = X, Y, Z. \qquad \text{(II-69)}$$

Thus from equations (II-68) and (II-69) the total average force acting on the j^{th} bead is given by

$$F_{u0} = -kT\frac{\partial(\ln\psi)}{\partial u_0} - \frac{3kT}{b^2}(u_0 - u_1), \; j = 0,$$

$$F_{uj} = -kT\frac{\partial(\ln\psi)}{\partial u_j} - \frac{3kT}{b^2}(-u_{j-1} + 2u_j - u_{j+1}), \qquad \text{(II-70)}$$

and $$F_{uN} = -kT\frac{\partial(\ln\psi)}{\partial u_j} - \frac{3kT}{b^2}(-u_{N-1} + u_N), \; j = N, \; u = X, Y, Z.$$

Hydrodynamic interaction between the various segments of the chain is introduced through the velocity $\vec{v}_j'$ of equation (II-66). $\vec{v}_j'$, the velocity that the fluid would have at the site of j if the j^{th} bead were absent, is different from the velocity v_j that would exist at the site of j if all forces due to the presence of the remainder of the chain were absent. The interaction of the chain segments by way of the suspending fluid is assumed to be given by the approximate form of the Oseen interaction tensor given by Kirkwood and Riseman (46). From equation (II-66), the force exerted on the liquid by the bead j has X, Y and Z components given by

$$F_{uj} = \zeta(\dot{u}_j - v'_{uj}), \quad u = X, Y, Z. \tag{II-66}$$

From the work of Oseen (5) the fluid velocity at a point located by a vector $\vec{R}$ from a given point P is modified by the application of a force $\vec{F}$ at the point P. The velocity of flow of the fluid is assumed to be small, and the force is assumed to vary sufficiently slowly with time t that

$$t > \frac{25\rho R^2}{\eta_s} \tag{II-71}$$

where ρ is the density of the fluid and t is the time between the instant of application of the force and the moment being considered. For such quasi-static conditions, the perturbing velocity $\vec{v}_p$ is given by

$$\begin{aligned} \vec{v}_p &= T(\vec{R})\,\vec{F} \\ &= \frac{1}{8\pi\eta_s}\left[1 + \vec{R}\vec{R}/R^2\right]\vec{F} \end{aligned} \tag{II-72}$$

if R is sufficiently small that $R \gg R^3$. $T(\vec{R})$ is a hydrodynamic interaction tensor and η_s is the viscosity of the suspending fluid (5, 34, 46). Thus $T(\vec{R})$ expressed in dyadic form is given by

$$T(\vec{R}) = \left[1 + \vec{R}\vec{R}/R^2\right]. \qquad \text{(II-73)}$$

Since the hydrodynamic interactions to be considered are interactions within the model chain, the values of R will be less than 10^{-4} cm. Thus from equation (II-71), assuming $\rho \simeq 1.4$ gm/cc and $\eta_s \geq 0.1$ poise, the minimum value of η_s encountered in the work presented herein, t must be greater than 3.5×10^{-6} seconds, so that for frequencies greater than approximately 1×10^5 cps equation (II-71) may not be valid.

Let $\vec{R}_{jk}$ denote the vector joining the locations of the two beads j and k. Since it is only possible to specify an average value for the vector $\vec{R}_{jk}$ denoted by $\langle R_{jk} \rangle_{av}$, $\langle R_{jk} \rangle_{av}$ is used in equation (II-72). This is equivalent to replacing the interaction tensor T_{jk} describing the influence of bead k at the site of bead j by its average value, if it is further assumed that the chain model will have a gaussian distribution function describing the R_{jk} vectors for the entire chain, and that such a distribution function will apply for all motions of the polymer chain being considered. Thus Kirkwood and Riseman obtain

$$\langle T_{jk} \rangle_{av} = \frac{1}{6\pi\eta_s} \left\langle \frac{1}{R_{jk}} \right\rangle_{av}. \qquad \text{(II-74)}$$

Further, if the extension of the model is not approaching the maximum extension of the chain,

$$\langle T_{jk} \rangle_{av} \simeq \left(\frac{6}{\pi}\right)^{\frac{1}{2}} \left(\frac{1}{b} |j-k|^{\frac{1}{2}}\right) \qquad \text{(II-75)}$$

where b is the average distance between two beads in the chain model. Combining equations (II-74) and (II-75), one obtains

$$\langle T_{jk} \rangle_{av} \simeq \left(\frac{1}{6\pi^3}\right)^{\frac{1}{2}} \left(\frac{1}{\eta_s b}\right) \left(|j-k|^{\frac{1}{2}}\right). \qquad \text{(II-76)}$$

Thus, making the assumptions noted above, the perturbing velocity $\vec{v}_{pj}$ at j caused by the bead k will be approximated by

$$\vec{v}_{pj} \simeq \left(\frac{1}{6\pi^3}\right)^{\frac{1}{2}} \left(\frac{1}{\eta_s b}\right) \left(|j-k|^{\frac{1}{2}}\right) \vec{F}_k = \langle T_{jk} \rangle_{av} \vec{F}_k \qquad \text{(II-77)}$$

from equation (II-72). The velocity v_j' at the site of j will be given by

$$\begin{aligned} \vec{v}_j' &\simeq \vec{v}_j + \sum_{\substack{k=0 \\ j \neq k}}^{N} \langle T_{jk} \rangle_{av} \vec{F}_k \\ &\simeq \vec{v}_j + \left(\frac{1}{6\pi^3}\right)^{\frac{1}{2}} \left(\frac{1}{\eta_s b}\right) \sum_{\substack{k=0 \\ j \neq k}}^{N} \left(|j-k|^{\frac{1}{2}}\right) \vec{F}_k \end{aligned} \qquad \text{(II-78)}$$

where $\vec{F}_k$ is the force exerted by the k^{th} bead on the suspending fluid.

The equation of motion--actually an equation of average motion, since equations (II-64) and (II-69) involve averages of the motions of the chain due to Brownian forces--may now be obtained. Assuming that

the mass of a bead is sufficiently small that inertial forces may be neglected for the frequencies of interest, the force exerted on the liquid by the bead j is equal to the force exerted on the bead by the linking springs and the Brownian motions. Hence, from equations (II-66) and (II-70)

$$\zeta(\dot{u}_0 - \tilde{v}'_{u0}) = -kT\frac{\partial(\ln\psi)}{\partial u_0} - \frac{3kT}{b^2}(u_0 - u_1),$$

$$\zeta(\dot{u}_j - \tilde{v}'_{uj}) = -kT\frac{\partial(\ln\psi)}{\partial u_j} - \frac{3kT}{b^2}(-u_{j-1} + 2u_j - u_{j+1}), \qquad \text{(II-79)}$$

$$\zeta(\dot{u}_N - \tilde{v}'_{uN}) = -kT\frac{\partial(\ln\psi)}{\partial u_N} - \frac{3kT}{b^2}(u_N - u_{N-1}), \quad u = x, y, z.$$

Solving equations (II-79) for $\dot{u}_j$ and inserting values for $\tilde{v}'_{uj}$ from equation (II-78) one obtains

$$\dot{u}_0 = \tilde{v}_{u0} - D\frac{\partial(\ln\psi)}{\partial u_0} - \sigma(u_0 - u_1) - \zeta\sum_{\substack{k=1\\k\neq j}}^{N-1} T_{0k}\left[D\frac{\partial(\ln\psi)}{\partial u_k} + \sigma(-u_{k-1} + 2u_k - u_{k+1})\right] - \zeta T_{00}\left[D\frac{\partial(\ln\psi)}{\partial u_0} + (u_0 - u_1)\right] - \zeta T_{0N}\left[D\frac{\partial(\ln\psi)}{\partial u_N} + \sigma(u_N - u_{N-1})\right]$$

$$\dot{u}_j = \tilde{v}_{uj} - D\frac{\partial(\ln\psi)}{\partial u_j} - \sigma(-u_{j-1} + 2u_j - u_{j+1}) - \zeta\sum_{\substack{k=1\\k\neq j}}^{N-1} T_{jk}\left[D\frac{\partial(\ln\psi)}{\partial u_k} + \sigma(-u_{k-1} + 2u_k - u_{k+1})\right] - \zeta T_{j0}\left[D\frac{\partial(\ln\psi)}{\partial u_0} + \sigma(u_0 - u_1)\right] - \zeta T_{jN}\left[D\frac{\partial(\ln\psi)}{\partial u_N} + \sigma(u_N - u_{N-1})\right] \qquad \text{(II-80)}$$

$$\dot{u}_N = \tilde{v}_{uN} - D\frac{\partial(\ln\psi)}{\partial u_N} - \sigma(u_N - u_{N-1}) - \zeta\sum_{k=1}^{N-1} T_{Nk}\left[D\frac{\partial(\ln\psi)}{\partial u_k} + \sigma(-u_{k-1} + 2u_k - u_{k+1})\right] - \zeta T_{N0}\left[D\frac{\partial(\ln\psi)}{\partial u_0} + \sigma(u_0 - u_1)\right] - \zeta T_{NN}\left[D\frac{\partial(\ln\psi)}{\partial u_N} - \sigma(u_N - u_{N-1}),\right.$$

where

$$D = \frac{kT}{f} \tag{II-81}$$

and

$$\sigma = \frac{3kT}{f b^2} \, . \tag{II-82}$$

It is mathematically convenient to introduce a matrix notation to indicate the method of solution of equation (II-80). Let the $(N+1)$ dimensional column vectors u, ν_u, F_u and $\frac{\partial}{\partial u}$ be defined as

$$u = \begin{pmatrix} u_0 \\ u_1 \\ \vdots \\ u_N \end{pmatrix}, \quad u = X, Y, Z, \tag{II-83}$$

$$\nu_u = \begin{pmatrix} \nu_{u0} \\ \nu_{u1} \\ \vdots \\ \nu_{uN} \end{pmatrix}, \quad u = X, Y, Z, \tag{II-84}$$

$$F_u = \begin{pmatrix} F_{u0} \\ F_{u1} \\ \vdots \\ F_{uN} \end{pmatrix}, \quad u = X, Y, Z, \tag{II-85}$$

and

$$\frac{\partial}{\partial u} = \begin{pmatrix} \frac{\partial}{\partial u_0} \\ \frac{\partial}{\partial u_1} \\ \vdots \\ \frac{\partial}{\partial u_N} \end{pmatrix}, \quad u = X, Y, Z. \tag{II-86}$$

Also, define square symmetric matrices A and H of order $(N+1)$ as

$$A \equiv \begin{pmatrix} 1 & -1 & 0 & 0 & \cdots & 0 \\ -1 & 2 & -1 & 0 & \cdots & 0 \\ 0 & -1 & 2 & -1 & \cdots & 0 \\ 0 & 0 & -1 & 2 & \cdots & 0 \\ \vdots & \vdots & \vdots & \vdots & & \vdots \\ 0 & 0 & 0 & 0 & \cdots & 2 \; -1 \\ 0 & 0 & 0 & 0 & \cdots & -1 \; 1 \end{pmatrix} \tag{II-87}$$

and

$$H \equiv \begin{pmatrix} 1 & \mathcal{J}T_{01} & \mathcal{J}T_{02} \cdots & \mathcal{J}T_{0N} \\ \mathcal{J}T_{10} & 1 & \mathcal{J}T_{12} \cdots & \mathcal{J}T_{1N} \\ \mathcal{J}T_{20} & \mathcal{J}T_{21} & 1 \cdots & \mathcal{J}T_{2N} \\ \vdots & \vdots & \vdots & \vdots \\ \mathcal{J}T_{N0} & \mathcal{J}T_{N1} & \mathcal{J}T_{N2} \cdots & 1 \end{pmatrix} . \tag{II-88}$$

Making use of equations (II-83) through (II-88), the differential equations of motion (II-80) may be written as

$$\dot{X} = \frac{\partial X}{\partial t} = \bar{v}_X - DH \cdot \left(\frac{\partial}{\partial X}\right) \ln \psi - \sigma H \cdot A \cdot X$$

$$\dot{Y} = \frac{\partial Y}{\partial t} = \bar{v}_Y - DH \cdot \left(\frac{\partial}{\partial Y}\right) \ln \psi - \sigma H \cdot A \cdot Y \tag{II-89}$$

$$\dot{Z} = \frac{\partial Z}{\partial t} = \bar{v}_Z - DH \cdot \left(\frac{\partial}{\partial Z}\right) \ln \psi - \sigma H \cdot A \cdot Z$$

where the dot between matrices indicates matrix multiplication.

Since the distribution function ψ may be considered to be a probability function describing the probability of finding the chain with a given configuration, the probability P of finding the chain in a volume element $d\tau = dX_0 dX_1 \cdots dZ_N$ located at $X_0, X_1, \cdots Z_N$ in the $(3N+3)$ dimensional space is given by

$$P = \psi(X_0, \cdots, Z_N, t)\, dX_0 \cdots dZ_N \tag{II-90}$$

Thus the variation of P with time will be given by

$$\frac{\partial P}{\partial t} = \frac{\partial \psi(X_0, \cdots Z_N, t)}{\partial t} d\tau . \tag{II-91}$$

Assuming that there are no sources or sinks for the creation or destruction of the chain, the entire change of P with time is given

by the influx and efflux of the chain from the volume element $d\tau$. Thus the divergence theorem yields the equation of continuity

$$\frac{\partial \psi}{\partial t} + div(\psi \mathcal{N}) = 0 \tag{II-92}$$

where $\mathcal{N}$ is the velocity matrix given by

$$\mathcal{N} = \left(\frac{\partial X}{\partial t}\right) + \left(\frac{\partial Y}{\partial t}\right) + \left(\frac{\partial Z}{\partial t}\right) = \begin{pmatrix} \frac{\partial X_0}{\partial t} & \frac{\partial Y_0}{\partial t} & \frac{\partial Z_0}{\partial t} \\ \frac{\partial X_1}{\partial t} & \frac{\partial Y_1}{\partial t} & \frac{\partial Z_1}{\partial t} \\ \vdots & \vdots & \vdots \\ \frac{\partial X_N}{\partial t} & \frac{\partial Y_N}{\partial t} & \frac{\partial Z_N}{\partial t} \end{pmatrix}. \tag{II-93}$$

Since the divergence operator in matrix notation is

$$div = \left(\frac{\partial}{\partial X}\right)^T + \left(\frac{\partial}{\partial Y}\right)^T + \left(\frac{\partial}{\partial Z}\right)^T, \tag{II-94}$$

where T indicates the transpose of the indicated matrix, equation (II-92), the equation of continuity, may be written as

$$\frac{\partial \psi}{\partial t} = -\sum_{u=X,Y,Z} \left\{ \left(\frac{\partial \psi}{\partial u}\right)^T \cdot \frac{\partial u}{\partial t} + \psi \left(\frac{\partial}{\partial u}\right)^T \cdot \frac{\partial u}{\partial t} \right\}. \tag{II-95}$$

Combining equations (II-89) and (II-95) one obtains the desired differential equation for ψ :

$$\frac{\partial \psi}{\partial t} = \sum_{u=X,Y,Z} \left\{ -\left(\frac{\partial \psi}{\partial u}\right)^T \cdot \mathcal{N}_u - \psi \left(\frac{\partial}{\partial u}\right)^T \cdot \mathcal{N}_u + D \left(\frac{\partial}{\partial u}\right)^T \cdot H \cdot \left(\frac{\partial \psi}{\partial u}\right) + \sigma \left(\frac{\partial \psi}{\partial u}\right)^T \cdot H \cdot A \cdot \mathcal{U} + \sigma \psi \left(\frac{\partial}{\partial u}\right)^T \cdot H \cdot A \cdot \mathcal{U} \right\}. \tag{II-96}$$

Equation (II-96) contains product terms that are not diagonal matrices in the X , Y , Z coordinate system. However, an appropriate transformation of coordinates can be performed such that the product terms will produce diagonalized matrices and hence simplify the mathematical analysis of the problem. This normal coordinate transformation is constructed from the characteristic vectors of the matrix $(H \cdot A)$. Note that although H and A are both symmetric matrices, $(H \cdot A)$ is not symmetric.

If the eigenvectors and eigenvalues of $(H \cdot A)$ are denoted by α_p and λ_p respectively, then the eigenvalue equation of $(H \cdot A)$ is

$$H \cdot A \cdot \alpha_p = \lambda_p \alpha_p \,. \tag{II-97}$$

This set of equations may be written in matrix form. Let the eigenvectors α_p be the $(N+1)$ columns of the $[(N+1) \times (N+1)]$ matrix Q defined by

$$Q \equiv \begin{pmatrix} \alpha_{00} & \alpha_{10} & \alpha_{20} \cdots \alpha_{N0} \\ \alpha_{01} & \alpha_{11} & \alpha_{21} \cdots \alpha_{N1} \\ \alpha_{02} & \alpha_{12} & \alpha_{22} \cdots \alpha_{N2} \\ \vdots & \vdots & \vdots \\ \alpha_{0N} & \alpha_{1N} & \alpha_{2N} \cdots \alpha_{NN} \end{pmatrix} \tag{II-98}$$

where α_{ij} denotes the j^{th} component of the eigenvector α_i . Let Q^{-1} be the inverse of Q so that

$$Q\,Q^{-1} = Q^{-1}Q = I \tag{II-99}$$

where I is the unit matrix. If a diagonal matrix Λ is defined by

$$\Lambda = \begin{pmatrix} \lambda_0 & 0 & 0 & 0 & \cdots & 0 \\ 0 & \lambda_1 & 0 & 0 & \cdots & 0 \\ 0 & 0 & \lambda_2 & 0 & \cdots & 0 \\ 0 & 0 & 0 & \lambda_3 & \cdots & 0 \\ \vdots & \vdots & \vdots & \vdots & & \vdots \\ 0 & 0 & 0 & 0 & \cdots & \lambda_N \end{pmatrix} \qquad \text{(II-100)}$$

then the family of equations (II-97) may be written as

$$H \cdot A \cdot Q = Q \Lambda . \qquad \text{(II-101)}$$

The matrix $(H \cdot A)$ may now be diagonalized by a similarity transformation if the λ_k are all distinct $(\lambda_k \neq \lambda_\ell, k \neq \ell)$. Multiplying equation (II-101) from the left by Q^{-1}, one obtains

$$Q^{-1} \cdot H \cdot A \cdot Q = Q^{-1} Q \Lambda = I \Lambda = \Lambda \qquad \text{(II-102)}$$

where Λ is the diagonal matrix having as elements the eigenvalues λ_p. Similarly, if all of the eigenvalues are distinct, A is diagonalized by

$$Q^{T} \cdot A \cdot Q = M \qquad \text{(II-103)}$$

where M has nonzero values μ_p on the diagonal only, and H is diagonalized by

$$Q^{-1} \cdot H \cdot Q^{-1 T} = M^{-1} \Lambda = N \qquad \text{(II-104)}$$

where N has nonzero diagonal elements ν_p only. Thus the matrix Q may be used to obtain the desired diagonal forms in equation (II-96), (36).

The normal coordinates adopted by Zimm are those given by the

transform matrix Q of equation (II-100). Thus if the normal coordinates are denoted by ξ , η , ζ , one has

$$\begin{aligned} X &= Q\xi \\ Y &= Q\eta \\ Z &= Q\zeta \end{aligned} \tag{II-105}$$

and,

$$\begin{aligned} \xi &= Q^{-1}X \\ \eta &= Q^{-1}Y \\ \zeta &= Q^{-1}Z . \end{aligned} \tag{II-106}$$

Partial derivatives will transform according to

$$\frac{\partial}{\partial X} = Q^{-1T}\frac{\partial}{\partial \xi} \tag{II-107}$$

and

$$\frac{\partial}{\partial \xi} = Q^{T}\frac{\partial}{\partial X} .$$

It is necessary to state the velocities v_u explicitly in order to transform equation (II-96) to normal coordinate form. Assume laminar flow with a velocity gradient such that the velocity gradient is essentially constant over a domain of molecular dimensions. That is, the shear wavelength λ_s at the driving frequency must be large with respect to the dimensions of the molecule. Thus for a given solution viscosity there will be an upper frequency limit set by the assumption of a constant velocity gradient acting on the molecule. The velocity is assumed to be given by

and

$$\begin{aligned} v_{xi} &= q\, z_i \\ v_{yi} &= v_{zi} = 0 \end{aligned} \tag{II-108}$$

where the velocity gradient g is a harmonic function of time with radian frequency ω, related to the frequency f in cps by $\omega = 2\pi f$. Thus g is given by

$$g = g_0 e^{i\omega t}. \tag{II-109}$$

The insertion of equations (II-108) into equation (II-96) yields

$$\frac{\partial \psi}{\partial t} = -\left(\frac{\partial \psi}{\partial x}\right)^T \cdot N_x + \sum_{u=x,y,z} \left\{ D\left(\frac{\partial}{\partial u}\right)^T \cdot H \cdot \left(\frac{\partial \psi}{\partial u}\right) + \sigma\left(\frac{\partial \psi}{\partial u}\right)^T \cdot H \cdot A \cdot u + \sigma \psi \left(\frac{\partial}{\partial u}\right)^T \cdot H \cdot A \cdot u \right\}. \tag{II-110}$$

From equations (II-106), (II-107), and (II-108),

$$N = N_x = g Q \mathcal{H} \tag{II-111}$$

and

$$\frac{\partial \psi}{\partial u} = Q^{-1T} \frac{\partial \psi}{\partial u'}, \quad u = x, y, z \quad u' = \xi, \eta, \mathcal{H}. \tag{II-112}$$

Thus the equation for ψ in normal coordinate form becomes after some manipulation

$$\frac{\partial \psi}{\partial t} = -g \mathcal{H}^T \cdot \left(\frac{\partial \psi}{\partial \xi}\right) + \sum_{u=\xi,\eta,\mathcal{H}} \left\{ D\left(\frac{\partial}{\partial u'}\right)^T \cdot N \cdot \frac{\partial \psi}{\partial u'} + \sigma\left(\frac{\partial \psi}{\partial u'}\right)^T \cdot \Lambda \cdot u' + \sigma \psi \left(\frac{\partial}{\partial u'}\right)^T \cdot \Lambda \cdot u' \right\}. \tag{II-113}$$

Or, writing equation (II-113) in terms of the matrix elements,

$$\frac{\partial \psi}{\partial t} = -g\, \mathcal{H}^{T} \cdot \left(\frac{\partial \psi}{\partial \xi}\right) + \sum_{u=\xi,\eta,\mathcal{H}} \sum_{p=0}^{N} \left[D v_p \frac{\partial^2 \psi}{\partial u_p'^2} + \sigma \lambda_p \left(u_p' \frac{\partial \psi}{\partial u_p'} + \psi \right) \right]. \tag{II-114}$$

The desired solutions to equation (II-114) are obtained by assuming a solution of the form

$$\psi = \Psi_0 \sum_{m=0}^{\infty} \psi_m g^m \tag{II-115}$$

with $\psi_0 = 1$ and

$$\Psi_0 = e^{\left[\left(\frac{-3}{2b^2}\right)\left\{\sum_{j=0}^{N-1}\left[(x_j - x_{j+1})^2 + (y_j - y_{j+1})^2 + (z_j - z_{j+1})^2\right]\right\}\right]} \tag{II-116}$$

from equation (II-58). Equation (II-116) becomes

$$\Psi_0 = e^{\left\{\left(\frac{-\sigma}{2D}\right)\left[\sum_{p=1}^{N} \mu_p (\xi_p^2 + \eta_p^2 + \mathcal{H}_p^2)\right]\right\}} \tag{II-117}$$

when written in the normal coordinate system. Thus

$$\frac{\partial \Psi_0}{\partial u_p'} = -\left(\frac{\sigma}{D}\right) \mu_p u_p' \Psi_0, \quad u_p' = \xi, \eta, \mathcal{H}. \tag{II-118}$$

Equating the coefficients of g^m in equation (II-114) making use of equations (II-115), (II-117) and (II-118) yields the set of equations

$$i m \omega \psi_m = \sum_{p=1}^{N} \left[(\sigma/D) \mu_p \xi_p \eta_p \psi_{m-1} - \eta_p \frac{\partial \psi_{m-1}}{\partial \xi_p} \right. \tag{II-119}$$

$$\left. + \sum_{u'=\xi,\eta,\zeta} \left(D \nu_p \frac{\partial^2 \psi_m}{\partial u_p'^2} - \sigma \lambda_p u_p' \frac{\partial \psi_m}{\partial u_p'} \right) \right], \quad m \geq 1.$$

Zimm obtained as a solution for ψ_1

$$\psi_1 = \sum_{p=1}^{N} c_p \xi_p \eta_p \tag{II-120}$$

where

$$c_p = \mu_p / 2D\lambda_p (1 + i\omega / 2\sigma\lambda_p). \tag{II-121}$$

It is possible to obtain any ψ_m from equations (II-120) and (II-121) using equation (II-119). However, Zimm obtained instead certain integrals that would permit a simpler evaluation of the viscoelastic and flow birefringence properties of the chain model without actually solving for ψ itself. Since ψ is a probability function, it is normalized so that

$$\underset{\text{ALL SPACE}}{\iiint \cdots \int} \psi \, dx_0 \, dx_1 \cdots dx_N = \underset{\text{ALL SPACE}}{\iiint \cdots \int} \psi \, d\tau = 1. \tag{II-122}$$

Or, converting to the normal coordinate system, since the volume element $d\tau$ is given by

$$d\tau = dx_0 \, dx_1 \cdots dx_i \cdots dz_N = J \, d\xi_0 \cdots d\zeta_N \tag{II-123}$$

where J is the Jacobian of the coordinate system ξ , η , $\mathcal{H}$ equation (II-122) yields

$$\underset{\text{ALL SPACE}}{\iint\cdots\int} \psi \, d\tau = \iint\cdots\int \psi \, J \, d\xi_0 \cdots d\mathcal{H}_N = 1. \qquad \text{(II-124)}$$

Or,

$$\underset{\text{ALL SPACE}}{\iint\cdots\int} \psi \, d\xi \cdots d\mathcal{H}_N = J^{-1}. \qquad \text{(II-125)}$$

From equation (II-125) and the boundary condition that ψ must vanish at infinity Zimm obtained the following important result:

$$J \int_{-\infty}^{+\infty}\cdots\int \xi_p \mathcal{H}_p \psi \, d\xi_0 \cdots d\mathcal{H}_N = \qquad \text{(II-126)}$$

$$g \, D / [\mu_p \sigma (2\sigma\lambda_p + i\omega)].$$

The transient term containing $e^{-2\sigma\lambda_p t}$ has been omitted in equation (II-126).

The solution viscosity may now be evaluated. The intrinsic viscosity $[\eta]$ of the solution may be computed using the method of Burgers (5) together with the calculated velocity perturbation of the flow velocity of the solvent due to the presence of the flexible chain in the solution as obtained by Kirkwood and Riseman (44, 46). Kirkwood and Riseman evaluated the velocity perturbation of the flow for a model chain consisting of a random coil model consisting of rigid links joined together at the proper bond angle for the macromolecule being modeled. The rotation around each bond at the valence angle is assumed to be hindered. The interaction of the solvent and

the chain is assumed to be the same as that given by equations (II-66) where the force now denotes the force on an entire link, not on a bead as for the Zimm model. The hydrodynamic interaction among the chain elements is assumed to follow the quasi-static expression of equation (II-73), subject to the assumptions noted previously. The solvent is assumed to be in a state of quasi-stationary two-dimensional laminar flow between plane parallel boundaries. If a polymer molecule is introduced into the solvent and allowed to reach an equilibrium state in the fluid, the center of gravity of the molecule will move with a mean velocity equal to that of the local velocity of the solvent. Also, since the particle is assumed to be in equilibrium, the mean external angular velocity of the overall chain with respect to the fluid is assumed to be such that the average hydrodynamic torques applied to the chain must be zero, where the averages are over a complete rotation of the coil. Also, the internal torques, i.e., the torques exerted on a segment of the model by the other segments, when summed over all segments and averaged over a complete rotation must be equal to zero, so that the average internal velocity must be zero. Thus if q is the velocity gradient and the unit vectors $\vec{i}$, $\vec{j}$ and $\vec{k}$ define a right handed coordinate system X, Y, Z with its origin at the center of gravity of the molecule, the solvent velocity $\vec{v_j}$ at the location of segment j with the chain removed from the solvent will be given by

$$\vec{v_j} = \vec{i}\, q\, R_{zl}, \qquad \text{(II-127)}$$

where R_{zl} is the Z component of the vector locating the segment l, assuming that the solvent is flowing in the X direction

and $\hat{z}$ is the direction normal to the plane parallel boundaries. The condition of zero average external torque is fulfilled if the coil is assigned an average angular velocity in the $-\hat{z}$ direction of $(g/2)$. Thus the average velocity $\vec{u}_j = (\dot{x}_j, \dot{y}_j, \dot{z}_j)$ for the j^{th} element of the chain is assumed to be given by

$$\vec{u}_j = -\frac{g}{2}(\vec{j} \times \vec{R}_L) . \tag{II-128}$$

Thus from equation (II-78) and (II-127) the forces exerted on the fluid by the segment j are given by

$$\vec{F}_j = -\frac{Jg}{2}\left[\vec{i} + \vec{j}\times\right] - \mathcal{J}\sum_{\substack{k=0 \\ j\neq k}}^{N} T_{jk}\vec{F}_k . \tag{II-129}$$

The velocity perturbation at some point located by the vector $\vec{R}$, where $\vec{R}$ is large compared to the linear dimensions of the chain, may be obtained from the quasi-static velocity perturbation expressions of Oseen as given by Burgers (5). For $\vec{R}$ large, the perturbing velocity $\vec{v}_p$ generated by the forces $\vec{F}_j$ yields

$$\langle \vec{v}_p \rangle_{av} = -\left(\frac{3JGg}{4\pi\eta_0 R^5}\right)(R_x R_z)\vec{R} \tag{II-130}$$

with

$$G = -\frac{1}{Jg}\left\langle \sum_{j=0}^{N} F_{xj} z_j \right\rangle_{av} \tag{II-131}$$

where the averages are over the internal configurations of the chain (44). It should be noted that equation (II-131) differs from the

erroneous expression given by Kirkwood and Riseman (46) but agrees with the corrected expression given later by Kirkwood (44).

The effect of the average perturbing velocity $\langle \vec{\nu}_p \rangle_{av}$ on the viscosity exhibited by the solvent is obtained following the method of Burgers (5). The motions are assumed to be sufficiently slow and the dimensions sufficiently small that inertial effects associated with either chain or solvent motions may be neglected. The solvent is assumed to be in a state of laminar flow with streamlines in the X direction and a velocity gradient g in the Z direction, and the number of chains per unit volume is assumed to be sufficiently small that no appreciable interaction between chains can occur. Thus the net average perturbation velocity will be given by the superposition of the average perturbation velocities for all of the chains in the solution. The presence of the chain also disturbs the value of the velocity gradient, but the total effect over a plane $Z = h_1$, that is infinite in extent in the X and Y directions, is zero. Thus the average frictional force per unit area (shear stress) acting on the plane $Z = h_1$, is unchanged by the presence of the chain. From equation (II-130) the X, Y and Z components of $\vec{\nu}_p$ are given by

$$\nu_{px} = -\frac{3G\int g}{4\pi\eta_s} \cdot \frac{R_x^2 R_z}{R^5} \qquad \text{(II-132)}$$

$$\nu_{py} = -\frac{3G\int g}{4\pi\eta_s} \cdot \frac{R_x R_y R_z}{R^5} \qquad \text{(II-133)}$$

and

$$v_{pz} = -\frac{3GJq}{4\pi\eta_s} \cdot \frac{R_x R_z^2}{R^5} \cdot \qquad \text{(II-134)}$$

Thus on the surface $z = h_1$, the integral of the velocity component v_{px}, using cylindrical coordinates, gives the following:

$$v_{xs}\Big|_{z=h_1} \equiv \int_{x=-\infty}^{+\infty} \int_{y=-\infty}^{+\infty} v_{px}\, dx\, dy$$

$$= -\frac{3Gh_1Jq}{4\pi\eta_s} \int_{\rho=0}^{\infty} \int_{\phi=0}^{2\pi} \frac{\rho^3}{(h^2+\rho^2)^{5/2}} \cos^2\phi\, d\phi\, d\rho \qquad \text{(II-135)}$$

$$= -\frac{GJq}{2\eta_s} \cdot$$

Repeating the same procedure for v_{py}, one obtains

$$\int_{x=-\infty}^{+\infty} \int_{y=-\infty}^{+\infty} v_{py}\, dx\, dy = -\frac{3Gh_1Jq}{4\pi\eta_s} \int_{\rho=0}^{+\infty} \int_{\phi=0}^{2\pi} \frac{\rho^3 \sin\phi\cos\phi}{(h^2+\rho^2)^{5/2}}\, d\phi\, d\rho \qquad \text{(II-136)}$$

$$= 0 \cdot$$

Similarly,

$$\int_{x=-\infty}^{+\infty} \int_{y=-\infty}^{+\infty} v_{pz}\, dx\, dy = -\frac{3Gh_1^2Jq}{4\pi\eta_s} \int_{\rho=0}^{+\infty} \int_{\phi=0}^{2\pi} \frac{\rho\cos\phi}{(h^2+\rho^2)^{5/2}}\, d\phi\, d\rho \qquad \text{(II-137)}$$

$$= 0 \cdot$$

Thus there is only an X component to the sum of the perturbing velocity contributions over the plane $Z = h_1$. If the same procedure is followed for the plane $Z = -h_2$, one obtains:

$$v_{xs}\Big|_{z=-h_2} \equiv \int_{x=-\infty}^{+\infty}\int_{y=-\infty}^{+\infty} v_{px}\,dx\,dy = +\frac{G\,\mathcal{J}q}{\partial \eta_s} \qquad \text{(II-138)}$$

and

$$\int_{x=-\infty}^{+\infty}\int_{y=-\infty}^{+\infty} v_{py}\,dx\,dy = \int_{x=-\infty}^{+\infty}\int_{y=-\infty}^{+\infty} v_{py}\,dx\,dy = 0. \qquad \text{(II-139)}$$

Thus the sums of the velocity perturbations on the planes $Z = +h_1$ and $Z = -h_2$ do not depend on the location of the chain between the planes as long as the chain is removed sufficiently far from the planes for the perturbed velocity expressions of (II-132), (II-133) and (II-134) to hold on these planes.

Consider a dilute solution of these chains having n_v particles per unit volume, all sufficiently remote from the planes $Z = h_1$ and $Z = -h_2$ that equations (II-135) and (II-138) are valid. For the infinite volume confined between these planes the sum of the perturbing velocities on a given plane $v_{x\,TOT}$ will be given by v_{xs} for the given plane per particle times the number of particles, where

$$\begin{aligned} v_{x\,TOT} &\equiv n_v v_{xs}\int_{x=-\infty}^{+\infty}\int_{y=-\infty}^{+\infty}(h_1+h_2)\,dx\,dy \\ &= n_v(h_1+h_2)\,v_{xs}\int_{x=-\infty}^{+\infty}\int_{y=-\infty}^{+\infty} dx\,dy\,. \end{aligned} \qquad \text{(II-140)}$$

Thus the average value of $\bar{v}_{XTOT}$ over the plane $z = h_1$ or $z = -h_2$ is

$$\overline{v_{XTOT}} = v_{XS} \cdot n_w (h_1 + h_2). \qquad \text{(II-141)}$$

Since the solvent is assumed to be in two-dimensional laminar flow with no chains present in the solution, the velocity of the solvent is constant in any given plane for which z is constant. Thus if the velocity of the solvent with all chains removed is given as $\vec{v}_1$ at $z = h_1$ and $\vec{v}_2$ at $z = -h_2$, where $\vec{v}_1$ and $\vec{v}_2$ have X components only, then the average velocities $\vec{v}_\lambda$ on the planes with the chains present will be given by

$$\vec{v}_1' = v_1 - \frac{G J g n_w}{2 \eta_s} (h_1 + h_2), \; z = +h_1, \qquad \text{(II-142)}$$

and

$$\vec{v}_2' = v_2 + \frac{G J g n_w}{2 \eta_s} (h_1 + h_2), \; z = -h_2. \qquad \text{(II-143)}$$

Thus the difference in the mean velocities at the two planes will be given by

$$\vec{v}_1' - \vec{v}_2' = -\vec{\imath} \frac{G J g n_w}{\eta_s} (h_1 + h_2) + \vec{v}_1 - \vec{v}_2. \qquad \text{(II-144)}$$

Since the velocity is assumed to increase linearly with z, the velocity gradient g_{eff} between the two planes will be given by

$$g_{eff} = \frac{N_1 - N_2}{(h_1 + h_2)} - \frac{G J g n_w}{\eta_s}. \qquad \text{(II-145)}$$

Thus since the average shear stresses acting on the planes $z = h_1$ and $z = -h_2$ are not altered by the presence of the chains, the viscosity exhibited by the solution will be different from that of the solvent. If the solution viscosity is denoted by η , then

$$\eta = \frac{\tau}{g_{eff}} = \frac{\tau}{g} \cdot \frac{g}{g_{eff}} = \eta_s \left(\frac{g}{g_{eff}}\right). \qquad \text{(II-146)}$$

From (II-145) the ratio (g/g_{eff}) will be given by

$$\frac{g}{g_{eff}} = \frac{1}{\left(1 - \frac{G J n_w}{\eta_s}\right)} \simeq 1 + \frac{G J n_w}{\eta_s} \qquad \text{(II-147)}$$

assuming that $(G J n_w/\eta_s) \gg (G J n_w/\eta_s)^2$, as would be expected for dilute solutions.

Thus from equations (II-146) and (II-147) the intrinsic viscosity of the solution will be given by

$$[\eta] \equiv \lim_{c \to 0} \frac{(\eta - \eta_s)}{\eta_s c} \simeq \frac{n_w J G}{\eta_s c} \qquad \text{(II-148)}$$

where c is the solution concentration in grams of solute per unit volume of the solution. Thus since n_w is given by

$$n_w = \frac{N_a c}{M}, \qquad \text{(II-149)}$$

where N_a is Avogadro's number and M is the gram molecular weight of the molecule, equation (II-148) may be written as

$$[\eta] \simeq \frac{N_a \mathcal{J} G}{M \eta_s} . \qquad \text{(II-150)}$$

Inserting G from equation (II-131) into equation (II-150) one obtains

$$[\eta] \simeq -\frac{N_a}{M \eta_s g} \left\langle \sum_{j=0}^{N} F_{xj} z_j \right\rangle_{av.} \qquad \text{(II-151)}$$

Kirkwood (44) later evaluated the intrinsic viscosity for oscillatory flow using a treatment in which the average hydrodynamic torques are equated not to zero, but to the rotatory diffusional torques due to Brownian motions. He found that the specification of $\vec{u}_j$ given by (II-128) is not sufficiently accurate to include the Brownian motions properly. After a more detailed calculation he found that the expressions for $[\eta]$ and G were not altered, although the quantity $\left\langle \sum_{j=0}^{N} F_{xj} z_j \right\rangle_{av}$ would be, so that equation (II-151) is applicable to oscillatory shears as long as the frequencies are sufficiently small so as to approximate the quasi-static restriction on the Oseen force equations (see equation II-71).

From equations (II-70), (II-85), and (II-87) the forces F_{xj} written in matrix form are

$$F_x = -kT\left(\frac{\partial}{\partial X}\right) \ln \psi - \frac{3kT}{f^2} A \cdot X \qquad \text{(II-152)}$$

which from equations (II-81) and (II-82) may be written as

$$F_x = -kT\left(\frac{\partial}{\partial x}\right)\ln\psi - \frac{kT\sigma}{D}A\cdot X. \qquad \text{(II-153)}$$

Thus, for example, the integral

$$\int_{-\infty}^{+\infty}\cdots\int \psi F_x \, dx_0 \cdots dz_N = -\frac{kT\sigma}{D}\int_{-\infty}^{+\infty}\cdots\int A\cdot X\psi \, dx_0\cdots dz_N, \qquad \text{(II-154)}$$

since the integration of the first term of F_x will equal zero since $\psi = 0$ at infinity. Consider the quantity $\left\langle \sum_{j=0}^{N} z_j F_{xj} \right\rangle_{av}$.

$$\left\langle \sum_{j=0}^{N} z_j F_{xj} \right\rangle_{av} = \left\langle z_0 F_{x0} + z_1 F_{x1} + \cdots + z_N F_{xN} \right\rangle_{av}$$
$$= \left\langle z^T \cdot F_x \right\rangle_{av}. \qquad \text{(II-155)}$$

Introducing the normal coordinates of equation (II-106) one obtains:

$$\begin{aligned}\left\langle z^T \cdot F_x \right\rangle_{av} &= \left\langle (Q\cdot H)^T \cdot F_x \right\rangle_{av} \\ &= \left\langle H^T \cdot Q^T \cdot F_x \right\rangle_{av} \\ &= -\frac{kT\sigma}{D}\left\langle H^T \cdot Q^T \cdot A \cdot X \right\rangle_{av} \\ &= -\frac{kT\sigma}{D}\left\langle H^T \cdot Q^T \cdot A \cdot Q \cdot \xi \right\rangle_{av}.\end{aligned} \qquad \text{(II-156)}$$

Or, writing equation (II-156) using matrix elements and equation (II-103),

$$\langle \underline{z}^T \cdot \underline{F}_x \rangle_{av} = -\frac{kT\sigma}{D} \sum_{p=1}^{N} \mu_p J \int_{-\infty}^{+\infty} \cdots \int \mathcal{H}_p \xi_p \psi \, d\underline{\xi}_0 \cdots d\mathcal{H}_N \,. \quad \text{(II-157)}$$

From equation (II-126), equation (II-157) yields

$$\langle \underline{z}^T \cdot \underline{F}_x \rangle_{av} = -kTq \sum_{p=1}^{N} \frac{1}{(2\sigma\lambda_p + i\omega)} \,. \quad \text{(II-158)}$$

The insertion of equation (II-158) in equation (II-151) yields

$$[\eta] = \frac{N_a kT}{M\eta_s} \sum_{p=1}^{N} \frac{1}{(2\sigma\lambda_p + i\omega)} \,. \quad \text{(II-159)}$$

If the p^{th} relaxation time τ_p is defined as

$$\tau_p = \frac{1}{2\sigma\lambda_p} = \frac{b^2 \zeta}{6kT\lambda_p} \,, \quad \text{(II-160)}$$

the intrinsic viscosity for a dilute solution of chains subject to oscillatory velocity gradients may be written as

$$[\eta] = \frac{N_a b^2 \zeta}{6M\eta_s} \sum_{p=1}^{N} \frac{1}{\lambda_p (1 + i\omega\tau_p)} \,. \quad \text{(II-161)}$$

Thus the viscoelastic properties of dilute solutions of linear chain molecules for which the bead and spring model is adequate will be

given by equation (II-161) for small velocity gradients, providing the eigenvalues λ_p of the eigenvalue equation, equation (II-97), are known. Zimm evaluated the λ_p assuming N to be large for the chain under consideration, so that the eigenvectors α_p of equation (II-97) may be replaced by a continuous function $\alpha(s)$:

$$\alpha_p = \left(\frac{2}{N}\right)^{\frac{1}{2}} \alpha(s) \tag{II-162}$$

where

$$s = \left[\left(\frac{2p}{N}\right) - 1\right] \tag{II-163}$$

relates the index p with the variable s . Similarly, let

$$r = \left[\left(\frac{2i}{N}\right) - 1\right] \tag{II-164}$$

relate the index i to the variable r . In a similar way the matrix operators A and H can be approximated by integral transform operators for N large. Making use of equations (II-162), (II-163) and the integral transform operators for A and H the eigenvalue equation (II-97) yields the following equation:

$$\alpha''(r) + h\int_{-1}^{+1} \alpha''(s)\left(|r-s|\right)^{-\frac{1}{2}} ds = -\frac{N^2}{4}\lambda\,\alpha(r) \tag{II-165}$$

subject to the boundary condition

$$\alpha'(\pm 1) = 0 \tag{II-166}$$

and where h is given by

$$h = \frac{N^{\frac{1}{2}} \zeta}{[(12\pi^3)^{1/2} b \eta_s]} \quad . \tag{II-167}$$

From equations (II-78), (II-66) and (II-80) it can be seen that the factor h is a measure of the quantity $(\vec{v}_f' - \vec{v}_f)$ and hence of the alteration of the velocity of the solvent inside the region occupied by the chain due to the interaction of the chain and the solvent. If h is vanishingly small, the solvent will flow with a velocity equal to that expected when the hydrodynamic interaction force term is negligible, and the chain will exhibit the so-called free-draining condition. If h is large, the solvent internal to the region occupied by the chain will move as if it is subject to forces originating mostly in the motions of other segments of the chain, the so-called non-free-draining condition. Equation (II-165) has been evaluated by Zimm for these two limiting draining conditions. For $h << 1$, the free-draining condition, the solution of (II-165) for N large yields

$$\lambda_p = \frac{\pi^2 p^2}{N^2}, \quad h << 1 \quad . \tag{II-168}$$

For $h >> 1$, the non-free-draining condition,

$$\lambda_p = \frac{4h}{N^2} \lambda_p' = \frac{2\zeta}{(3\pi^3)^{1/2} b \eta_s N^{3/2}} \lambda_p' \tag{II-169}$$

where the λ'_p are numbers that have been evaluated by Zimm, Roe and Epstein for N large (105). Values of λ'_p for p ranging from 0 to 7 are given in Table I.

TABLE I

NON-FREE-DRAINING EIGENVALUES FOR LARGE N

p	λ'_p
0	0
1	4.04
2	12.79
3	24.20
4	37.90
5	53.50
6	70.70
7	89.40

For p greater than 7, the λ'_p can be obtained from the asymptotic formula (109)

$$\lambda'_p \simeq \frac{\pi^2 p^{3/2}}{2}\left(1 - \frac{1}{2\pi p}\right), p > 7. \quad \text{(II-170)}$$

For reasons of mathematical simplicity the values of λ_p obtained from equations (II-168), (II-169), (II-170) and Table I were used for all theoretical computations in the work presented herein although the number of segments is not considered to be large for all cases considered. That the use of these approximate values of λ_p is reasonable can be seen by noting that Rouse has given an expression for λ_p for the free-draining case that is valid for any N (69, 75). He

obtains:

$$\lambda_p = 4 \sin^2\left[\frac{p\pi}{2(N+1)}\right]. \qquad \text{(II-171)}$$

If the argument in equation (II-171) is sufficiently small, the sine may be replaced by the argument. Thus if p is such that $p < \frac{N}{5}$, then

$$\lambda_p \simeq \frac{p^2\pi^2}{N^2} \qquad \text{(II-172)}$$

which is identical to equation (II-168) of Zimm. For $p < \frac{N}{5}$ the approximate expression (II-172) is within 3% of the exact expression (II-171), while for $p < \frac{N}{10}$ the two equations provide values of that are within 1% of each other. Thus except for small values of N, the major effect of the use of the approximate expressions (II-172) will be to alter slightly the high frequency end of the viscosity versus frequency curve obtained from equation (II-161). Since the free-draining and non-free-draining approximate λ_p of Zimm are not drastically different, it is assumed that for the non-free-draining case the exact values of λ_p would also not be much different from those given by Table I and the asymptotic formula equation (II-170).

The intrinsic birefringence exhibited by a dilute solution of the bead and spring chain model subject to oscillatory velocity gradients may now be evaluated. From the analysis of the intrinsic polarizability of a flexible unbranched molecule as evaluated by Kuhn and Grün (see the previous section), the intrinsic polarizability tensor associated with any one of the subchains of the Zimm model should be of

the form obtained by Kuhn and Grün for an entire chain, since the Zimm subchain is assumed to have a gaussian distribution function. Thus the intrinsic polarizability tensor will have its principal axis system oriented such that the $\vec{h}$ direction of Figure 1 is parallel to the major axis of the ellipsoid describing the polarizability of the subchain. From equations (II-51), (II-52), (II-55), (II-56), and (II-57)

$$\gamma_{1i} = p + 2q l_i^2 \qquad \text{(II-173)}$$

$$\gamma_{2i} = p - q l_i^2 \qquad \text{(II-174)}$$

where γ_{1i} and γ_{2i} are the polarizabilities of the subchain associated with directions along and normal to the vector joining the end points of the subchain, p and q are constants depending on the constitution of the system and l_i is the length of the segment i.

The polarizability tensor for the whole molecule is assumed to be equal to the sum of the polarizability tensors for the separate subchains, so that no optical interaction between subchains is included. The polarizability tensors for the various subchains are referred to the X, Y, Z coordinate system and added, making use of the matrix notation. The average values of the elements of the resultant intrinsic polarizability tensor are computed, and the principal polarizabilities of the averaged intrinsic polarizability tensor are extracted to obtain the magnitude of the birefringence of the solution.

Consider the i^{th} subchain, having the vector $\vec{l}_i$ joining its endpoints as shown in Figure 4. Since the principal polarizabilities corresponding to the 1, 2, 3 coordinate system are the γ_{1i} and γ_{2i} of equations (II-173) and (II-174), the elements of the polarizability tensor γ_i associated with the X_i, Y_i, Z_i coordinate system and hence with the X, Y, Z coordinate system may be obtained using the equations (II-35) and (II-36). Thus the elements of the polarizability tensor γ_i for the X, Y, Z system

$$\gamma_i = \begin{pmatrix} (\gamma_{xx})_i & (\gamma_{xy})_i & (\gamma_{xz})_i \\ (\gamma_{yx})_i & (\gamma_{yy})_i & (\gamma_{yz})_i \\ (\gamma_{zx})_i & (\gamma_{zy})_i & (\gamma_{zz})_i \end{pmatrix} \tag{II-175}$$

are given by

$$(\gamma_{xx})_i = (\gamma_1 - \gamma_2)\sin^2\theta\cos^2\phi + \gamma_2 \tag{II-176}$$

$$(\gamma_{yy})_i = (\gamma_1 - \gamma_2)\sin^2\theta\sin^2\phi + \gamma_2 \tag{II-177}$$

$$(\gamma_{zz})_i = \gamma_1\cos^2\theta + \gamma_2\sin^2\theta \tag{II-178}$$

$$(\gamma_{xy})_i = (\gamma_{yx})_i = (\gamma_1 - \gamma_2)\sin^2\theta\cos\phi\sin\phi \tag{II-179}$$

$$(\gamma_{xz})_i = (\gamma_{zx})_i = (\gamma_1 - \gamma_2)\sin\theta\cos\theta\cos\phi \tag{II-180}$$

$$(\gamma_{yz})_i = (\gamma_{zy})_i = (\gamma_1 - \gamma_2)\sin\theta\cos\theta\sin\phi. \tag{II-181}$$

Note that γ_i is a symmetric tensor in the X, Y, Z coordinate system. From Figure 4 the angles θ and ϕ are related

to the magnitude l_i of the end-to-end vector $\vec{l}_i$ by the following:

$$\sin\theta = \frac{(l_{xi}^2 + l_{yi}^2)^{\frac{1}{2}}}{l_i} \tag{II-182}$$

$$\cos\theta = \frac{l_{zi}}{l_i} \tag{II-183}$$

$$\sin\phi = \frac{l_{yi}}{(l_{xi}^2 + l_{yi}^2)^{1/2}} \tag{II-184}$$

$$\cos\phi = \frac{l_{xi}}{(l_{xi}^2 + l_{yi}^2)^{1/2}} \tag{II-185}$$

where l_{xi} , l_{yi} and l_{zi} are the X , Y and Z components of l_i . Combining equations (II-176) through (II-181) with equations (II-182) through (II-185) one obtains:

$$(\gamma_{xx})_i = (\gamma_1 - \gamma_2)_i \frac{l_{xi}^2}{l_i^2} + \gamma_{2i} \tag{II-186}$$

$$(\gamma_{yy})_i = (\gamma_1 - \gamma_2)_i \frac{l_{yi}^2}{l_i^2} + \gamma_{2i} \tag{II-187}$$

$$(\gamma_{zz})_i = \gamma_{1i} \frac{l_{zi}^2}{l_i^2} + \gamma_{2i} \frac{(l_{xi}^2 + l_{yi}^2)}{l_i^2} \tag{II-188}$$

$$(\gamma_{xy})_i = (\gamma_{yx})_i = (\gamma_1 - \gamma_2) \frac{l_{xi} l_{yi}}{l_i^2} \tag{II-189}$$

$$(\gamma_{xz})_i = (\gamma_{zx})_i = (\gamma_1 - \gamma_2) \frac{l_{xi} l_{zi}}{l_i^2} \tag{II-190}$$

$$(\gamma_{yz})_i = (\gamma_{zy})_i = (\gamma_1 - \gamma_2) \frac{l_{zi} l_{yi}}{l_i^2} . \tag{II-191}$$

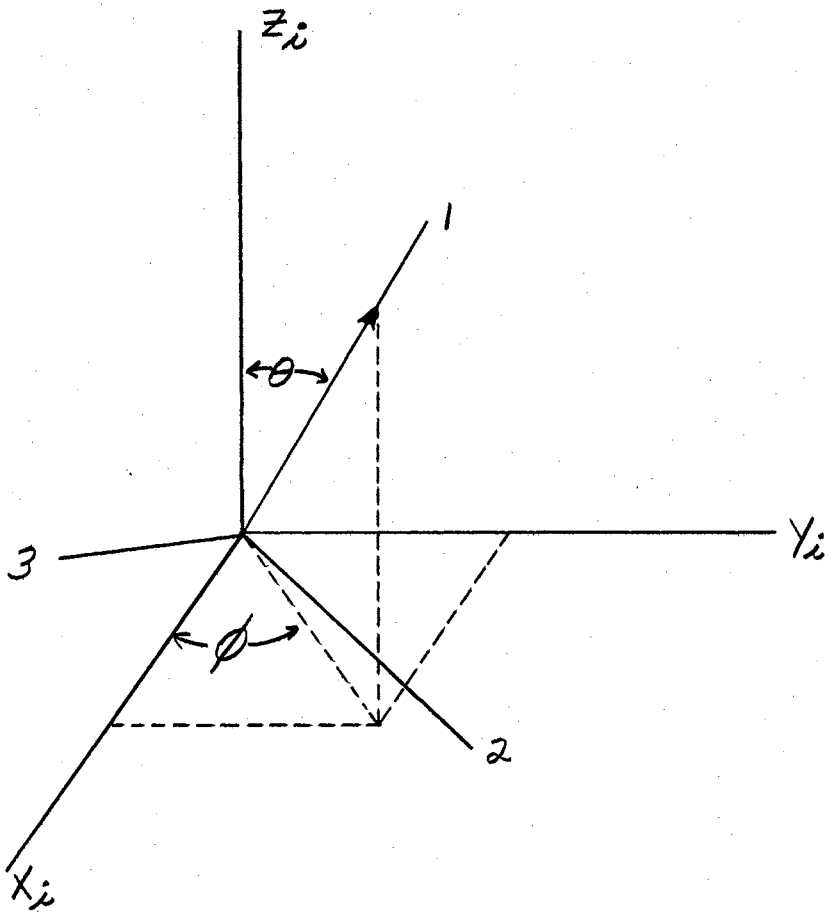

Figure 4. Coordinate Systems for the Specification of the Polarizability of a Zimm Subchain.

Introducing equations (II-173) and (II-174) into equations (II-186) and summing over all N subchains, one obtains

$$(\gamma_{xx})_{TOT.} = \sum_{i=1}^{N} (\gamma_{xx})_i = Np - q\sum_{i=1}^{N} l_i^2 + 3q\{X_0^2 + 2X_1^2 + 2X_2^2 + 2X_3^2 + \cdots + 2X_{N-1}^2 + X_N^2 - 2X_1X_0 - 2X_2X_1 - 2X_3X_2 - 2X_4X_3 - \cdots - 2X_NX_{N-1}\}. \quad \text{(II-192)}$$

The bracketed quantity $\{\ \}$ in equation (II-192) may be simplified by noting that from equations (II-83) and (II-87)

$$\{X_0^2 + 2X_1^2 + 2X_2^2 + \cdots + X_N^2 - 2X_1X_0 - 2X_2X_1 \cdots - 2X_NX_{N-1}\} = X^T \cdot A \cdot X. \quad \text{(II-193)}$$

Thus equation (II-192) becomes

$$(\gamma_{xx})_{TOT.} = Np - q\sum_{i=1}^{N} l_i^2 + 3q(X^T \cdot A \cdot X). \quad \text{(II-194)}$$

Similarly, the other elements of the polarizability tensor for the entire chain will be given by

$$(\gamma_{yy})_{TOT.} = Np - q\sum_{i=1}^{N} l_i^2 + 3q(Y^T \cdot A \cdot Y), \quad \text{(II-195)}$$

$$(\gamma_{zz})_{TOT.} = Np - q\sum_{i=1}^{N} l_i^2 + 3q(Z^T \cdot A \cdot Z), \quad \text{(II-196)}$$

$$(\gamma_{xy})_{TOT.} = (\gamma_{yz})_{TOT.} = 3q(X^T \cdot A \cdot Y) = 3q(Y^T \cdot A \cdot X), \quad \text{(II-197)}$$

$$(\gamma_{xz})_{TOT.} = (\gamma_{zx})_{TOT.} = 3q(X^T \cdot A \cdot Z) = 3q(Z^T \cdot A \cdot X), \quad \text{(II-198)}$$

$$(\gamma_{yz})_{TOT.} = (\gamma_{zy})_{TOT.} = 3q(Y^T \cdot A \cdot Z) = 3q(Z^T \cdot A \cdot Y). \quad \text{(II-199)}$$

Thus the average intrinsic polarizability tensor Γ for the entire chain expressed in the X, Y, Z coordinate system is given by

$$\Gamma = N(p - qb^2)I + 3q \begin{pmatrix} \langle X^T \cdot A \cdot X \rangle_{av.} & \langle X^T \cdot A \cdot Y \rangle_{av.} & \langle X^T \cdot A \cdot Z \rangle_{av.} \\ \langle Y^T \cdot A \cdot X \rangle_{av.} & \langle Y^T \cdot A \cdot Y \rangle_{av.} & \langle Y^T \cdot A \cdot Z \rangle_{av.} \\ \langle Z^T \cdot A \cdot X \rangle_{av.} & \langle Z^T \cdot A \cdot Y \rangle_{av.} & \langle Z^T \cdot A \cdot Z \rangle_{av.} \end{pmatrix} \quad \text{(II-200)}$$

where I is the unity matrix. Only the second term of equation (II-200) is of importance here since this term represents the anisotropic part of Γ. Assuming that the light ray incident upon the medium is travelling along the Y axis, the second row and column of Γ may be omitted to obtain the trace of the tensor on the X, Z plane and thus the intersection of the polarizability ellipsoid and the X, Z plane (4). Thus consider the tensor Γ' obtained from the anisotropic part of (II-200) by setting the second row and column equal to zero.

$$\Gamma' = 3q \begin{pmatrix} \langle X^T \cdot A \cdot X \rangle_{av.} & \langle X^T \cdot A \cdot Z \rangle_{av.} \\ \langle Z^T \cdot A \cdot X \rangle_{av.} & \langle Z^T \cdot A \cdot Z \rangle_{av.} \end{pmatrix} \quad \text{(II-201)}$$

Since Γ' is a symmetric tensor, it can be diagonalized by choosing a new coordinate system rotated about the Y axis by an angle χ. For a tensor A given by

$$A = \begin{vmatrix} A_1 & 0 \\ 0 & A_2 \end{vmatrix} \tag{II-202}$$

in the principal axis coordinate system 1, 2, the rotation of the 1, 2 coordinate system about the Y axis by an angle χ yields tensor elements given by

$$A = \begin{vmatrix} a_{11} & a_{12} \\ a_{21} & a_{22} \end{vmatrix} = U^T A(1,2)\, U$$

$$= \begin{vmatrix} A_1\cos^2\chi + A_2\sin^2\chi & (A_1 - A_2)\sin\chi\cos\chi \\ (A_1 - A_2)\sin\chi\cos\chi & A_1\sin^2\chi + A_2\cos^2\chi \end{vmatrix} \tag{II-203}$$

where U is a rotator matrix (18).

$$U = \begin{vmatrix} \cos\chi & \sin\chi \\ -\sin\chi & \cos\chi \end{vmatrix} \tag{II-204}$$

Thus from equation (II-203) it is possible to evaluate χ and the principal axis tensor elements A_1 and A_2 from the X, Z coordinate system tensor elements. Thus from equation (II-203) it is seen that

$$\frac{2a_{21}}{a_{11} - a_{22}} = \frac{2\cos\chi\sin\chi}{\cos^2\chi - \sin^2\chi} = \tan 2\chi \tag{II-205}$$

and

$$\left[(a_{11} - a_{22})^2 + 4a_{21}^2\right]^{\frac{1}{2}} = \left\{\left[(\cos 2\chi)(A_1 - A_2)\right]^2 + (A_1 - A_2)^2\sin^2 2\chi\right\}^{\frac{1}{2}} \tag{II-206}$$

$$= \left[(A_1 - A_2)^2\right]^{\frac{1}{2}} = |A_1 - A_2|.$$

Equation (II-206) may be further simplified by the substitution of $2a_{12}$ from equation (II-205) in (II-206). Thus

$$|A_1 - A_2| = \pm 2a_{21}\left[\cot^2(2\chi) + 1\right]^{\frac{1}{2}}. \qquad \text{(II-207)}$$

Applying equation (II-207) to the polarizability tensor Γ' of equation (II-201) one obtains for the magnitude of the difference of the polarizabilities $\Delta\Gamma'$ along the principal axes the following:

$$|\Delta\Gamma'| = \pm 6q\langle Z^T \cdot A \cdot X\rangle_{av}\left[\cot^2(2\chi) + 1\right]^{\frac{1}{2}}. \qquad \text{(II-208)}$$

From equation (II-152), (II-153), (II-154), (II-155), and (II-156),

$$\langle Z^T \cdot A \cdot X\rangle_{av} = \left\langle Z^T \cdot \left(\frac{b^2}{3kT}\right) F_X \right\rangle_{av} \qquad \text{(II-209)}$$

$$= \frac{b^2}{3kT}\langle Z^T \cdot F_X\rangle_{av} = \frac{b^2}{3kT}\left\langle \sum_{j=0}^{N} Z_j F_{Xj}\right\rangle_{av}.$$

Or, introducing equation (II-151),

$$\langle Z^T \cdot A \cdot X\rangle_{av} = \frac{b^2}{3kT} \cdot \frac{M\eta_s g[\eta]}{N_a}. \qquad \text{(II-210)}$$

Thus from equations (II-208) and (II-210) the difference $\Delta\Gamma'$ of the intrinsic polarizabilities along the principal axes is given by

$$|\Delta\Gamma'| = \pm \frac{2qb^2}{kT} \frac{M\eta_s[\eta]g}{N_a}\left[\cot^2(2\chi) + 1\right]^{\frac{1}{2}} \qquad \text{(II-211)}$$

where χ is the so-called extinction angle. From equation (II-17), the birefringence Δn will be proportional to the number of chains per unit volume times $|\Delta \Gamma'|$, assuming that the number of chains is sufficiently small to avoid optical interaction between the chains. Thus since the number of chains per unit volume n_c will be given by

$$n_c = \frac{c N_a}{M}, \tag{II-212}$$

the birefringence due to the intrinsic anisotropy of the subchains will be given by

$$\frac{\Delta n}{g} = \pm g'\left(\frac{b^2}{kT}\right)[\eta]\eta_s c\left[\cot^2(2\chi)+1\right]^{\frac{1}{2}} \tag{II-213}$$

where c is the solution concentration in grams of solute per unit volume of solution. g' is an optical constant characteristic of the chain-solvent system given by

$$\begin{aligned} g' &= \frac{4\pi}{9}\cdot\frac{(n_s^2+2)^2}{n_s}\cdot g \\ &= \frac{4\pi}{45}\cdot\frac{(n_s^2+2)^2}{n_s}\cdot\frac{(\alpha_1-\alpha_2)}{b^2} \end{aligned} \tag{II-214}$$

where n_s is the solvent index of refraction [see equations (II-17), (II-34), (II-173), and (II-174)]. For sufficiently small velocity gradients, the factor $\left[\cot^2(2\chi)+1\right]^{\frac{1}{2}}$ of equation (II-213) is essentially equal to 1. Thus, combining equations (II-213) and (II-161) the oscillatory flow birefringence will be given by

$$\frac{\Delta n}{g} = \pm g'\left(\frac{N_a}{6M}\right)\left(\frac{c}{kT}\right) b^4 \mathcal{J} \sum_{p=1}^{N} \frac{1}{\lambda_p(1+i\omega\tau_p)} , \qquad \text{(II-215)}$$

assuming that g is sufficiently small that

$$\left[\cot^2(2\chi)+1\right]^{\frac{1}{2}} \simeq 1 , \qquad \text{(II-216)}$$

where λ_p and τ_p are given by equations (II-160), (II-168), and (II-169) and ω is the radian frequency of the velocity gradient in the solution. It should be noted that equation (II-213) differs from the erroneous expression contained in the original paper by Zimm, (103), but does agree with the zero frequency birefringence expressions given by Copic for the elastic dumbbell model and by Tsvetkov for the Zimm model (19, 98).

3. Analysis of the Frequency and Temperature Dependence of the Viscoelasticity and Flow Birefringence Expressions Given by the Zimm Theory

The viscoelasticity and oscillatory flow birefringence expressions of equations (II-161) and (II-215) involve the factors c, b^2, λ_p, τ_p, N, $\mathcal{J}$ and g'. The analysis of the polymer molecule in terms of the freely flexing chain as given by Kuhn and Kuhn (49, 50, 51, 55) indicates that b^2 should be approximately independent of temperature. The Zimm model of the polymer assumes that N is independent of temperature and frequency while g' is assumed to be independent of frequency. From equation (II-214) the temperature dependence of g' will probably be governed by the

temperature dependence of the solvent index of refraction. Thus for many solute-solvent combinations q' will be essentially independent of temperature. Similarly, the concentration c will be independent of frequency and only weakly dependent on temperature for most solutions. From equation (II-66) $\mathcal{F}$ is assumed to be frequency independent while from equations (II-66) and (II-67) a reasonable assumption concerning the temperature dependence of $\mathcal{F}$ would appear to be that $\mathcal{F}$ follows the temperature dependence of η_s. That is,

$$\frac{\mathcal{F}}{\mathcal{F}_r} \simeq \frac{\eta_s}{\eta_{sr}} \qquad \text{(II-217)}$$

where the subscript r is used to denote quantities at a reference temperature T_r. Nonsubscripted quantities denote values at any other temperature T. From equations (II-168), (II-169), (II-170) and Table I the λ_p are independent of both frequency and temperature, in view of the constancy of b^2 and N and the assumed temperature dependence of $\mathcal{F}$ given by equation (II-217). From equation (II-160) the factor τ_p is independent of frequency but dependent on temperature. The ratio (τ_p/τ_1) is independent of temperature, however, since from equations (II-160), (II-168), (II-169) and Table I

$$\frac{\tau_p}{\tau_1} = \frac{\lambda_1}{\lambda_p} \qquad \text{(II-218)}$$

so that

$$\frac{\tau_p}{\tau_1} = \frac{1}{p^2}, \text{ for } h \ll 1, \qquad \text{(II-219)}$$

and

$$\frac{\tau_p}{\tau_1} = \frac{4.04}{\lambda'_p}, \text{ for } h \gg 1. \qquad \text{(II-220)}$$

Equations (II-161) and (II-215) may be written in a more convenient form by defining a temperature dependent quantity a_T by

$$a_T \equiv \frac{\tau_p}{\tau_{pr}} \qquad \text{(II-221)}$$

where τ_p is the value at some temperature T and τ_{pr} is the value at the reference temperature T_r. Thus from equations (II-160) and (II-218)

$$a_T \equiv \frac{\tau_p}{\tau_{pr}} = \frac{\mathcal{J} T_r}{\mathcal{J}_r T} . \qquad \text{(II-222)}$$

Or, if the assumption concerning the temperature dependence of $\mathcal{J}$ given by equation (II-217) is valid,

$$a_T \simeq \left(\frac{T_r}{T}\right)\left(\frac{\eta_s}{\eta_{sr}}\right). \qquad \text{(II-223)}$$

The intrinsic viscosity $[\eta]$ of equation (II-161) may be used to obtain the quantity $(\eta^* - \eta_s)$ for dilute solutions where $c \to 0$, where

$$\eta^* = \eta' - i\,\eta'' = \eta_M e^{-i\phi_\eta} \qquad \text{(II-224)}$$

denotes the complex viscosity coefficient (26). From equations (II-151) and (II-161)

$$\eta^* - \eta_s \Big|_{c\to 0} = \frac{c N_a b^2 \mathcal{J}}{6M} \sum_{p=1}^{N} \frac{1}{\lambda_p (1 + i\omega\tau_p)} \quad \text{(II-225)}$$

Inserting equation (II-218) into (II-220), the frequency dependence of the viscosity is given by

$$\eta^* - \eta_s = \frac{c N_a}{6M} \cdot \frac{b^2 \mathcal{J}}{\lambda_1} \sum_{p=1}^{N} \frac{(\tau_p/\tau_1)}{[1 + i\omega\tau_1(\tau_p/\tau_1)]} \quad \text{(II-226)}$$

From equation (II-226), the zero frequency viscosity will be given by

$$\eta^* - \eta_s \Big|_{\omega\to 0} = \eta_0 - \eta_s = \frac{c N_a}{6M} \cdot \frac{b^2 \mathcal{J}}{\lambda_1} \sum_{p=1}^{N} (\tau_p/\tau_1) \quad \text{(II-227)}$$

Computation of the theoretical variation of viscosity with frequency is simplified by considering the ratio $\dfrac{(\eta^* - \eta_s)}{(\eta_0 - \eta_s)}$. Thus from equations (II-226) and (II-227)

$$\frac{(\eta^* - \eta_s)}{(\eta_0 - \eta_s)} = \frac{\sum_{p=1}^{N} \dfrac{(\tau_p/\tau_1)}{[1 + i\omega\tau_1(\tau_p/\tau_1)}}{\sum_{p=1}^{N} (\tau_p/\tau_1)} \quad \text{(II-228)}$$

so that $\dfrac{(\eta^* - \eta_s)}{(\eta_0 - \eta_s)}$ may be computed as a function of $\omega\tau_1$, using values of (τ_p/τ_1) from equations (II-219) and (II-220).

The magnitude $\left|\frac{(\eta^* - \eta_s)}{(\eta_o - \eta_s)}\right|$ and the angle ϕ'_η defined by

$$\phi'_\eta = \tan^{-1}\frac{\eta''}{(\eta' - \eta_s)} \qquad \text{(II-229)}$$

may be obtained from equations (II-224) and (II-228). One obtains:

$$\left|\frac{(\eta^* - \eta_s)}{(\eta_o - \eta_s)}\right| = \frac{\left\{\left[\sum_{p=1}^{N}\frac{(\tau_p/\tau_1)}{[1+\omega^2\tau^2(\tau_p/\tau_1)^2]}\right]^2 + \left[\omega\tau_1\sum_{p=1}^{N}\frac{(\tau_p/\tau_1)^2}{[1+\omega^2\tau_1^2(\tau_p/\tau_1)^2]}\right]^2\right\}^{\frac{1}{2}}}{\sum_{p=1}^{N}(\tau_p/\tau_1)} \qquad \text{(II-230)}$$

and,

$$\phi'_\eta = \tan^{-1}\frac{\omega\tau_1\sum_{p=1}^{N}\frac{(\tau_p/\tau_1)^2}{[1+\omega^2\tau_1^2(\tau_p/\tau_1)^2]}}{\sum_{p=1}^{N}\frac{(\tau_p/\tau_1)}{[1+\omega^2\tau_1^2(\tau_p/\tau_1)^2]}} . \qquad \text{(II-231)}$$

The temperature dependence of the viscosity may be obtained from equations (II-226), (II-227) and (II-222). It is convenient to form the ratio of $(\eta^* - \eta_s)$ at temperature T and $(\eta_o - \eta_s)_r$ at temperature T_r. One obtains:

$$\frac{(\eta^* - \eta_s)}{(\eta_o - \eta_s)_r} = \left(\frac{c}{c_r}\right)\left(\frac{T}{T_r}\right)a_T\frac{\sum_{p=1}^{N}\frac{(\tau_p/\tau_1)}{[1+i\omega a_T\tau_{1r}(\tau_p/\tau_1)]}}{\sum_{p=1}^{N}(\tau_p/\tau_1)} . \qquad \text{(II-232)}$$

The zero frequency temperature dependence of the viscosity is obtained from equation (II-232) as

$$\frac{(\eta_o-\eta_s)}{(\eta_o-\eta_s)_r} = \left(\frac{c}{c_r}\right)\left(\frac{T}{T_r}\right)a_T \qquad \text{(II-233)}$$

so then for a solution for which the Zimm theory is applicable,

$$\frac{(\eta_o-\eta_s)}{(\eta_o-\eta_s)_r}\cdot\left(\frac{T_r}{T}\right)\cdot\left(\frac{c}{c_r}\right) = a_T \qquad \text{(II-234)}$$

and

$$\frac{\mathcal{J}}{\mathcal{J}_r} = \frac{(\eta_o-\eta_s)}{(\eta_o-\eta_s)_r}\cdot\left(\frac{c_r}{c}\right) \qquad \text{(II-235)}$$

from equation (II-222). Equation (II-232) may be written in terms of $\left|\frac{(\eta^*-\eta_s)}{(\eta_o-\eta_s)_r}\right|$ and ϕ_η'. Thus

$$\left|\frac{(\eta^*-\eta_s)}{(\eta_o-\eta_s)_r}\right| = \left(\frac{c}{c_r}\right)\left(\frac{T}{T_r}\right)a_T \cdot \frac{\left\{\left[\sum_{p=1}^{N}\frac{(\tau_p/\tau_1)}{[1+\omega^2 a_T^2\tau_{1r}^2(\tau_p/\tau_1)^2]}\right]^2+\left[\omega a_T\tau_{1r}\sum_{p=1}^{N}\frac{(\tau_p/\tau_1)^2}{[1+\omega^2 a_T^2\tau_{1r}^2(\tau_p/\tau_1)^2]}\right]^2\right\}^{1/2}}{\sum_{p=1}^{N}(\tau_p/\tau_1)} \qquad \text{(II-236)}$$

and

$$\phi_\eta' = \tan^{-1} \frac{\omega a_T \tau_{1r} \sum_{p=1}^{N} \frac{(\tau_p/\tau_1)^2}{[1+\omega^2 a_T^2 \tau_{1r}^2 (\tau_p/\tau_1)^2}}{\sum_{p=1}^{N} \frac{(\tau_p/\tau_1)}{[1+\omega^2 a_T^2 \tau_{1r}^2 (\tau_p/\tau_1)^2]}} \quad \text{(II-237)}$$

As is seen from equations (II-236) and (II-237), plotting $\left|\frac{(\eta^*-\eta_s)}{(\eta_o-\eta_s)_r}\right| \cdot \left(\frac{C_r T_r}{C T}\right)$ and ϕ_η' versus ωa_T yields universal curves to which any $\left|\frac{(\eta^*-\eta_s)}{(\eta_o-\eta_s)}\right|$ or ϕ_η' versus frequency f curve may be fitted for a given temperature, provided that a_T, (C_r/C), (T_r/T) and ϕ_η' are known. Or, given a sufficient set of $\left|\frac{(\eta^*-\eta_s)}{(\eta_o-\eta_s)}\right|$ and ϕ_η' curves for various temperatures, the "universal curves" of equation (II-236) and (II-237) may be constructed. This procedure is the basis for the reduced parameter method of data handling developed by Ferry (26). Note that the "universal curves" obtained as above are the frequency response curves given by equations (II-230) and (II-231) for the temperature T_r. Thus curves of $\left|\frac{(\eta^*-\eta_s)}{(\eta_o-\eta_s)}\right|$ and ϕ_η' versus f at various T can be superimposed to obtain the $\left|\frac{(\eta^*-\eta_s)}{(\eta_o-\eta_s)}\right|$ and ϕ_η' versus f curves for $T=T_r$.

The theoretical frequency and temperature dependence of the oscillatory flow birefringence may be examined conveniently in terms of a complex oscillatory flow birefringence coefficient S^* defined as

$$S^* = S_M e^{i\theta} = \pm \frac{\Delta n}{g} \quad \text{(II-238)}$$

where the sign is selected in accordance with the specified coordinate system (90, 92). From equations (II-215), (II-238) and (II-218)

is given as

$$S^* = \pm q' \left(\frac{Na}{6M}\right)\left(\frac{c}{kT}\right)\left(\frac{b^4 J}{\lambda_1}\right) \sum_{p=1}^{N} \frac{(\tau_p/\tau_1)}{[1 + i\omega\tau_1(\tau_p/\tau_1)]} \qquad \text{(II-239)}$$

for dilute solutions $(c \to 0)$ subjected to velocity gradients sufficiently small that equation (II-216) is satisfied. The low frequency limit for S^* is defined as

$$S^*\Big|_{\omega \to 0} = S_0 = S_{M0} e^{i\theta_0} \qquad \text{(II-240)}$$

so that as ω approaches zero S_0 is given by

$$S_0 = \pm q' \left(\frac{Na}{6M}\right)\left(\frac{c}{kT}\right)\left(\frac{b^4 J}{\lambda_1}\right) \sum_{p=1}^{N} (\tau_p/\tau_1) \qquad \text{(II-241)}$$

from equation (II-239). Thus the limiting angle θ_0 is either 0 degrees or 180 degrees depending on the sign of the optical factor and the coordinate system specified. It is convenient for purposes of computation of the theoretical frequency dependence of the flow birefringence to form the ratio (S^*/S_0) from equations (II-239) and (II-241). Thus

$$\frac{S^*}{S_0} = \frac{\sum_{p=1}^{N} \frac{(\tau_p/\tau_1)}{[1 + i\omega\tau_1(\tau_p/\tau_1)]}}{\sum_{p=1}^{N} (\tau_p/\tau_1)} . \qquad \text{(II-242)}$$

$\frac{S_M}{S_{MO}}$ and $(\theta - \theta_o)$ may be evaluated from equations (II-238), (II-241) and (II-242). One obtains:

$$\frac{S_M}{S_{MO}} = \frac{\left\{\left[\sum_{p=1}^{N} \frac{(\tau_p/\tau_1)}{[1+\omega^2\tau_1^2(\tau_p/\tau_1)^2]}\right]^2 + \left[\omega\tau_1 \sum_{p=1}^{N} \frac{(\tau_p/\tau_1)^2}{[1+\omega^2\tau_1^2(\tau_p/\tau_1)^2]}\right]^2\right\}^{\frac{1}{2}}}{\sum_{p=1}^{N} (\tau_p/\tau_1)} \qquad \text{(II-243)}$$

and

$$(\theta - \theta_o) = \tan^{-1} \frac{-\omega\tau_1 \sum_{p=1}^{N} \frac{(\tau_p/\tau_1)^2}{[1+\omega^2\tau_1^2(\tau_p/\tau_1)^2]}}{\sum_{p=1}^{N} \frac{(\tau_p/\tau_1)}{[1+\omega^2\tau_1^2(\tau_p/\tau_1)^2]}} \qquad \text{(II-244)}$$

Calculations of (S_M/S_{MO}) and $(\theta - \theta_o)$ versus $\omega\tau_1$ were performed on a digital computer and are shown in Figures 5 and 6 for free-draining molecules and in Figures 7 and 8 for non-free-draining molecules, using values of N of 1, 3, 10, 20, 30, 40, 50, 100 and 400. The values of (τ_p/τ_1) used for the computations were obtained from equations (II-219), (II-220) and (II-170) and Table I.

The temperature dependence of the oscillatory flow birefringence is conveniently examined by introducing the quantity a_T given by equation (II-222). Thus from equations (II-239) and (II-241)

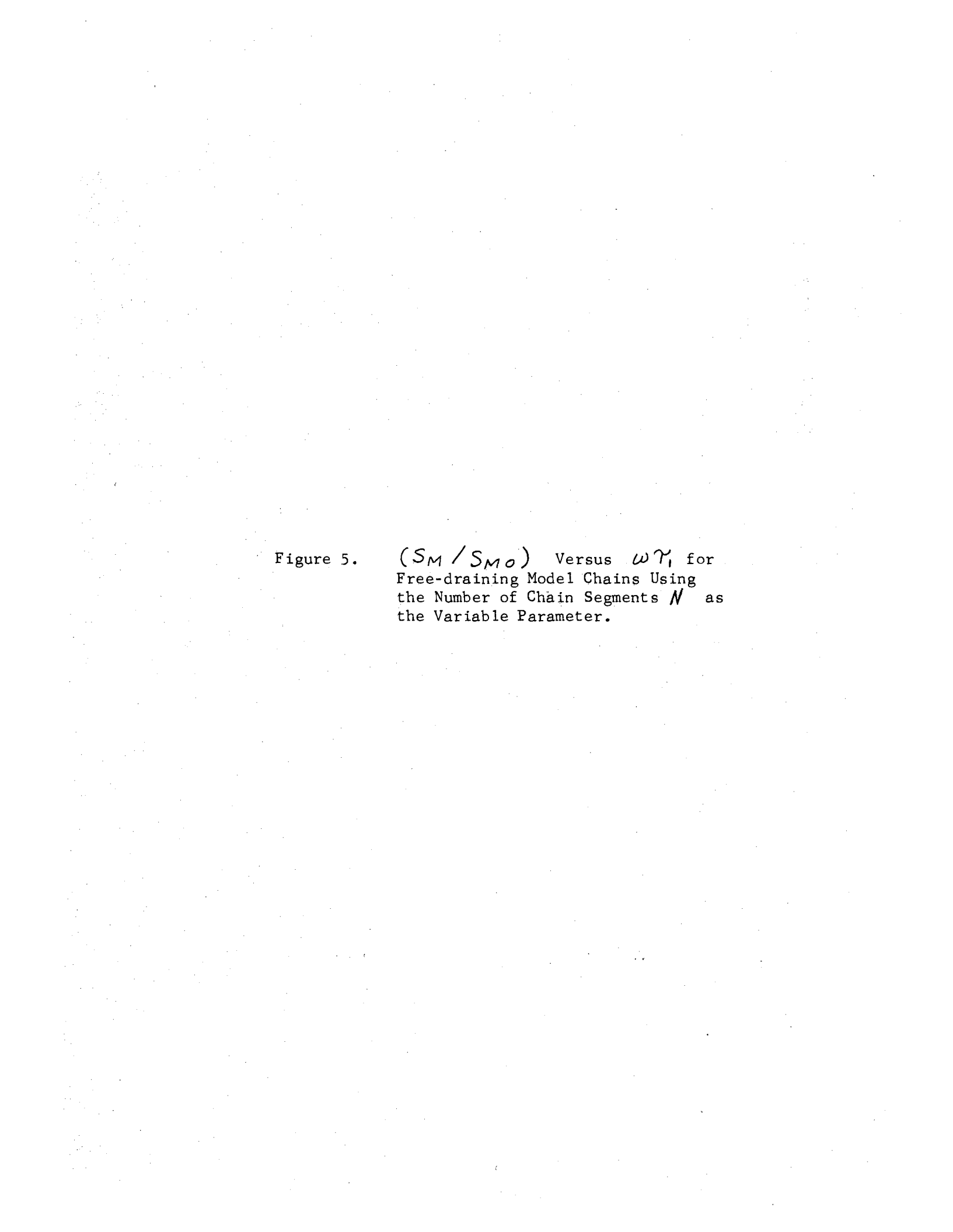

Figure 5. (S_M / S_{MO}) Versus $\omega\tau_1$ for Free-draining Model Chains Using the Number of Chain Segments N as the Variable Parameter.

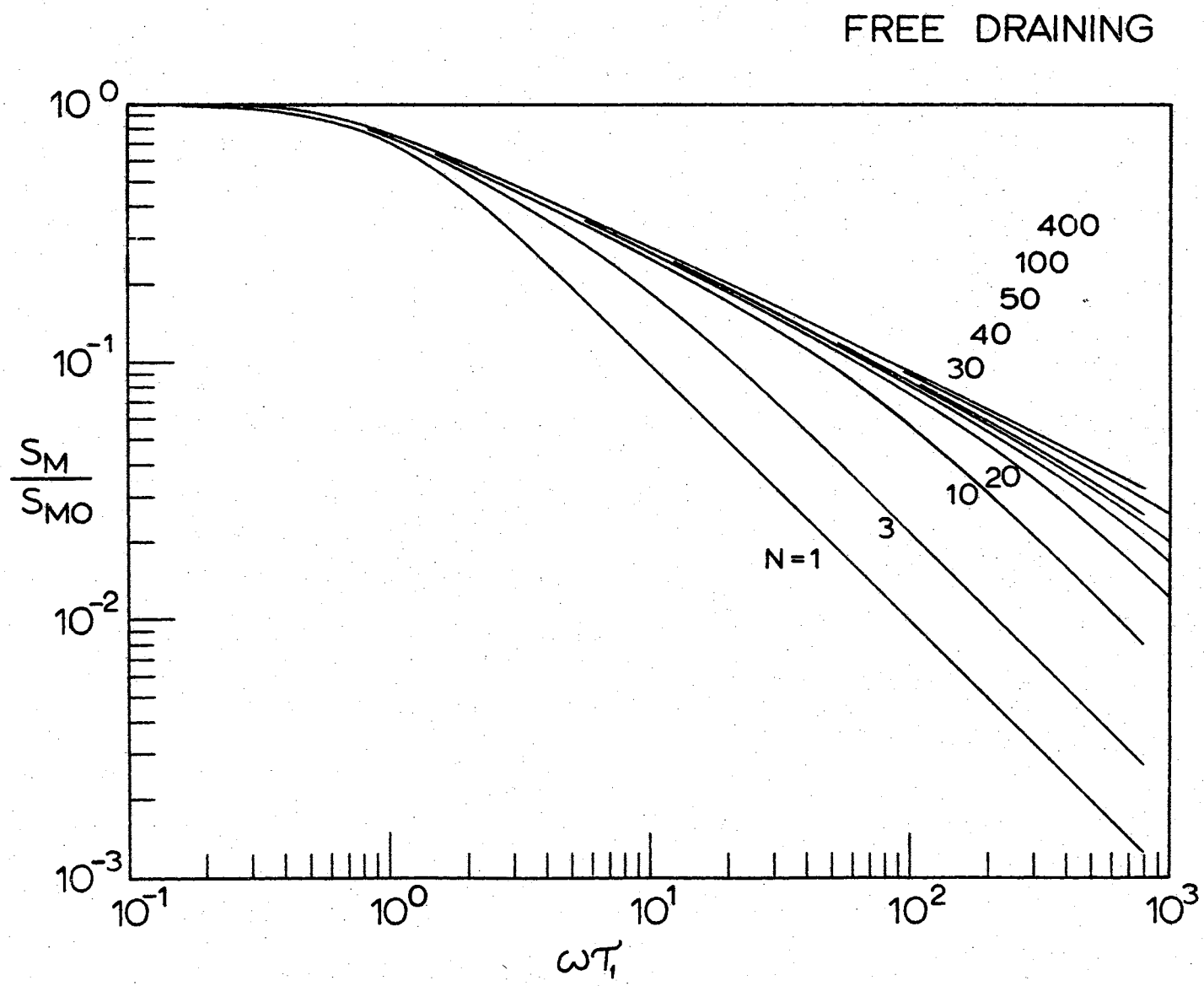
FREE DRAINING
10^0
10^{-1}
10^{-2}
10^{-3}
$\frac{S_M}{S_{MO}}$
10^{-1}
10^0
10^1
10^2
10^3
$\omega\tau_1$
400
100
50
40
30
20
10
3
N=1

Figure 6. $(\theta - \theta_o)$ Versus $\omega\tau_1$ for Free-draining Model Chains Using the Number of Chain Segments N as the Variable Parameter.

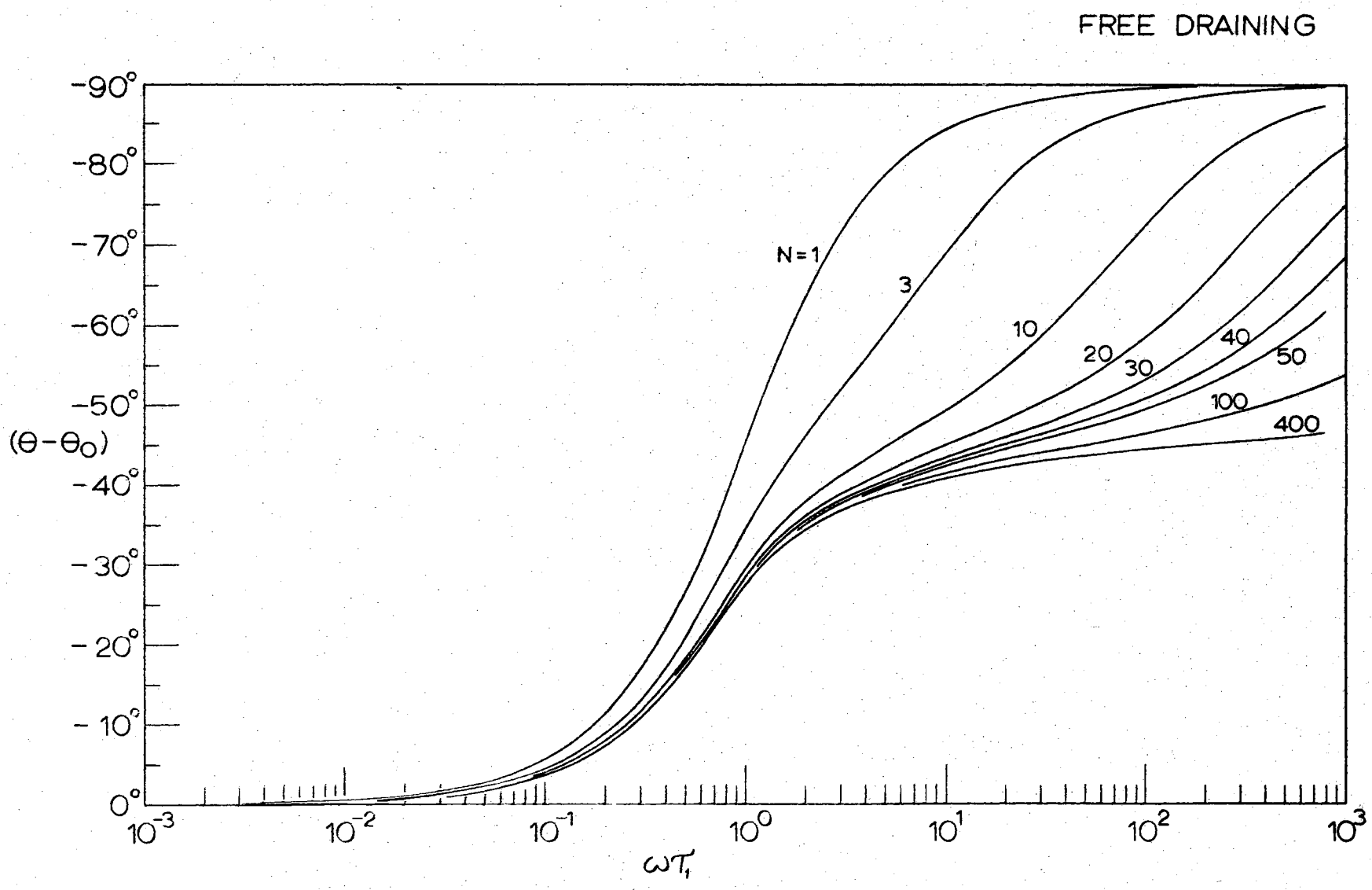
FREE DRAINING
-90°
-80°
-70°
-60°
-50°
-40°
-30°
-20°
-10°
0°
(θ-θo)
N=1
3
10
20
30
40
50
100
400
10^-3
10^-2
10^-1
10^0
10^1
10^2
10^3
ωT1

Figure 7. (S_M/S_{MO}) Versus $\omega\tau_1$ for Non-free-draining Model Chains, Using the Number of Chain Segments N as the Variable Parameter.

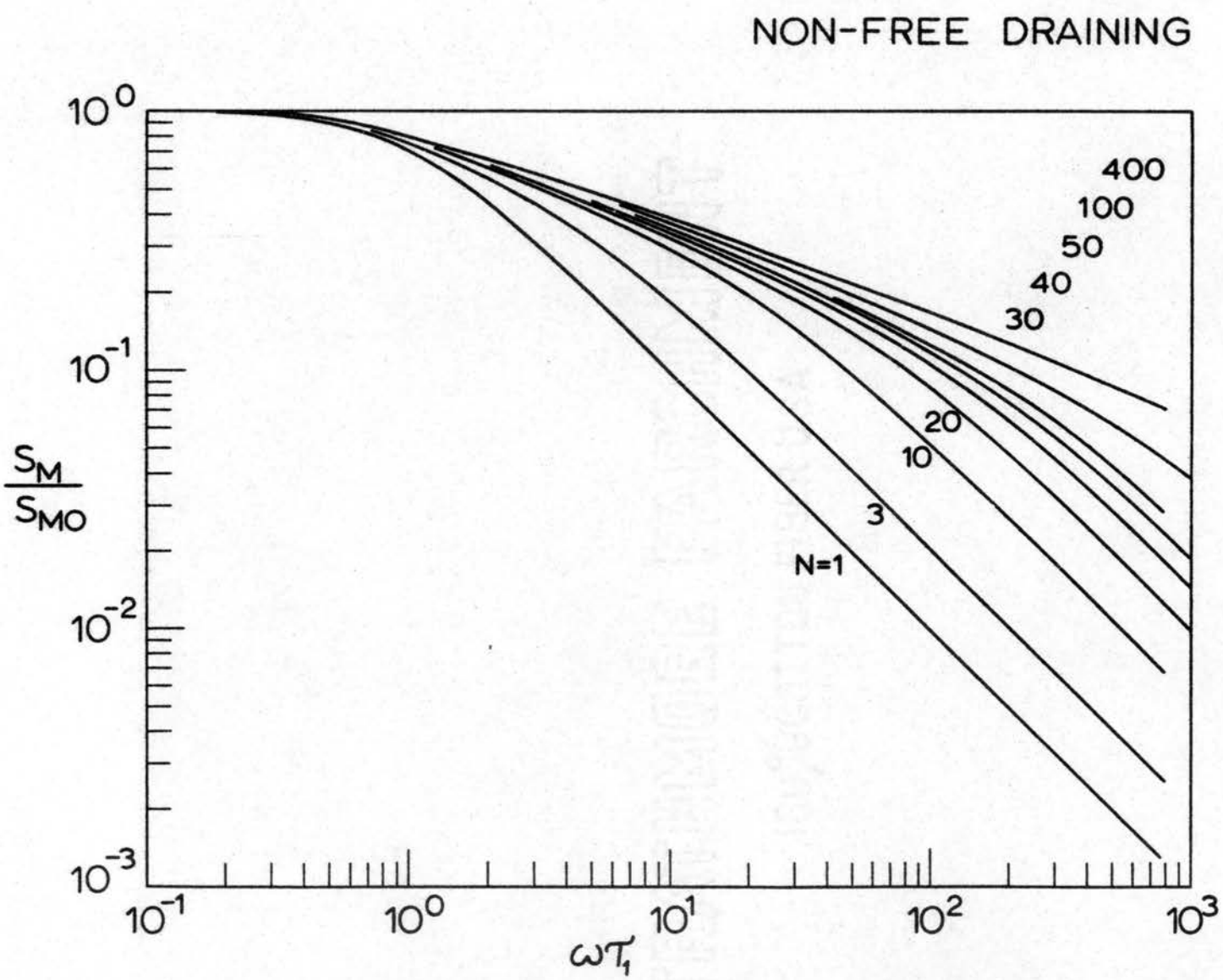
NON-FREE DRAINING
10^0
10^{-1}
10^{-2}
10^{-3}
$\frac{S_M}{S_{MO}}$
400
100
50
40
30
20
10
3
N=1
10^{-1}
10^0
10^1
10^2
10^3
$\omega\tau_1$

Figure 8. $(\theta - \theta_o)$ Versus $\omega\tau_1$ for Non-free-draining Model Chains, Using the Number of Chain Segments N as the Variable Parameter.

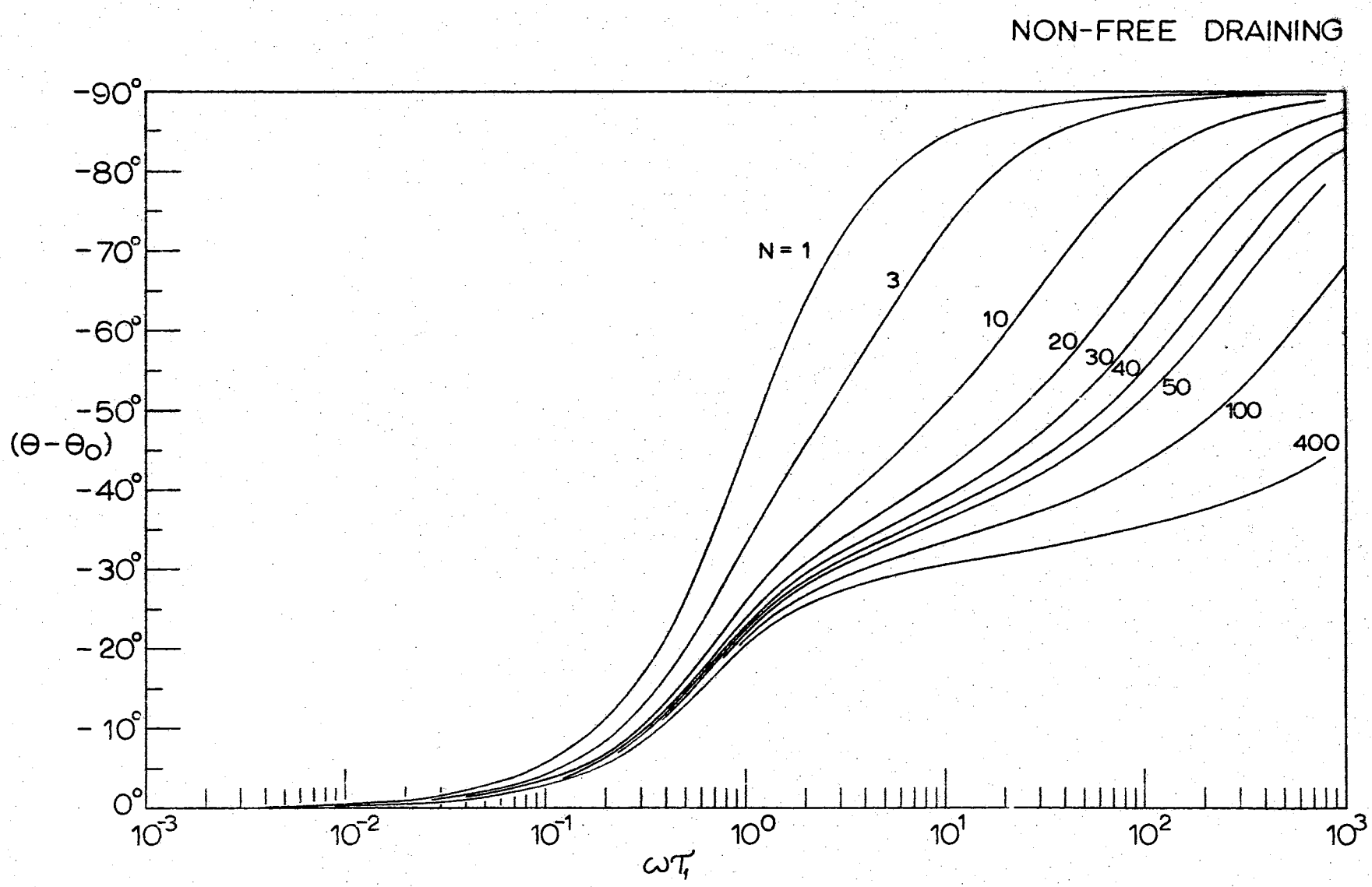
NON-FREE DRAINING
-90°
-80°
-70°
-60°
-50°
-40°
-30°
-20°
-10°
0°
(θ - θ0)
N = 1
3
10
20
30
40
50
100
400
10^-3
10^-2
10^-1
10^0
10^1
10^2
10^3
ωτ1

$$\frac{S^*}{S_{or}} = \left(\frac{q'}{q'_r}\right)\left(\frac{c}{c_r}\right) a_T \frac{\sum_{p=1}^{N} \frac{(\tau_p/\tau_1)}{[1 + i\omega a_T \tau_{1r}(\tau_p/\tau_1)]}}{\sum_{p=1}^{N} (\tau_p/\tau_1)} \quad \text{(II-245)}$$

Thus from equations (II-238) and (II-245) (S_M/S_{Mor}) and $(\theta - \theta_{or})$ are given by

$$\frac{S_M}{S_{Mor}} = \left(\frac{q'}{q'_r}\right)\left(\frac{c}{c_r}\right) a_T \cdot \left\{ \frac{\left[\sum_{p=1}^{N} \frac{(\tau_p/\tau_1)}{[1 + \omega^2 a_T^2 \tau_{1r}^2 (\tau_p/\tau_1)^2]}\right]^2 + \left[\omega a_T \tau_{1r} \sum_{p=1}^{N} \frac{(\tau_p/\tau_1)^2}{[1 + \omega^2 a_T^2 \tau_{1r}^2 (\tau_p/\tau_1)^2]}\right]^2}{\sum_{p=1}^{N} (\tau_p/\tau_1)} \right\}^{\frac{1}{2}} \quad \text{(II-246)}$$

and

$$(\theta - \theta_{or}) = \tan^{-1} \frac{-\omega a_T \tau_{1r} \sum_{p=1}^{N} \frac{(\tau_p/\tau_1)^2}{[1 + \omega^2 a_T^2 \tau_{1r}^2 (\tau_p/\tau_1)^2}}{\sum_{p=1}^{N} \frac{(\tau_p/\tau_1)}{[1 + \omega^2 a_T^2 \tau_{1r}^2 (\tau_p/\tau_1)^2]}} \quad \text{(II-247)}$$

If the frequency of the velocity gradient is denoted by f, then it is seen that by plotting $\left(\frac{S_M}{S_{Mor}}\right)\left(\frac{q'}{q'_r}\right)\left(\frac{1}{a_T}\right)$ versus $f a_T$ and

$(\theta - \theta_{or})$ versus $f a_T$ one obtains a superposition of various $\left(\frac{S_M}{S_{MO}}\right)$ versus f and $(\theta - \theta_o)$ versus f curves obtained at various temperatures, similar to the superposition obtained for the viscosity from equations (II-236) and (II-237). The resultant curve obtained by the superposition of the various $\left(\frac{S_M}{S_{MO}}\right)$ and $(\theta - \theta_o)$ curves is identical to that obtained from equations (II-243) and (II-244) for $T = T_r$. Thus by plotting the quantities noted above the frequency dependence curve for the oscillatory flow birefringence corresponding to $T = T_r$ may be obtained by a superposition of frequency response curves taken at several temperatures. Experimentally this reduction procedure is quite valuable if it is applicable to the material being studied, since if a_T varies rapidly with temperature, one can obtain the frequency dependence curve for a wide range in ωa_T without having to cover a wide range in ω .

An important result of equation (II-245) is obtained by setting $\omega = 0$. Thus,

$$\frac{S_o}{S_{or}} = \left(\frac{q'}{q'_r}\right)\left(\frac{c}{c_r}\right) a_T \qquad \text{(II-248)}$$

so that the factor a_T may be obtained from zero frequency birefringence values. For materials for which q' and c are essentially independent of temperature, a_T can be obtained from the zero frequency birefringence values only.

The close relationship between the complex viscosity and the oscillatory flow birefringence predicted by the Zimm theory can be seen by a comparison of equations (II-228) and (II-242), (II-230) and

(II-243) and (II-231) and (II-244). One obtains

$$\frac{S^*}{S_0} = \frac{(\eta^* - \eta_s)}{(\eta_0 - \eta_s)} \qquad \text{(II-249)}$$

so that

$$\frac{S_M}{S_{M0}} = \left| \frac{(\eta^* - \eta_s)}{(\eta_0 - \eta_s)} \right| \qquad \text{(II-250)}$$

and

$$\tan(\theta - \theta_0) = -\tan \phi_\eta' \,. \qquad \text{(II-251)}$$

Thus Figures 5, 6, 7, and 8 also describe the frequency dependence of the viscosity as is seen from equations (II-250) and (II-251). From equations (II-232) and (II-245) the temperature dependence of the viscosity and the birefringence are related by

$$\frac{S^*}{S_{or}} = \frac{q_r'}{q'} \cdot \frac{T_r}{T} \cdot \frac{(\eta^* - \eta_s)}{(\eta_0 - \eta_s)} \,. \qquad \text{(II-252)}$$

4. <u>The Flow Birefringence Exhibited by a Simple Multiple Component System</u>

Assume that an incident light ray is propagating along the Y axis so that the anisotropic part of the polarizability for a single component system is given by a symmetric polarizability tensor of the form of equation (II-201). The relation between the components of such a tensor expressed in the X , Y , Z coordinate system and the components of the same tensor expressed in the principal axis

system is given by equations (II-202) through (II-207). Similar symmetric polarizability tensors are obtained for rigid particles (4). Consider two such symmetric polarizability tensors A and B expressed in the X , Y , Z coordinate system as

$$A = \begin{vmatrix} a_{11} & a_{12} \\ a_{21} & a_{22} \end{vmatrix} \tag{II-253}$$

and

$$B = \begin{vmatrix} b_{11} & b_{12} \\ b_{21} & b_{22} \end{vmatrix} , \tag{II-254}$$

the elements of which can be related to their principal axis system elements by equations (II-202), (II-203) and (II-204). Let the rotation angle (extinction angles for flow birefringence) between the X or Z axis and the corresponding principal axis be denoted by χ_A for tensor A and χ_B for tensor B . If two components giving rise to such polarizability tensors are present in a solution, and the components are sufficiently isolated from each other that neither polarizability tensor is modified by the presence of the other component, the polarizability tensor C for the system will be given by the sum of the tensors for the components. Thus from equation (II-252) and (II-253) C will be given by

$$C = A + B = \begin{vmatrix} c_{11} & c_{12} \\ c_{21} & c_{22} \end{vmatrix} = \begin{vmatrix} a_{11}+b_{11} & a_{12}+b_{12} \\ a_{21}+b_{21} & a_{22}+b_{22} \end{vmatrix} , \tag{II-255}$$

which is also a symmetric tensor. Thus if the principal polarizabilities for the principal axis systems are given by a_1 , a_2 , b_1 ,

b_2 , c_1 and c_2 respectively, then from equation (II-203) the polarizability tensor C when written in terms of principal polarizabilities is equal to

$$C = \begin{pmatrix} \left[a_1\cos^2\chi_A + a_2\sin^2\chi_A + b_1\cos^2\chi_B + b_2\sin^2\chi_B\right] & \left[(a_1-a_2)\cos\chi_A\sin\chi_A + (b_1-b_2)\cos\chi_B\sin\chi_B\right] \\ \left[(a_1-a_2)\cos\chi_A\sin\chi_A + (b_1-b_2)\cos\chi_B\sin\chi_B\right] & \left[a_1\sin^2\chi_A + a_2\cos^2\chi_A + b_1\sin^2\chi_B + b_2\cos^2\chi_B\right] \end{pmatrix} \quad \text{(II-256)}$$

Thus if χ_c denotes the rotation angle between the X , Z axes and the principal axis system, then from equation (II-205) $\tan(2\chi_c)$ will be given by

$$\tan(2\chi_c) = \frac{(a_1-a_2)\sin(2\chi_A) + (b_1-b_2)\sin(2\chi_B)}{(a_1-a_2)\cos(2\chi_A) + (b_1-b_2)\cos(2\chi_B)} \quad \text{(II-257)}$$

and from equation (II-206) (c_1-c_2) will be given by

$$(c_1-c_2)^2 = \left[(a_1-a_2)\cos(2\chi_A) + (b_1-b_2)\cos(2\chi_B)\right]^2 + \left[(a_1-a_2)\sin(2\chi_A) + (b_1-b_2)\sin(2\chi_B)\right]^2 . \quad \text{(II-258)}$$

Equations (II-257) and (II-258) may be generalized readily to a system composed of N components all assumed to be noninteracting so that the individual polarizability tensors will add according to equation (II-255). If $(C_1 - C_2)$ is denoted by $\Delta\gamma_C$ and the difference of the principal polarizabilities of the i^{th} component by $\Delta\gamma_i$, then from a generalization of equations (II-257) and (II-258) one obtains

$$\tan 2\chi_C = \frac{\sum_{i=1}^{N} \Delta\gamma_i \sin 2\chi_i}{\sum_{i=1}^{N} \Delta\gamma_i \cos 2\chi_i} \qquad \text{(II-259)}$$

and

$$(\Delta\gamma_C)^2 = \left[\sum_{i=1}^{N} \Delta\gamma_i \cos(2\chi_i)\right]^2 + \left[\sum_{i=1}^{N} \Delta\gamma_i \sin(2\chi_i)\right]^2 \qquad \text{(II-260)}$$

where χ_i denotes the angle between the X or Z axis and the principal axis system for the i^{th} component. Since from equation (II-17) the $\Delta\gamma_i$ are proportional to the birefringence Δn_i which in turn is proportional to the optical retardation δ_i given by

$$\delta_i = \Delta n_i L \qquad \text{(II-261)}$$

where L is the length of fluid traversed by the light ray, the quantities $\Delta\gamma_i$ and $\Delta\gamma_C$ of equations (II-259) and (II-260) may be replaced by either Δn_i and Δn_C or δ_L and δ_C.

Equations (II-259) and (II-260) describe the vector addition of N vectors $\Delta\vec{Y}_i$, all contained in the given X, Z plane, each oriented at an angle $2\chi_i$ with respect to either the X or Z coordinate line in the plane. This is illustrated for a two-component system in Figure 9. Thus it is possible to compute the birefringence and extinction angle for a given component i from the measured birefringence and extinction angle for the total solution by performing a vector subtraction, provided the values of the birefringence and extinction angles for the other components of the system are known.

Sadron has obtained equations (II-259) and (II-260) by working out the polarizabilities of the components of a system of suspended particles oriented by flow, assuming that the particles were noninteracting (dilute solutions), and also obtained experimental verification of these expressions (76, 77). These same expressions have been used to correct birefringence measurements for the solvent birefringence contribution when the solvent itself showed appreciable birefringence (70, 71, 92). For a dilute solution in which each solute molecule may be considered to be surrounded by only solvent material, one can probably consider a small volume element surrounding the solute molecule to be the region subject to the influence of the molecule. Thus one might argue that the polarizability characterizing the small volume element is independent of the polarizability of the surrounding solvent, so that the two polarizabilities could be separated using equations (II-259) and (II-260). However, in the present work, the polarizability of interest is that of the molecule in a nonbirefringent solvent having a mean index of refraction equal to that of the weakly

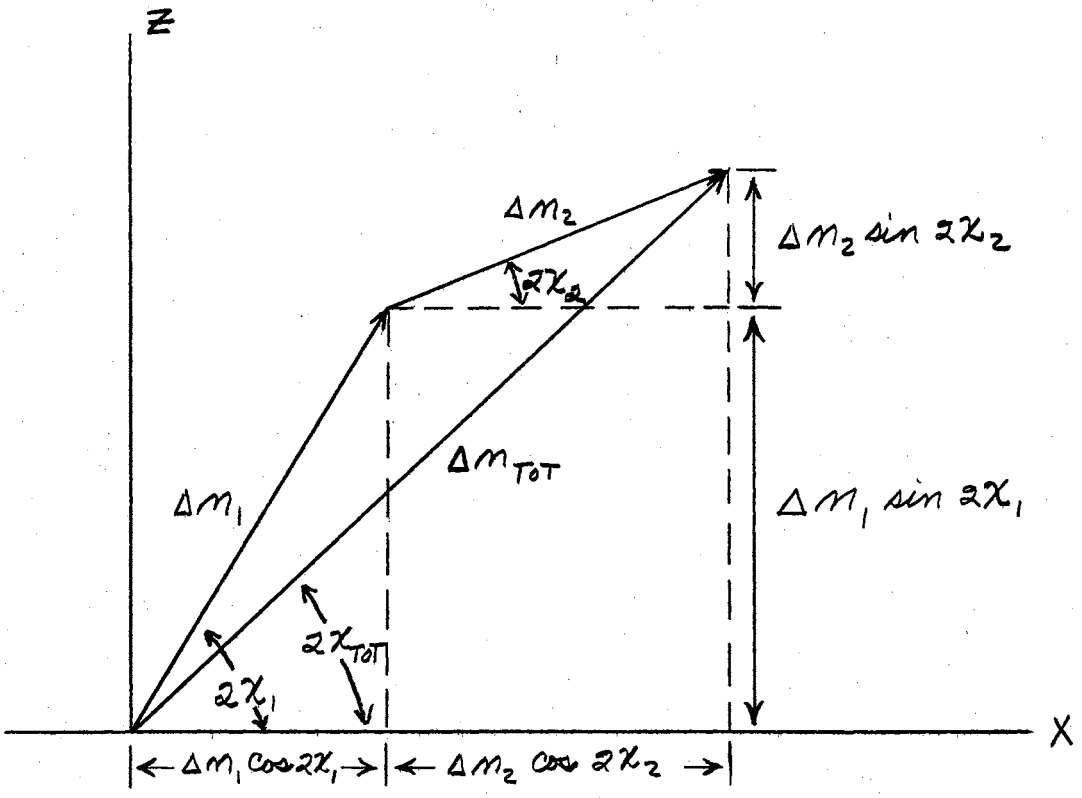

$$\text{Sum of } Z \text{ Components} = \Delta n_1 \sin 2\chi_1 + \Delta n_2 \sin 2\chi_2$$

$$\text{Sum of } X \text{ Components} = \Delta n_1 \cos 2\chi_1 + \Delta n_2 \cos 2\chi_2$$

$$\tan(2\chi_{TOT}) = \frac{\text{Sum of } Z \text{ Components}}{\text{Sum of } X \text{ Components}} = \frac{\sum_i \Delta n_i \sin 2\chi_i}{\sum_i \Delta n_i \cos 2\chi_i}$$

$$(\Delta n_{TOT})^2 = (\text{Sum of } X \text{ Components})^2 + (\text{Sum of } Z \text{ Components})^2$$

$$= \left[\sum_i \Delta n_i \cos 2\chi_i\right]^2 + \left[\sum_i \Delta n_i \sin^2 \chi_i\right]^2$$

Figure 9. Illustration of the Vector Addition of the Optical Birefringences Δn_i exhibited by Optically Non-interacting Components of a Two-component System to Obtain the Birefringence Δn_{TOT} of the System.

birefringent solvent. The polarizability of the small volume element containing both solvent and the solute molecule might be different from that of the molecule when immersed in a nonbirefringent solvent of the same mean refractive index, especially when the solvent contained in the small volume element contributes a birefringence comparable to that of the molecule. Since the birefringence of the solute molecule will be decreasing with frequency, possibly as given by equation (II-239), the difference between the molecular birefringence and the molecule plus birefringent solvent birefringence may become significant at high frequencies, even though the solvent contribution is initially insignificant at low frequency. Further, since the solvent and the molecule are intimately related in the small volume element, the birefringence of the solvent and the molecule probably cannot be separated by means of equations (II-259) and (II-260), but likely follows a much more complex additive process. For the work contained herein it is assumed that the birefringence contribution of such a birefringent solvent may be removed from the solution birefringence by a vector subtraction according to equations (II-259) and (II-260).

CHAPTER III

EXPERIMENTAL METHODS

Measurements of the flow birefringence of three polystyrene solutions have been carried out using two different flow conditions, sinusoidally time varying velocity gradients and non-time varying (steady flow or zero frequency) velocity gradients. Two different types of apparatus were used to generate these differing velocity gradient conditions; a closely spaced plane and reflector system for the time varying gradient measurements, and a coaxial cylinder (Couette) system for the non-time varying gradient measurements.

1. The Closely Spaced Oscillating Plane and Fixed Reflector System

Since the flow birefringence measurement involves the determination of both the birefringence produced by the fluid in shear and the velocity gradient inducing the birefringence, for accurate flow birefringence determinations it is essential that the velocity gradients used be known precisely. One method for producing a known and simple velocity gradient condition for sinusoidally time varying flow is the closely spaced oscillating plane and reflector system (80, 90). Figure 10 illustrates such a system. The surface of the plane which is oscillating sinusoidally in the X direction is located at $Z = -D$ with the surface of the fixed reflecting plane at $Z = 0$. The region between the planes is filled with the test solution. If the velocity of motion $\dot{\xi}_{PL}$ of the plane oscillating with angular

Figure 10. Arrangement of the Optical Elements of the Optical Transmission System of the Closely Spaced Oscillating Plane and Fixed Reflector System.

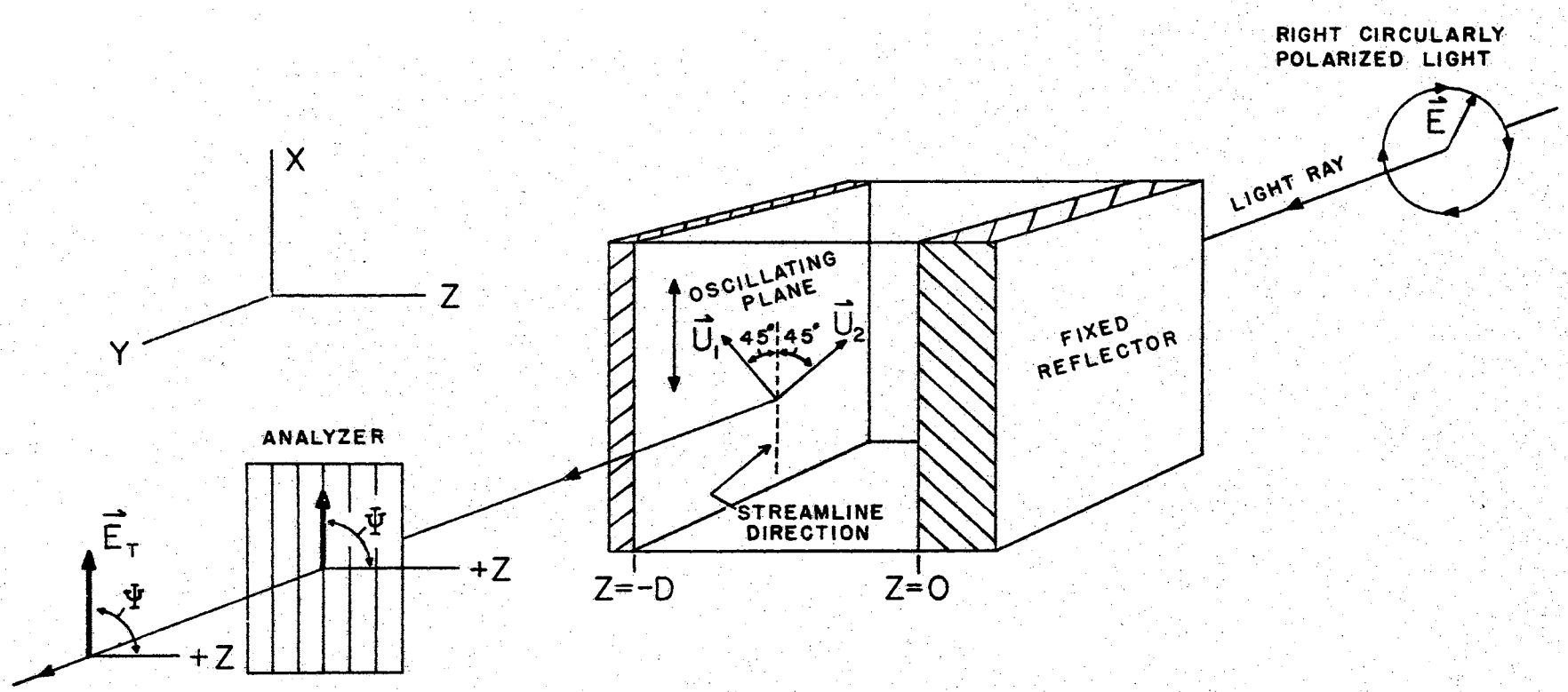
RIGHT CIRCULARLY
POLARIZED LIGHT
$\vec{E}$
LIGHT RAY
X
Z
Y
OSCILLATING
PLANE
$\vec{U}_1$
45°
45°
$\vec{U}_2$
FIXED
REFLECTOR
ANALYZER
$\vec{E}_T$
Ψ
+Z
STREAMLINE
DIRECTION
Z=-D
Z=0

frequency ω is given by the real part of

$$\dot{\xi}_{PL} = \dot{\xi}_o e^{i\omega t} \tag{III-1}$$

and the planes extend far enough in the X , Y plane to approximate planes of infinite extent, then the shear wave field generated in the viscoelastic test solution between the planes will be such that the velocity gradient q generated at any point z in the region will be given by the real part of

$$q = \left(\frac{\partial \dot{\xi}}{\partial z}\right) = -\dot{\xi}_o \gamma_s \left[\cos(\gamma_s z)/\sin(\gamma_s D)\right] e^{i\omega t} \tag{III-2}$$

where $\gamma_s = \beta_s - i\alpha_s$ is the complex shear wave propagation constant for the medium. γ_s is related to the complex viscosity coefficient

$$\eta^* = \eta' - i\eta'' = \eta_M e^{i\phi_\eta} \tag{III-3}$$

by

$$\gamma_s^2 = -\frac{i\omega\rho}{\eta^*} \tag{III-4}$$

where ρ denotes the density of the medium. For a viscoelastic medium ϕ may range from 0 degrees, corresponding to purely viscous behavior, to 90 degrees, corresponding to purely elastic behavior.

The shear wavelength λ_s for a freely propagating plane shear wave propagating in the viscoelastic medium is given by

$$\lambda_s = \frac{2\pi}{\beta_s} = 2\pi\left(\frac{\eta_M}{\rho\omega}\right)^{\frac{1}{2}} \sec\left[\frac{\phi_\eta}{2} - \frac{\pi}{4}\right]. \tag{III-5}$$

The velocity gradient given by equation (III-2) reduces to the important limiting value g_c when the ratio (D/λ_s) approaches zero.

$$\lim_{\frac{D}{\lambda_s}\to 0} g \equiv g_c = -\frac{\dot{\xi}_o}{D} e^{i\omega t} \qquad \text{(III-6)}$$

Thus for an infinitesimal gap width the velocity gradient g_c is constant throughout the gap and is 180 degrees out of phase with the oscillating plane velocity. The maximum variation of the magnitude and phase of the velocity gradient for a given value of (D/λ_s) as given by equation (III-2) occurs when the medium is purely viscous. For a viscous medium and (D/λ_s) ratio of 1/20, g will differ from g_c by at most 0.5% in magnitude and 2.8 degrees in phase. Hence if (D/λ_s) can be maintained sufficiently small, equation (III-6) may be taken as the relation between the plane velocity and the velocity gradient in the test medium.

Figure 10 also illustrates the optical system used to measure the flow birefringence of the solution. A monochromatic beam of right circularly polarized light is incident on the solution being examined. The flow birefringence induced by the shearing action of the driving plane modifies the polarization state of the light so that the light beam emerges from the fluid elliptically polarized. A polarizing prism employed as an analyzer transmits a plane polarized component of the elliptically polarized beam to a photomultiplier tube which responds to the intensity of this transmitted plane polarized component. Such a system for the detection of small flow birefringence has been analyzed in detail in the literature (88, 91).

To analyze the optical system quantitatively, consider the

following. A solution which exhibits flow birefringence has two orthogonal preferred directions, denoted by the unit vectors $\vec{u}_1$ and $\vec{u}_2$ of Figure 10, such that a plane polarized light ray having an electric vector polarization direction parallel to either $\vec{u}_1$ or $\vec{u}_2$ will pass through the solution with its polarization state unaltered. However, in general, these directions will vary as the velocity gradient is varied, usually exhibiting an orientation of $\vec{u}_1$ such that $\vec{u}_1$ and $\vec{u}_2$ make an angle of 45° to the streamline direction only for velocity gradients approaching zero. For the oscillatory shear measurements presented herein the velocity gradients used were kept sufficiently small that $\vec{u}_1$ and $\vec{u}_2$ were essentially at 45° to the streamline direction throughout the entire cycle of motion of the moving plane as is indicated in Figure 10. The electric vector $\vec{E}$ of the incident circularly polarized light beam may be resolved into components along the directions $\vec{u}_1$ and $\vec{u}_2$. Thus $\vec{E}$ is given by the real part of

$$\vec{E} = (\vec{u}_2 + \vec{u}_1 i) E_0 e^{i(\omega t - \chi_0 Y)} \qquad \text{(III-7)}$$

where $i = \sqrt{-1}$ and χ_0 is the propagation constant for the electromagnetic wave in free space. It is assumed herein that the propagation of the $\vec{u}_1$ and $\vec{u}_2$ components of the electric vector through the birefringent solution of thickness L in the Y direction can be described by the propagation constants χ_1 and χ_2 given by

$$\chi_{0j} = \aleph_{0j} - i\mu_0 \qquad \text{(III-8)}$$

where μ_0 is the attenuation factor and $\mathcal{H}_{oj}$ the phase factor of the propagation constant, related to the optical wavelengths in the solution λ_{oj} by

$$\mathcal{H}_{oj} = \frac{2\pi}{\lambda_{oj}} . \qquad \text{(III-9)}$$

Thus it is assumed that the space rate of attenuation of the two components will be identical (no dichroism). Neglecting complicating features having to do with transmission through the interfaces at the entering and exiting fluid surfaces (25), the transmitted electric vector $\vec{E}'$ exiting from the fluid layer is given by

$$\vec{E}' = \left[\vec{u}_2 e^{-i\chi_{o2}L} + \vec{u}_1 e^{-i\chi_{o1}L}\right] E_o e^{i(\omega t - \chi_o Y)} . \qquad \text{(III-10)}$$

The analyzer, which consists of a plane polarizer with transmission direction in the direction of the unit vector $\vec{u}$, will transmit the component $\vec{E}_T$ of the electric vector $\vec{E}'$ given by

$$\vec{E}_T = \vec{u} E_T e^{i(\omega t - \chi_o Y)} \qquad \text{(III-11)}$$

where

$$E_T = E_o e^{-\mu_o L}\left[\cos(\theta - \tfrac{\pi}{4}) e^{-i\mathcal{H}_{o2}L} + i \sin(\theta - \tfrac{\pi}{4}) e^{-i\mathcal{H}_{o1}L}\right] . \qquad \text{(III-12)}$$

If the transmitted electric vector is incident on a photomultiplier tube, then the photomultiplier output current I is proportional to the product of E_T and its complex conjugate E_T^* (90).

$$I \propto (E_T E_T^*) \tag{III-13}$$

Or, combining (III-12) and (III-13),

$$I = I_0 \left\{ 1 + 2 \cos\left(\Psi - \frac{\pi}{4}\right) \sin\left(\Psi - \frac{\pi}{4}\right) \cdot \sin\left[(\mathcal{H}_{01} - \mathcal{H}_{02})L\right] \right\} \tag{III-14}$$

where I_0 is a constant current determined by E_0, μ_0 and the photomultiplier sensitivity. Since the index of refraction of a medium is defined as the ratio of the propagation velocity of the electromagnetic wave in free space to the propagation velocity of the wave in the medium, the quantity $(\mathcal{H}_{01} - \mathcal{H}_{02})L$ of equation (III-14) may be related to the indices of refraction n_1 and n_2 of the fluid associated with the $\vec{u}_1$ and $\vec{u}_2$ directions. Thus from (III-8) and (III-9)

$$\begin{aligned}(\mathcal{H}_{01} - \mathcal{H}_{02})L &= \left(\frac{2\pi}{\lambda_{01}} - \frac{2\pi}{\lambda_{02}}\right)L = \frac{2\pi L}{\lambda_0}\left[\frac{\lambda_0}{\lambda_{01}} - \frac{\lambda_0}{\lambda_{02}}\right] \\ &= \frac{2\pi L}{\lambda_0}\left[\frac{c}{v_1} - \frac{c}{v_2}\right] = \frac{2\pi L}{\lambda_0}(n_1 - n_2)\end{aligned} \tag{III-15}$$

where λ_{01} and λ_{02} are the wavelengths in the solution of the components of the electromagnetic wave in the $\vec{u}_1$ and $\vec{u}_2$ directions, v_1 and v_2 are the propagation velocities of these same two components in the solution, and λ_0 and c are the wavelength and propagation velocity of the components in free space. If the relative retardation δ is defined as

$$\delta = \Delta m L = (n_2 - n_1) L \qquad \text{(III-16)}$$

the insertion of (III-16) and (III-15) in (III-14) yields

$$I = I_o \left\{ 1 - 2 \cos\left(\Psi - \frac{\pi}{4}\right) \sin\left(\Psi - \frac{\pi}{4}\right) \sin\left(\frac{2\pi\delta}{\lambda_o}\right) \right\}. \qquad \text{(III-17)}$$

Two analyzer orientations of particular interest are the orientations $\Psi = 0$ degrees and $\Psi = 90$ degrees. For these orientations, equation (III-17) reduces to

$$I_{\Psi=0^\circ} = I_o \left\{ 1 + \sin\left(\frac{2\pi\delta}{\lambda_o}\right) \right\} \qquad \text{(III-18)}$$

and

$$I_{\Psi=90^\circ} = I_o \left\{ 1 - \sin\left(\frac{2\pi\delta}{\lambda_o}\right) \right\}. \qquad \text{(III-19)}$$

If the retardation δ is restricted to sufficiently small values that

$$\sin\left(\frac{2\pi\delta}{\lambda_o}\right) \simeq \frac{2\pi\delta}{\lambda_o} \qquad \text{(III-20)}$$

equations (III-18) and (III-19) reduce to

$$I_{\Psi=0^\circ} = I_o \left\{ 1 + \frac{2\pi\delta}{\lambda_o} \right\} \qquad \text{(III-21)}$$

and

$$I_{\Psi=90^\circ} = I_o \left\{ 1 - \frac{2\pi\delta}{\lambda_o} \right\} . \qquad \text{(III-22)}$$

These relations are good to within related experimental accuracies if δ is less than 1/12 of the optical wavelength λ_o . As was noted in the previous chapter, the shear induced birefringence and the velocity gradient producing it will, in general, be out of phase, the phase difference being a function of the frequency of the driving plane motion. The complex mechano-optic constant S^* used herein to characterize the flow birefringence $\Delta n = n_2 - n_1$ at a given velocity gradient g has been defined by equation (II-238). Using complex representation,

$$S^* = + S_M e^{i\theta} = + \frac{\Delta n}{g} = + \frac{(n_2 - n_1)}{g} = + \frac{\delta}{\lambda g} \qquad \text{(III-23)}$$

for the coordinate system of Figure 10, where n_2 and n_1 are the indices of refraction corresponding to the directions $\vec{u}_2$ and $\vec{u}_1$, respectively. This relation thus specifies the relative magnitudes of Δn and g through S_M , and their relative phasing through θ . Combining equation (III-23) with equations (III-6) and (III-16) yields an expression for the complex retardation δ for small values of (D/λ_s) for the coordinate system of Figure 10.

$$\delta = S^* L g \simeq - \frac{S_M L \dot{\xi}_0}{D} e^{i(\omega t + \theta)} . \qquad \text{(III-24)}$$

The photocurrent generated by the retardation may be evaluated by the insertion of the real part of (III-20) in (III-18) and (III-19). Or, if the magnitude of the retardation is less than 1/12 the optical wavelength, the photocurrent may be evaluated from (III-20), (III-21) and (III-22) retaining the complex notation. Thus for $|\delta| < \lambda_0/12$ the photocurrent obtained for the cases $\Psi = 0$ degrees and $\Psi = 90$ degrees are given by the real parts of

$$I_{\Psi=0^\circ} \simeq I_0 \left\{ 1 + \frac{2\pi}{\lambda_0} \cdot \frac{S_M L \dot{\xi}_0}{D} e^{i(\omega t + \theta + \pi)} \right\}$$
$$= I_0 + I_1 e^{i(\omega t + \theta + \pi)} \qquad \text{(III-25)}$$

and

$$I_{\Psi=90^\circ} \simeq I_0 \left\{ 1 + \frac{2\pi}{\lambda_0} \cdot \frac{S_M L \dot{\xi}_0}{D} e^{i(\omega t + \theta)} \right\} \qquad \text{(III-26)}$$
$$= I_0 + I_1 e^{i(\omega t + \theta)} .$$

All measurements presented herein were made under conditions such that equations (III-25) and (III-26) would apply. From equations (III-24) and (III-25) it is seen that the photocurrent is composed of a constant

term of magnitude I_0 which is independent of the birefringence of the medium, and a time varying component of magnitude I_1 varying at the driving frequency ω . From either (III-24) or (III-26) S_M, the magnitude of S^*, may be obtained readily from measurements of the constant and the time varying components of I and the plane velocity according to the relation

$$S_M = \left(\frac{\lambda_0 D}{2\pi L}\right)\left(\frac{I_1}{I_0 \xi_0}\right). \qquad \text{(III-27)}$$

The angle θ may be evaluated readily from measurements of the phase angle between the plane velocity and the birefringence, as is seen from equations (III-1), (III-24) and (III-25). The phase angle between the driving plane velocity and the photocurrent will be θ for the case $\Psi = 90$ degrees or will be $\theta + 180$ degrees for the case $\Psi = 0$ degrees.

Figure 11 presents a simplified block diagram of the closely spaced plane and reflector system used for the sinusoidally time varying birefringence measurements. The oscillating plane and reflector are located in the fluid cell FC. Three driving planes were used, a narrow black glass plane, a wide brass plane, and a wide black glass plane. The wide glass and brass planes have dimensions of 0.750" x 1.1" in directions parallel to the light ray propagation direction and the plane displacement respectively, and are made so that the part of the plane that is immersed in the test solution is 0.125" thick. The narrow black glass plane has corresponding dimensions of 0.153" x 0.375" x 0.125". The narrow black glass plane was used to reduce the mechanical loading when the solution under test exhibited a high

Figure 11. Diagram of the Closely Spaced Oscillating Plane and Reflector System Showing the Light Source LS, the Diffuser D, the Slit S, the Lens L, the Interference Filter IF, the Polarizer P, the Quarter Wave Plate $(\lambda/4)$, the Fluid Cell FC, the Analyzer A, the Photomultiplier PM, the Steel Mass M, and the Drive Head DH Containing the Velocity Monitor VM, the Electrodynamic Driver DR and the Displacement Monitor DM.

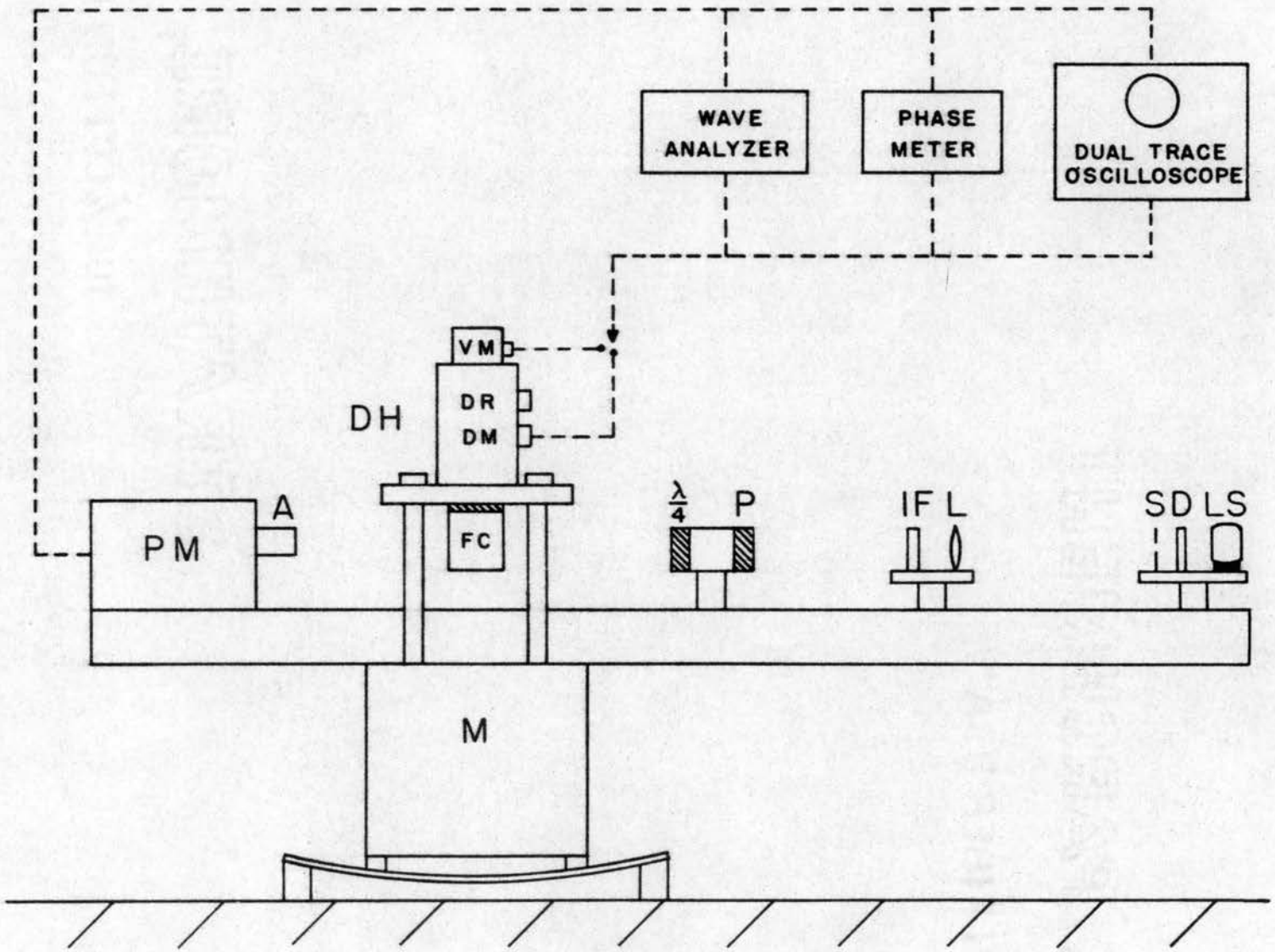
WAVE ANALYZER
PHASE METER
DUAL TRACE OSCILLOSCOPE
VM
DR
DM
DH
FC
PM
A
λ/4
P
IF
L
SD
LS
M

viscosity. The plane is mechanically attached to the shaft of the driving head DH but is thermally isolated from it by a Delrin insulator. The fixed brass reflector has a reflecting surface of 0.750" x 0.750" in directions parallel to the light ray propagation direction and the plane displacement. The gap between the plane and reflector may be varied from 0.0" to 0.100" by repositioning the reflector. The gap widths are determined by feeler gauges placed between the reflector and plane, or by measurement of the distance between scribed lines on the edges of the reflector and plane using a traveling microscope. There is an uncertainty in gap width of somewhat less than 0.001" for feeler gauge measurements and of less than 0.0002" for the traveling microscope measurements. Thus for materials with a viscosity requiring the use of gaps of less than 0.002" to maintain the desired (D/λ_s) ratio as well as an adequate optical retardation at the higher frequencies it is necessary to make additional measurements at lower frequencies using a wider gap width, so that the smaller gap width may be determined by a comparison of the data. The reflector is mounted on a brass plate which also supports the fluid cell. The plate is attached mechanically to the driving head DH but is insulated from it by a Delrin spacer between the plate and the driving head. The fluid cell is equipped with passages for the circulation of liquid from a constant temperature circulator so that the cell, the plane and reflector combination, and the brass mounting plate achieve essentially the same temperature as the test fluid. The temperature of the reflector is monitored by measuring the resistance of a thermistor imbedded in the reflector near the reflecting surface, using a Wheatstone bridge and galvanometer. Temperature changes of the reflector of $\pm$ 0.02°C can be

detected readily for temperatures between -5°C and +90°C, the temperature limits attainable using a Haake constant temperature circulator. The driving head DH houses an electrodynamic driver, an electrodynamic velocity monitor, and a capacitive displacement monitor for measurements at low frequencies. Below 0.1 cps the velocity monitor output voltage is too small to be usable, so the plane motion must be monitored by the displacement monitor. The moving elements of these systems as well as the oscillating plane are attached to a common shaft which is held by a wire suspension system. The driving head is capable of attaining displacements of up to 1/4 inch peak to peak for frequencies near the fundamental resonance frequency of the system, and is usable for frequencies from 0.01 cps to approximately 1,000 cps. The driving current is supplied by a Hewlett-Packard low frequency oscillator driving a DC coupled Kron Hite 10 watt amplifier. The driving head is supported above the optical bench as shown, and is coupled to a 150-lb steel mass M to reduce motions of the overall system. A flexible aluminum plate suspension below the steel mass is used to provide additional isolation from mechanical room noise.

The optical bench is also attached to the mass M. A tungsten projection lamp LS , diffuser D and vertical slit S serve as the light source for the system. The adjustable slit S is oriented vertically. The lens L forms an image of S in the gap between the plane and reflector approximately 0.5" from the entering surfaces of the plane and reflector, to avoid reflections from the metal walls of the gap. The lens is equipped with a variable aperture stop so that the light beam may be kept away from the plane and reflector walls for gap widths greater than 0.010", if desired. However, no difference in

the birefringence measurements for lighting conditions in which the light beam is allowed to strike the entering edges of the gap by opening the lens stop and for conditions in which the light beam does not strike the entering edges has been detected. Since the transmitted light intensity is increased appreciably for the wide beam illumination condition, it was used for the measurements presented here. The light beam is rendered semi-monochromatic by the use of an interference filter IF having its transmission peak at 5790 Å. The Glan-Thompson prism polarizer P and quarter wave plate $\lambda/4$ combination produces the right circular polarization state of the light that illuminates the fluid cell. A second Glan-Thompson prism is used as the analyzer A to transmit the desired plane polarized component of the light emerging from the fluid to a photomultiplier tube PM. The output voltages from the velocity or displacement monitors and the photomultiplier tube are analyzed by means of a Hewlett-Packard model 302A wave analyzer for the measurement of the magnitudes of the respective voltages, and a Phazor Model 210AB phase meter for the measurement of relative phasing of the signals, for frequencies above 15 cps. For frequencies less than 15 cps, the output voltages are displayed on a Tektronix type 564 storage oscilloscope, so that the magnitudes and relative phasing of the signals may be determined visually from the stored oscilloscope traces.

Two measurement procedures were used to measure the oscillatory flow birefringence. Since the light beam is sufficiently large to fill the entire gap at the entering side, any lateral plane motion causing a variation in the gap during the cycle of motion results in a modulation of the light beam. Such modulation is emphasized as the

gap width is decreased. If the modulation is at the driving frequency, it can produce an appreciable error if it amounts to as little as 5 percent of the birefringence signal. Hence before making any measurements, the analyzing prism was removed and the photomultiplier output analyzed to determine if an appreciable driving frequency component due to improper plane motion was present. If the modulation was negligible, the analyzer was replaced with Ψ set equal to 45 degrees so that the behavior of the preferential directions corresponding to $\vec{u}_1$ and $\vec{u}_2$ of Figure 10 could be examined. Since the analysis presented is valid only for $\vec{u}_1$ and $\vec{u}_2$ at 45 degrees to the streamline direction throughout the entire cycle of motion, the driving plane velocity was reduced until no variation of the photomultiplier output could be observed on the oscilloscope. The corresponding displacement or velocity monitor output was noted, the test being carried out for all frequencies at which the birefringence measurement was to be made. Having thus determined the maximum plane velocities to be used at the various frequencies at which birefringence measurements were to be made, the analyzer was set to Ψ = 90 degrees and the drive level adjusted to provide an appropriate plane velocity. Then the magnitude and relative phasing of the photomultiplier and velocity or displacement monitor outputs were determined, using the wave analyzer and phase meter where possible, and the oscilloscope for frequencies below the limits of the other instruments.

A second measurement procedure was used if appreciable modulation of the light beam at the driving frequency due to improper plane motion was detected. Such a modulation may be treated by considering the photocurrent expressions in equations (III-25) and (III-26) to have a

time varying I_o given by

$$I_o = I_o'\{1 + k\cos(\omega t + \phi)\} \tag{III-28}$$

where k is some constant less than 1. The insertion of (III-28) into (III-26) and (III-25) yields the following photocurrent expressions:

$$I_{\Psi=0^\circ} = I_o'\{1 - \frac{kA}{2}\cos(\theta-\phi) + k\cos(\omega t+\phi) - A\cos(\omega t+\theta) - \frac{kA}{2}\cos(2\omega t+\theta+\phi)\} \tag{III-29}$$

and

$$I_{\Psi=90^\circ} = I_o'\{1 + \frac{kA}{2}\cos(\theta-\phi) + k\cos(\omega t+\phi) + A\cos(\omega t+\theta) + \frac{kA}{2}\cos(2\omega t+\theta+\phi), \tag{III-30}$$

where

$$A = \left(\frac{L S_M \dot{S}_o}{D}\right)\left(\frac{2\pi}{\lambda_o}\right). \tag{III-31}$$

Only the driving frequency component and the constant component of the photocurrent are of interest. If the driving frequency component of the photocurrent given by equations (III-29) and (III-30) is denoted by I_1', then

$$I'_{1\,\Psi=0^\circ} = I'_o\left[k\cos(\omega t+\phi) - A\cos(\omega t+\theta)\right] \tag{III-32}$$

and

$$I'_{1\,\Psi=90^\circ} = I'_o\left[k\cos(\omega t+\phi) + A\cos(\omega t+\theta)\right]. \tag{III-33}$$

Either the birefringence or the modulation component of the photocurrent may be recovered by the subtraction or addition of (III-32) and (III-33).

$$I'_{1\,\Psi=90^\circ} - I'_{1\,\Psi=0^\circ} = 2I'_o A\cos(\omega t+\theta) \tag{III-34}$$

$$= 2I'_o\left(\frac{LS_M\dot{\xi}_e}{D}\right)\left(\frac{2\pi}{\lambda_o}\right)\cos(\omega t+\theta)$$

and,

$$I'_{1\,\Psi=90^\circ} + I'_{1\,\Psi=0^\circ} = 2I'_o k\cos(\omega t+\phi). \tag{III-35}$$

For k and A small, as is the case for the measurements presented herein, the constant term in (III-29) is essentially equal to that in (III-30) so that

$$I'_o \simeq 1 - \frac{kA}{2}\cos(\theta-\phi) \simeq 1 + \frac{kA}{2}\cos(\theta-\phi). \tag{III-36}$$

Thus a measurement of the constant and driving frequency components of the photocurrent and the relative phasing of the driving frequency components of the photocurrent with respect to either the velocity or

displacement monitor outputs for Ψ equal to 0 degrees and 90 degrees will permit the determination of either the birefringence or the modulation component of the photocurrent by making phazor plots of $I_1' \underline{\Psi = 90°}$ and $I_1' \underline{\Psi = 0°}$ and forming the vector sum and difference given by equations (III-34) and (III-35). As is indicated by the equations, the vector difference will yield a vector corresponding to twice the birefringence component, while the vector sum will yield a vector corresponding to twice the modulation component. Figure 12 illustrates such a phazor plot. Thus the measurement procedure for the case of appreciable intensity modulation due to improper plane motion is to note the maximum drive levels to be used to avoid deviation of $\vec{u}_1$ and $\vec{u}_2$ from 45 degrees to the streamline direction by examining the photocurrent for $\Psi = 45$ degrees, noting the drive level at which the photocurrent takes on an additional modulation due to the variation of $\vec{u}_1$ and $\vec{u}_2$. Then, having determined the maximum plane velocities to be used at each frequency at which measurements are to be made, measurements of the magnitude and relative phasing of the photocurrent and the velocity or displacement monitor output are made as before, except that instead of making measurements for $\Psi = 90$ degrees only, measurements are made for both $\Psi = 0$ degrees, and $\Psi = 90$ degrees at each frequency. The appropriate birefringence component is then extracted by the vector subtraction given by equation (III-34).

The velocity monitor as well as the photomultiplier circuit was found to be sensitive to electrical loading especially at frequencies above 200 cps. The velocity monitor was found to be sensitive to mechanical loading also. Hence to check the equipment, measurements of

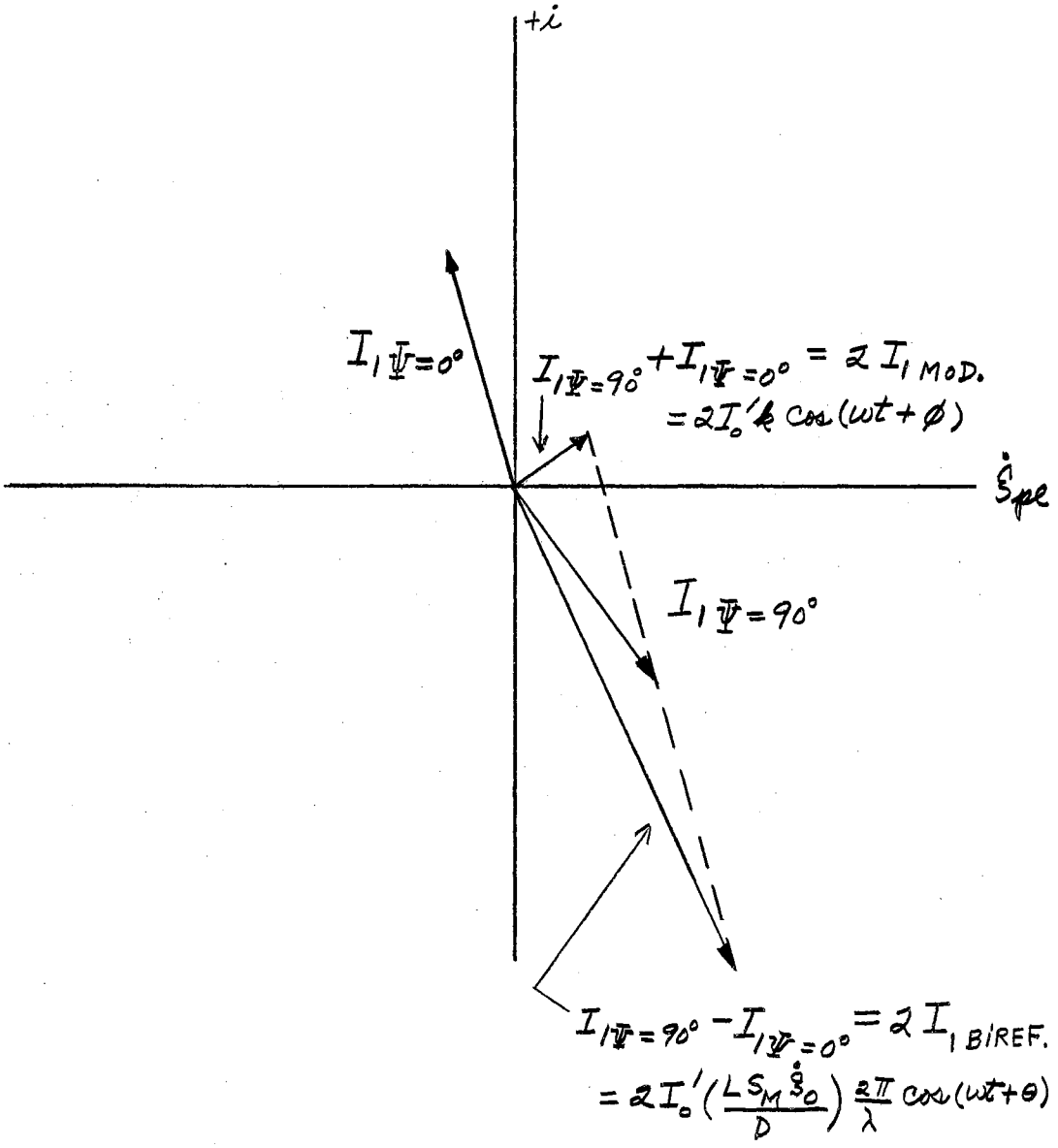

Figure 12. Illustration of the Determination of the Modulation and Birefringence Components $I_{1,MOD}$ and $I_{1,BIREF.}$, of the Photomultiplier Current From the Meassured Values of $I_{1,\Psi=0°}$ and $I_{1,\Psi=90°}$.

S_M and θ versus frequency were made for materials for which it was felt that the relaxation times should be sufficiently short that S_M should be constant and θ be either 0 or -180 degrees throughout the frequency range of the instrument. The materials used were Aroclors 1248 and 1254, and Oronite polybutene N-18. The velocity monitor was found to have a phase error of less than 5 degrees for frequencies to 800 cps, provided the mechanical loading was kept sufficiently small. From 250 cps to 15 cps the phase error was less than 3 degrees. The magnitude of the velocity monitor output was proper up to 1,000 cps.

The closely spaced plane and reflector system can detect a birefringence Δn of 5×10^{-9} with a probable error of 5%. Thus using a gap width of approximately .0015", the narrowest gap width feasible with the tungsten light source, the system will measure values of S_M down to $S_M \simeq 10^{-11}$ sec.

2. The Coaxial Cylinder System

The concentric cylinder apparatus used for the measurement of the shear induced birefringence of the polystyrene solutions in steady flow is capable of covering a range of velocity gradients corresponding to those obtainable for the oscillatory flow birefringence measurements as made on the thin fluid layer system described in the previous section. The maximum and minimum velocity gradients are approximately 640 per second and 1 per second, respectively. The apparatus is of the rotating outer cylinder design, having inner and outer cylinders of 5.00 centimeter axial length and diameters of 2.000 inches and 2.060 inches, respectively. Thus the sheared medium is confined to an annular ring of thickness 0.030 inches. The light beam used to analyze

the flow birefringence of the medium propagates through the annular ring in a direction parallel to the axes of the cylinders, so that if end effects are neglected, the beam may be considered to traverse 5.00 centimeters of the sheared medium.

The optical birefringence of the medium under test is analyzed by means of a Senarmont compensator scheme (40). Figure 13 shows the elements of the optical system, and the coordinate system adopted for the specification of the flow birefringence exhibited by the sheared medium. As for the oscillatory flow experiment, the $+X$ direction is taken to be the streamline direction at the observation point P, with the direction of propagation of the light ray in the $+Y$ direction. The $+Z$ axis is directed inward along a radial line as shown in the figure. As for the thin fluid layer system, the intersection of the Z axis and the outer (rotating) cylinder is designated as the point $Z = -D$, D being the gap width, with the intersection of the Z axis and the inner cylinder being designated as the point $Z = 0$. In shear, the medium contained in the gap becomes optically birefringent. The birefringence is characterized herein by the sign of the difference Δn of the indices of refraction n_2 and n_1 corresponding to the preferential directions in the medium specified by the unit vectors $\vec{u}_2$ and $\vec{u}_1$ of Figure 13, and the angle χ between $\vec{u}_1$ and the streamline direction ($+X$ axis). Since for certain mixtures of solutions the preferential directions may move from one quandrant of the Z, X plane to another, for the work presented herein the vector $\vec{u}_1$ is taken to be the vector describing the orientation of the preferred direction to be found in the Z, X quadrant defined by vectors in the $-Z$ and

Figure 13. Arrangement of the Optical Elements of the Optical Transmission System of the Coaxial Cylinder System.

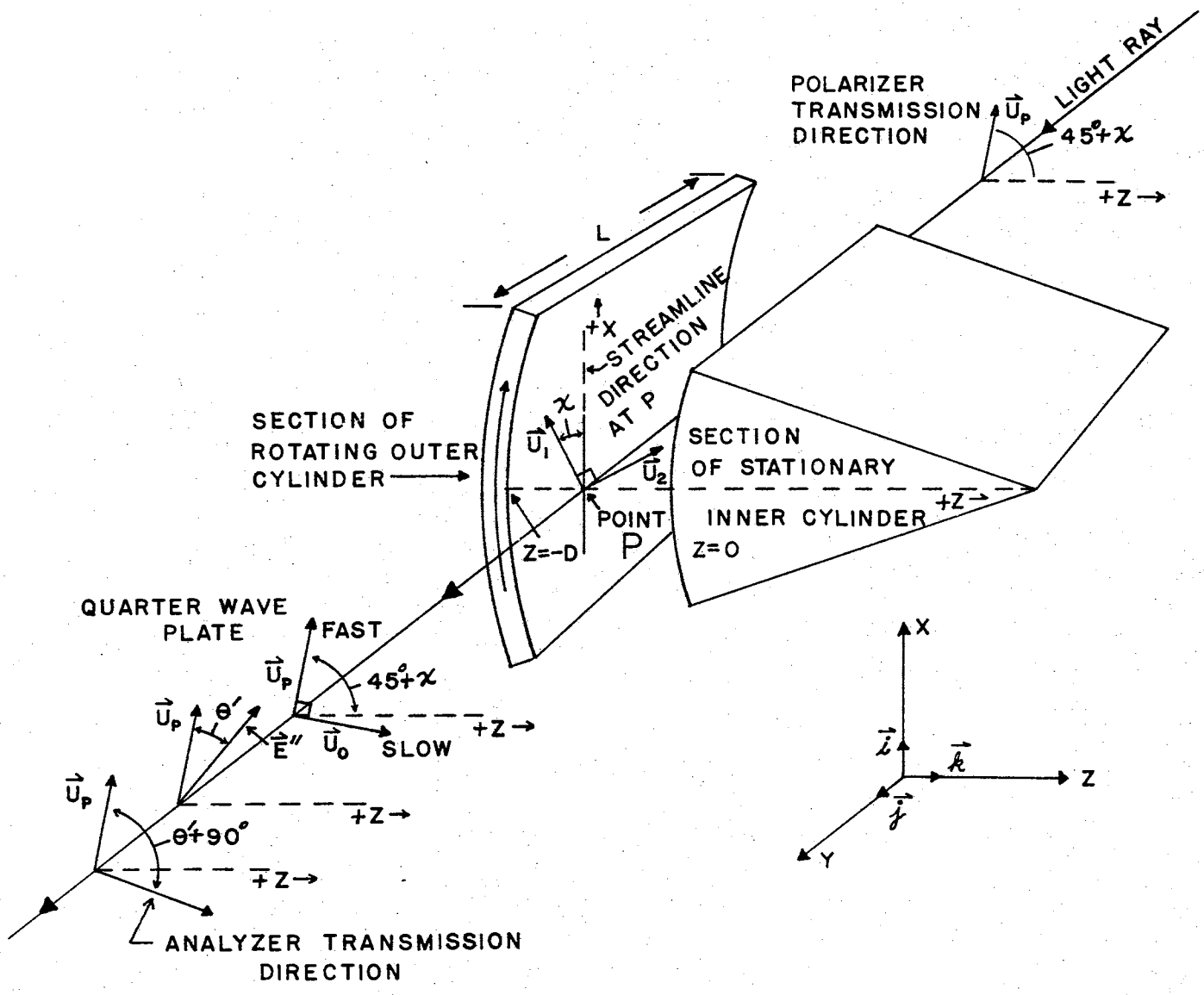
POLARIZER
TRANSMISSION
DIRECTION
$\vec{U}_p$
LIGHT RAY
$45°+\chi$
+Z
L
STREAMLINE
DIRECTION
AT P
SECTION OF
ROTATING OUTER
CYLINDER
$\vec{U}_1$
χ
$\vec{U}_2$
SECTION
OF STATIONARY
INNER CYLINDER
POINT
P
Z=-D
Z=0
QUARTER WAVE
PLATE
FAST
$\vec{U}_p$
$45°+\chi$
θ'
$\vec{E}''$
$\vec{U}_0$
SLOW
$\theta'+90°$
ANALYZER TRANSMISSION
DIRECTION
X
Y
Z
$\vec{i}$
$\vec{j}$
$\vec{k}$

$+X$ directions as shown in the figure. Thus the angle χ is such that

$$0° \leq \chi \leq 90° \tag{III-37}$$

and the sign of the difference of the indices of refraction Δn given by

$$\Delta n = n_2 - n_1 \tag{III-38}$$

is such that it may change sign during the course of an experiment.

To analyze the operation of the Senarmont compensator quantitatively, consider Figure 13. A monochromatic light ray having a free space wavelength λ_0 propagating in the $+Y$ direction passes through the polarizer P. The electric vector of the light ray transmitted by the polarizer is given by

$$\vec{E} = \vec{u}_p E_m e^{i(\omega t - \gamma_0 Y)}, \tag{III-39}$$

where $\vec{u}_p$ is a unit vector describing the transmission direction of the polarizer and γ_0 is the free space propagation constant for the electromagnetic wave. γ_0 is related to the free space wavelength λ_0 by

$$\gamma_0 = \frac{2\pi}{\lambda_0} . \tag{III-40}$$

The plane polarized ray proceeds to the birefringent fluid. Neglecting complicating effects associated with the propagation of the ray at the fluid interfaces (25), the propagation of the ray may be treated by considering the components of the ray having polarization directions

corresponding to the unit vectors $\vec{u}_1$ and $\vec{u}_2$ to have associated complex propagation constants γ_{o1} and γ_{o2} (91). If the polarizer transmission direction described by the unit vector $\vec{u}_p$ is adjusted so that it makes a 45 degree angle with $\vec{u}_1$ and $\vec{u}_2$ as shown in the figure, then

$$\vec{u}_p = \frac{\vec{u}_1}{\sqrt{2}} + \frac{\vec{u}_2}{\sqrt{2}} . \qquad \text{(III-41)}$$

Thus the electric vector entering the fluid may be written as

$$\vec{E} = \frac{E_M}{\sqrt{2}}(\vec{u}_1 + \vec{u}_2) e^{i(\omega t - \gamma_o Y)} . \qquad \text{(III-42)}$$

The electromagnetic wave propagation constants γ_{o1} and γ_{o2} characterizing the medium are, in general, complex.

$$\gamma_{oi} = \beta_{oi} - i\mu_{oi} , \qquad \text{(III-43)}$$

where β_{oi} is the phase factor of the propagation constant and μ_{oi} is the attenuation constant for the medium being considered. β_{oi} is related to the electromagnetic wavelength λ_{oi} for the component i in the medium and thus to the corresponding index of refraction n_i by

$$\beta_{oi} = \frac{2\pi}{\lambda_{oi}} = \frac{2\pi n_i}{\lambda_o} . \qquad \text{(III-44)}$$

It is assumed that the two components of $\vec{E}$ will show the same space rate of attenuation when passing through the birefringent medium (no dichroism), so that

$$\mu_{o1} = \mu_{o2} = \mu_o \,. \tag{III-45}$$

Thus the electric vector E' emerging from the fluid layer of thickness L is given by

$$\vec{E}' = \frac{E_M}{\sqrt{2}} \left\{ \vec{u}_1 e^{i\kappa_{o1}L} + u_2 e^{-i\kappa_{o2}L} \right\} e^{-\mu_o L} e^{i(\omega t - \gamma_o Y)} \,. \tag{III-46}$$

The ray next encounters the quarter wave plate, assumed to have negligible absorption, which is oriented with its fast axis parallel to the polarizer axis. Thus the fast and slow axes have the directions specified by the orthogonal unit vectors $\vec{u}_p$ and $\vec{u}_o$ of Figure 13. Again, the propagation of the ray through the plate may be analyzed in terms of the components of the vector $\vec{E}'$ along $\vec{u}_p$ and $\vec{u}_o$. Thus upon entering the plate the electric vector is given by

$$\vec{E}' = \frac{E_M}{2} \left[\vec{u}_p \left(e^{-i\kappa_{o1}L} + e^{-i\kappa_{2}L} \right) + \vec{u}_o \left(e^{-i\kappa_{o2}L} - e^{-i\kappa_{o1}L} \right) \right] e^{-\mu_o L} e^{i(\omega t - \gamma_o Y)} \,. \tag{III-47}$$

Equation (III-47) may be simplified by the use of the following:

$$\begin{aligned} e^{-i\kappa_{o1}L} + e^{-i\kappa_{o2}L} &= \cos(\kappa_{o1}L) + \cos(\kappa_{o2}L) \\ &\quad - i\left[\sin(\kappa_{o1}L) + \sin(\kappa_{o2}L)\right] \\ &= 2\cos\left[\tfrac{1}{2}(\kappa_{o1} - \kappa_{o2})L\right] e^{-i\left[\frac{1}{2}(\kappa_{o1} + \kappa_{o2})L\right]} \end{aligned} \tag{III-48}$$

and,

$$e^{-i\beta_{o2}L} - e^{-i\beta_{o1}L} = \cos(\beta_{o2}L) - \cos(\beta_{o1}L) - i\left[\sin(\beta_{o2}L) - \sin(\beta_{o1}L)\right] \quad \text{(III-49)}$$
$$= 2\sin\left[\tfrac{1}{2}(\beta_{o1}-\beta_{o2})L\right] e^{-i\left[\frac{1}{2}(\beta_{o1}+\beta_{o2})L + \frac{\pi}{2}\right]}.$$

Thus from equation (III-48) and (III-49) equation (III-47) may be written as (III-50)

$$\vec{E}' = E_M\left\{\vec{u}_p \cos\left[\tfrac{1}{2}(\beta_{o1}-\beta_{o2})L\right] - \vec{u}_o \sin\left[\tfrac{1}{2}(\beta_{o1}-\beta_{o2})L\right] e^{-i\frac{\pi}{2}}\right\} \cdot e^{-\mu_o L} e^{i\left[\omega t - \gamma_o Y - \frac{1}{2}(\beta_{o1}+\beta_{o2})L\right]}.$$

The passage of the ray through the quarter wave plate produces a spatial retardation between the components of one quarter wavelength. Thus if the phasing of the faster component is altered by an angle ϕ upon passage through the plate, then the phasing of the slower component is altered by an amount $\left(\phi + \frac{\pi}{2}\right)$. Thus the ray $\vec{E}''$ exiting from the quarter wave plate is given by

$$\vec{E}_M'' = E_M\left\{\vec{u}_p \cos\left[\tfrac{1}{2}(\beta_{o1}-\beta_{o2})L\right] - \vec{u}_o \sin\left[\tfrac{1}{2}(\beta_{o1}-\beta_{o2})L\right] e^{-i\pi}\right\} \cdot e^{-\mu_o L} e^{i\left[\omega t - \gamma_o Y - \frac{1}{2}(\beta_{o1}+\beta_{o2})L - \phi\right]} \quad \text{(III-51)}$$

$$= E_M\left\{\vec{u}_p \cos\left[\tfrac{1}{2}(\beta_{o1}-\beta_{o2})L\right] + \vec{u}_o \sin\left[\tfrac{1}{2}(\beta_{o1}-\beta_{o2})L\right]\right\} \cdot e^{-\mu_o L} e^{i\left[\omega t - \gamma Y - \frac{1}{2}(\beta_{o1}+\beta_{o2})L - \phi\right]}.$$

Hence the ray emerging from the quarter wave plate is plane polarized, having a polarization direction that is dependent on the magnitude and sign of $(\gamma_{o1} - \gamma_{o2})$. The polarization direction of $\vec{E}''$ may be specified by the angle θ' of Figure 13. Thus

$$\tan\theta' = \frac{\vec{u}_o \text{ COMPONENT}}{\vec{u}_p \text{ COMPONENT}} = \frac{\sin\left[\frac{1}{2}(\gamma_{o1}-\gamma_{o2})L\right]}{\cos\left[\frac{1}{2}(\gamma_{o1}-\gamma_{o2})L\right]} \qquad \text{(III-52)}$$

so that

$$\theta' = \left[\frac{1}{2}(\gamma_{o1} - \gamma_{o2})L\right] \pm 2m\pi, \qquad \text{(III-53)}$$
$$m = 0, 1, 2, \cdots .$$

If the optical retardation δ produced by the sheared medium is measured in radians, then it is related to the difference between the indices of refraction of the medium by

$$\delta = \frac{(n_2 - n_1)L}{\lambda_o} \cdot 2\pi = \Delta n\left(\frac{2\pi L}{\lambda_o}\right). \qquad \text{(III-54)}$$

Thus from equations (III-44) and (III-54) the real parts γ_{oi} of the propagation constants for the medium are related to the optical retardation δ by

$$(\gamma_{o1} - \gamma_{o2})L = \frac{2\pi}{\lambda_o}(n_1 - n_2)L = -\delta. \qquad \text{(III-55)}$$

Thus from equations (III-53) and (III-55)

$$\theta' = -\frac{1}{2}\delta \pm 2m\pi = -\left(\frac{\pi L}{\lambda_0}\right)\Delta n \pm 2m\pi \qquad \text{(III-56)}$$

where θ' is measured in radians, so that the magnitude and the sign of δ, and hence of Δn, may be determined by measuring the polarization direction of the plane polarized ray emerging from the quarter wave plate. A positive angle θ' corresponds to a negative value of Δn and vice versa. As is shown in Figure 13, the orientation of the plane polarized ray exiting from the quarter wave plate is determined by rotating a plane polarizing prism analyzer until no light is transmitted through the analyzer. The analyzer is thus oriented so that its transmission direction is orthogonal to the polarization direction of $\vec{E}''$ and hence is at an angle $(\theta' + \frac{\pi}{2})$ to $\vec{u}_p$. Figure 14 illustrates the principle of operation of the Senarmont compensator in simplified form.

The velocity gradients produced in a medium sheared in a concentric cylinder apparatus have been analyzed in detail in the literature (24, 32). The velocity gradient g at a point P in the gap is defined herein as

$$g_P = \left.\frac{\partial \dot{\xi}}{\partial z}\right|_P \qquad \text{(III-57)}$$

where $\dot{\xi}$ is the velocity of the fluid at the point and the coordinate system is that shown in Figure 13. This specification of the velocity gradient is identical to that used for the oscillatory measurements already discussed. From equation (III-57) the velocity gradient

Figure 14. Diagram Illustrating the Principle of Operation of the Senarmont Compensator.

A. Plane polarized light incident on the fluid layer. $\vec{u}_1$ and $\vec{u}_2$ are the principal directions of the polarizability tensor for the fluid. $\omega t = \frac{\pi}{2}$.

B. Elliptically polarized light entering the $(\lambda/4)$ plate after passage through the fluid layer with retardation δ , assuming that the slow axis of the fluid is in the $\vec{u}_1$ direction and that there is no attenuation on passage through the fluid. $\omega t = (\pi/2)$. $\vec{E}$ is confined to the box indicated, and will touch all four sides of the box during one period unless $\vec{E}$ is plane polarized. The ellipse drawn illustrates the motion of the end point of $\vec{E}$ during one cycle corresponding to the values of $\vec{E}_{u_1}$ and $\vec{E}_{u_2}$ drawn in the figure.

C. Plane polarized light leaving the $(\lambda/4)$ plate assuming that the slow axis of the plate is along the $+\vec{y}$ axis. $\omega t = \frac{\pi}{2}$. The transmitted $\vec{E}$ is plane polarized and is oriented at an angle θ' to the $\vec{y}$ vector. Note that the $|\vec{E}|$ is given by $|\vec{E}| = (E_M/\sqrt{2})[1 - \cos\delta + 1 + \cos\delta]^{\frac{1}{2}} = E_M$ so that the maximum value of $\vec{E}$ lies on the circle for all values of δ .

A.

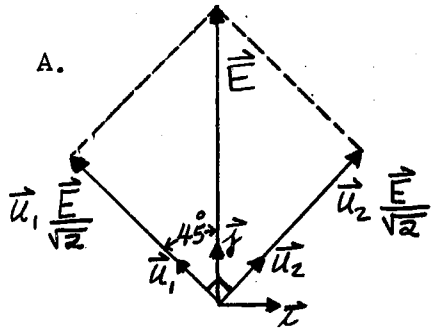

$$\vec{E} = \vec{j}\, E_M \sin \omega t = \vec{E}_{u_1} + \vec{E}_{u_2}$$

$$= \frac{(\vec{u}_1 + \vec{u}_2)}{\sqrt{2}} E_M \sin \omega t$$

$$\vec{E}_{u_1} = \vec{u}_1 \frac{E_M}{\sqrt{2}} \sin \omega t$$

$$\vec{E}_{u_2} = \vec{u}_2 \frac{E_M}{\sqrt{2}} \sin \omega t$$

B.

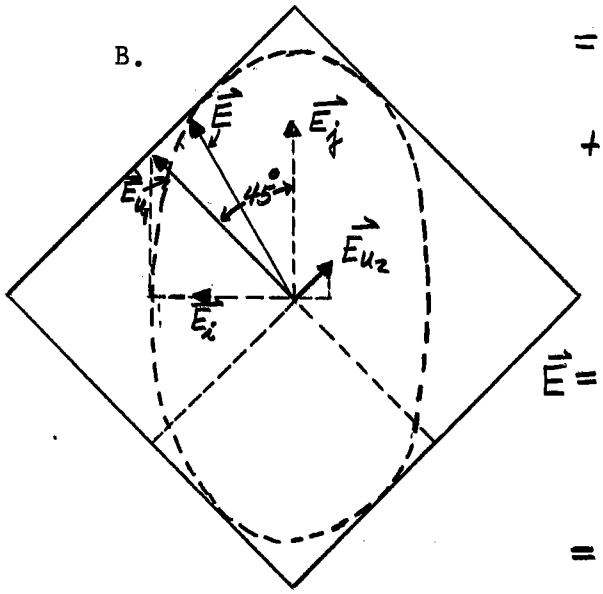

$$\vec{E} = \vec{E}_{u_1} + \vec{E}_{u_2} = \vec{E}_i + \vec{E}_j$$

$$= \left[\vec{u}_1 \frac{E_M}{\sqrt{2}} \sin(\omega t' + \delta) + \vec{u}_2 \frac{E_M}{\sqrt{2}} \sin \omega t'\right]$$

$$\vec{E} = E_M \left\{\vec{i}\left[\tfrac{1}{2}\sin \omega t' - \tfrac{1}{2}\sin(\omega t' - \delta)\right] + \vec{j}\left[\tfrac{1}{2}\sin \omega t' + \tfrac{1}{2}\sin(\omega t' - \delta)\right]\right\}$$

$$= \frac{E_M}{\sqrt{2}}\left[\vec{i}\,(1 - \cos\delta)^{\frac{1}{2}} \sin\left(\omega t' - \tfrac{\pi}{2} - \tfrac{\delta}{2}\right) + \vec{j}\,(1 + \cos\delta)^{\frac{1}{2}} \sin\left(\omega t' - \tfrac{\delta}{2}\right)\right]$$

c.

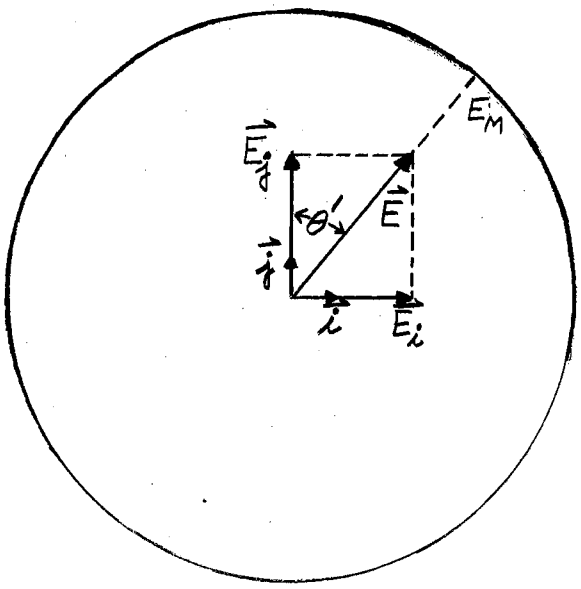

$$\vec{E} = \vec{E}_i + \vec{E}_j$$

$$= \frac{E_M}{\sqrt{2}}\left[\vec{i}\,(1-\cos\delta)^{\frac{1}{2}}\sin\left(\omega t'' - \frac{\delta}{2} - \frac{\pi}{2}\right) + \vec{j}\,(1+\cos\delta)^{\frac{1}{2}}\sin\left(\omega t'' - \frac{\delta}{2} - \frac{\pi}{2}\right)\right]$$

$$\tan\theta' = \frac{|\vec{E}_i|}{|\vec{E}_j|} = \frac{(1-\cos\delta)^{\frac{1}{2}}}{(1+\cos\delta)^{\frac{1}{2}}}$$

$$\therefore \tan\theta' = \pm\tan\left(\frac{\delta}{2}\right)$$

$$\theta' = \pm\left(\frac{\delta}{2}\right) \pm n\pi, \quad n = 0, 1, 2, \cdots.$$

$$|\vec{E}| = \frac{E_M}{\sqrt{2}}\left[1-\cos\delta+1+\cos\delta\right]^{\frac{1}{2}} = E_M$$

generated at the point P in a concentric cylinder system with rotating outer cylinder is given by (32)

$$g_P = -2\Omega \frac{1/(R_i - z)^2}{1/R_i^2 - 1/R_o^2} \qquad \text{(III-58)}$$

where Ω is the angular velocity of the rotating outer cylinder, R_o is the radius of the outer cylinder and R_i is the radius of the inner cylinder. Note that the velocity gradient defined as above will always be negative in sign. If the gap width $D = R_o - R_i$ is sufficiently small that $D << R_i$, then equation (III-58) yields a constant value for the velocity gradient given by

$$g \simeq -\frac{R_i \Omega}{D} \simeq -\frac{R_o \Omega}{D} \simeq -\frac{(R_i - z)\Omega}{D}. \qquad \text{(III-59)}$$

For the apparatus described, the magnitude of the velocity gradient will vary about 6 percent over the 0.030" gap. The use of the approximation expression (III-59) with $(R_i - z) = 1.015"$ yields a value for g that is within 1 percent of the exact value obtained at the same point using equation (III-58). All gradient values listed in this work were computed from equation (III-59) using $(R_i - z) = 1.015"$, $D = 0.030"$ and values of Ω computed from measurements of the period of rotation of the inner cylinder.

The mechano-optic constant S^* was defined for oscillatory flow $(\omega \neq 0)$ by equation (II-238) and for steady flow $(\omega = 0)$ by equation (II-240). For the coordinate system of Figure 13,

$$S_o = S_{Mo} e^{i\theta_o} = + \frac{\Delta n}{g}\Big|_{\omega=0}. \qquad \text{(III-60)}$$

Thus from equations (III-56) and (III-57),

$$S_0 = + \frac{\theta' \lambda D}{\pi L (R_i - Z) \Omega} = \pm S_{MO} \qquad \text{(III-61)}$$

so that S_0 may be computed from the measured values of θ' and Ω. Since the velocity gradient g is always negative, the sign of S_0 is opposite to that of Δn, so that for Δn positive, θ_0 is ± 180 degrees and for Δn negative, θ_0 is 0 degrees. For the polystyrene solutions studied, Δn is positive, so that $S_0 = -S_M$ giving $\theta_0 = \pm$ 180 degrees.

Figure 15 shows a simplified block diagram of the concentric cylinder apparatus. A super pressure mercury arc lamp serves as the light source S. Lens L_1 is used to reduce the effective source size seen by lens L_2 and to produce a small pencil of light to be interrupted by the chopper assembly LC. Lens L_2 forms an image of the image formed by L_1 in the gap between the concentric cylinders contained in the head H. The beam size in the gap converges from approximately 0.014" at the entering edge of the gap to 0.010" at the focus and then diverges to approximately 0.012", assuming an aperture setting of f-32 for lens L_2. The front surfaced mirror M may be adjusted to send the light beam through the gap parallel to the cylinder axes. The beam shifter BS is used to displace the beam without altering its propagation direction. The polarizer P, analyzer A and quarter wave plate $\lambda/4$ are mounted on a rotating arm assembly RH which can be moved so that the polarizer transmission axis may be rotated approximately 50 degrees either side

Figure 15. Diagram of the Coaxial Cylinder System Showing the Light Source S, the Lens L, the Light Chopper Assembly LC, the Lens L_2, the Beam Shifter BS, the Mirror M, the Polarizer P, the Rotating Handle RH of the Vertical Optical Bench, the Analyzer A, the Quarter Wave Plate $(\lambda/4)$, the Air Bearing AB, the Torsion Fiber W, the Interference Filter IF, the Photomultiplier PM, the Drive Head H, the Temperature Control Coils C and the Insulating Spacers IS and I.

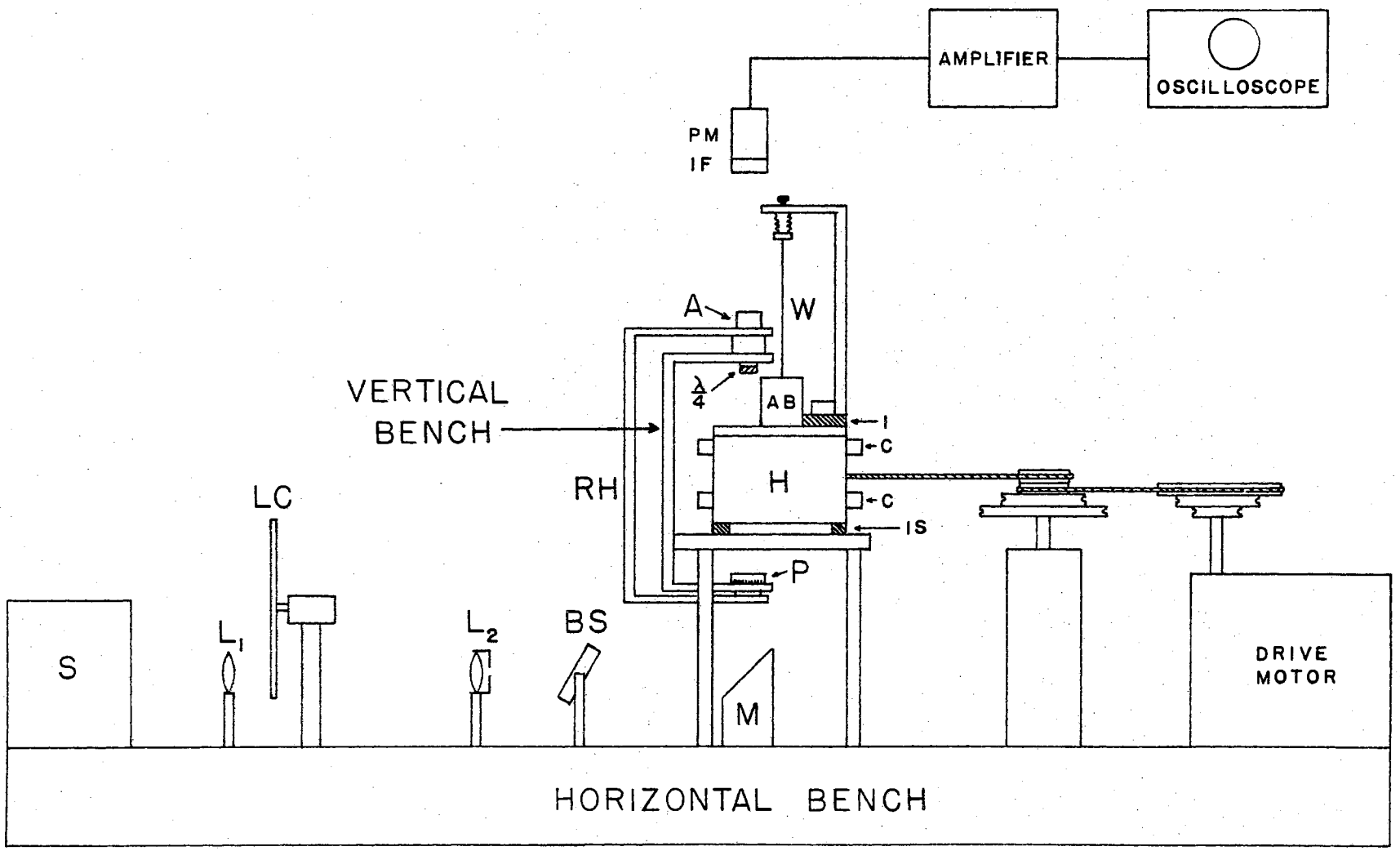
AMPLIFIER
OSCILLOSCOPE
PM
IF
A
W
VERTICAL
BENCH
λ/4
AB
I
C
H
C
RH
IS
P
LC
S
L1
L2
BS
M
DRIVE
MOTOR
HORIZONTAL BENCH

of the streamline direction in the gap. The polarizer and analyzer are Glan Thompson polarizing prisms. A scale mounted on the polarizer reads the angle χ directly. The $(\lambda/4)$ plate ($\lambda/4$ at 5800 Å) is a mica plate sandwiched between optical glass, and is attached to the rotating arm assembly so that the fast direction of the plate is parallel to the polarizer transmission direction for all arm positions. The analyzer may be rotated separately from the arm assembly, and is equipped with scales to read the angle θ' in degrees between the normal to its transmission direction and the polarizer transmission direction corresponding to the angle θ' of Figure 13. The analyzer is followed by a 5800 Å second order interference filter IF that can be removed to improve the setting accuracy for measurement of the angle χ. The transmitted intensity may be detected by a photomultiplier assembly PM, or by eye, using a telescope to view the liquid in the gap. The photomultiplier output is fed to an amplifier providing either 20 or 40 db gain which feeds the vertical amplifier of an oscilloscope. With chopping rates of near 200 per second this detection scheme readily detects optical retardations of less than 0.01 degrees, although the dials used to measure θ' and χ are accurate to only ± 0.1 degree.

The driving head H consists of the concentric cylinders, the precision angular contact ball bearings which position the rotating outer cylinder and the air bearing-torsion wire assembly used for viscosity measurements. Since the outer cylinder is rotating, the entire bottom of this cylinder is made of a Schott optical glass, number SFS-09PF. Residual retardations in the glass are sufficiently small to be almost undetectable. The upper window is made from selected

microscope cover glass and likewise has almost undetectable residual birefringence. The sides of the driving head are surrounded by cooling coils in which flows an ethylene glycol solution from a constant temperature circulator. The head is mounted on spacers IS made of Delrin to insulate it from the steel supporting bench. The temperature of the head may be varied from about -5°C to +90°C. The measurement of the fluid temperature is accomplished by measuring the resistance of a thermistor imbedded in the inner cylinder near the outer surface of the cylinder.

The outer cylinder is rotated by means of a belt and pulley system as shown in Figure 2. The driving motor is a reversible 1/15 horse power motor equipped with a variable speed control. This motor-pulley arrangement will generate usable velocity gradients from about 1 to 640 per second. The velocity gradients are determined from measurements of the time T required for 1/20 of a complete rotation of the moving cylinder, as obtained by feeding the output of a photodetector, mounted behind an illuminated slotted chopping ring attached to the rotating cylinder, to a counter. Thus from equation (III-59) and the stated dimensions of the cylinder the velocity gradient at the center of the gap is related to the time interval by

$$g = -\frac{10.63}{T} \qquad \text{(III-62)}$$

where g has units of sec^{-1} if T is measured in seconds.

The method of measurement of the flow birefringence is to determine the angle χ by rotating the crossed polarizer-analyzer system by moving the rotating handle until no light is transmitted through the analyzer, then to set the polarizer transmission direction to

$(\chi + \pi/4)$, as indicated in Figure 12, followed by a rotation of the analyzer only, until a minimum transmitted intensity is obtained. From the angle θ' read on the analyzer dial the magnitude and sign of Δn are obtained, while the time interval measurement yields the magnitude of the velocity gradient from equation (III-62). From equation (III-56) Δn is related to θ' by

$$\Delta n = -6.444 \times 10^{-8} \theta', \qquad \text{(III-63)}$$

for θ' measured in degrees, with $\lambda_0 = 5800$ Å and $L = 5.00$ cm. The interference filter may be removed for the extinction angle measurement, but should be inserted for the measurement of θ'. The calibration of the extinction angle dial is accomplished by repeatedly reversing the rotation direction of the cylinder, resetting the scales until the same value of χ is obtained for both directions of rotation. The calibration of the analyzer scale is accomplished by removing the driving head and quarter wave plate and setting the prisms for extinction. The analyzer scale should indicate 0 degrees with the prisms crossed. It should be noted that for fluids exhibiting dichroism the value obtained for Δn from equation (III-56) will be erroneous.

The coaxial cylinder system may also be used to measure the steady flow viscosity. As is shown in Figure 15, the inner cylinder is suspended on a torsion wire W held by a superstructure attached to the top plate of the system. An air bearing AB centers the inner cylinder and provides an almost frictionless guide for the shaft extending upward from the cylinder. Thus when the outer cylinder is rotated, the viscous drag on the inner cylinder due to the viscosity of the liquid

in the gap causes it to rotate through a small angle. The angle of rotation depends on the viscosity of the medium in the gap, the torsion constant of the wire and the rotation rate of the outer cylinder. The measurement of the angle of rotation is accomplished by detecting a change in the electrical capacitance of two metal plates separated by a narrow air gap. The plates are mounted so that the rotation of the inner cylinder alters the engagement of the plates, thus producing a change in capacitance. The capacitance of the plates is in the charging circuit of a transistorized unijunction relaxation oscillator so that a change in capacitance produces a change in frequency of the oscillator which is then measured by a counter. A micrometer screw is utilized to calibrate the oscillator by rotating the inner cylinder through a known angle. Thus if the torsion constant of the wire is known, the viscosity may be determined by measuring the oscillator frequency change and the velocity gradient as described previously. The torsion fibers used are made from tempered beryllium copper and have diameters ranging from 0.016 inch to 0.125 inch. The fibers were calibrated by using liquids of known viscosity, namely, distilled water for the smaller and a glycerol solution for the larger fibers. Utilizing the velocity gradient range capability of the instrument as well as the range of torsion fiber constants, one can measure viscosities from less than 1 centipoise to approximately 800 poises to within 6 percent, the uncertainty being due largely to speed variations of the drive motor.

CHAPTER IV

EXPERIMENTAL RESULTS

1. Preparation of Solutions

Oscillatory flow birefringence measurements as well as steady flow birefringence and viscosity measurements have been carried out for three different polystyrene solutions containing different molecular weights of polystyrene, using the same viscous solvent, Aroclor 1248, lot KD-507, a chlorinated biphenyl manufactured by and obtained from the Organic Chemicals Division of the Monsanto Chemical Corporation. The Aroclor 1248, lot KD-507, has a density of 1.44 gm/cc at 25°C, a viscosity of 2.24 poises at 25°C and a molecular weight of approximately 292. The polystyrene samples obtained from Dr. H. W. McCormick of the Dow Chemical Company were as follows: polystyrene S102, having a weight average molecular weight of 82,000; polystyrene S111, having a weight average molecular weight of 239,000; polystyrene S13, having a weight average molecular weight of 968,000. The polystyrene samples were fairly sharp fractions, especially the lower molecular weight samples, as indicated by the ratios of weight average molecular weight $\overline{M}_w$ to number average molecular weight $\overline{M}_N$ of 1.51 for the S13 sample, 1.08 for the S111 sample and 1.05 for the S102 sample. The polystyrene samples were put into solution by combining the desired amount of the solid polystyrene and Aroclor 1248 in a glass bottle, then placing the bottle in a thermostatted oven for

approximately three weeks at a temperature of 65°C. Occasionally the contents of the bottle were stirred gently using a glass rod. After the solutions had been heated for three weeks, the bottles were removed from the oven and stored in a dark cabinet in an air conditioned room. The solutions were prepared in different concentrations in an attempt to obtain a convenient level of birefringence for each solution. The S102 was prepared as a 4 percent solution, the S111 as a 2 percent solution and the S13 as a 1 percent solution, where the concentration figure given, denoted by c_w , designates the ratio of the weight of the polymer to the total weight of the final solution, in percent. These concentrations give a mass of polymer per unit volume of solution of 5.70×10^{-2} gm/cm^3 for the S102 solution, 2.86×10^{-2} gm/cm^3 for the S111 solution and 1.44 gm/cm^3 for the S13 solution. Another solution of 2 percent polystyrene S111 in Aroclor 1248 obtained from Dr. W. Philippoff of the Esso Research and Engineering Company has been studied previously in this laboratory. No significant difference between the oscillatory flow birefringence exhibited by this solution and that exhibited by the solution prepared in our laboratory for the present study could be detected, indicating that the preparation techniques employed yielded equivalent solutions. Measurements of the steady flow birefringence and viscosity as well as oscillatory flow birefringence of solutions of S111 in Aroclor 1248 have been reported previously (72, 92). Viscosity measurements for solutions subjected to oscillatory shear have also been given for solutions of S111 in toluene, methyl ethyl ketone and cyclohexane and for solutions of S102 and S111 in Aroclor 1248 (29, 57).

Polystyrene is obtained from the polymerization of the monomer

styrene. Styrene has a molecular weight of 104.14, a density of 0.9074 gm/cc at 20°C and an index of refraction of 1.546 for the Sodium D line at 20°C (74). The styrene molecule is one of the arene family, a family of compounds that contain both aliphatic and aromatic elements. The chemical structure is indicated below, where the ring structure is the phenyl ring C_6H_5 (63).

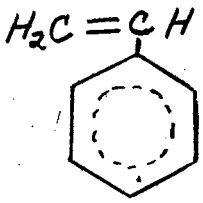

The phenyl ring is thought to have a width of about 6 Å and a thickness of 3.7 Å (28). An anionic polymerization procedure was used for the preparation of the polystyrene samples S102, S111, and S13. The anionic procedure apparently produces sharper molecular weight fractions for polystyrene than other polymerization techniques (1, 85, 87). The polystyrene molecule obtained by this polymerization procedure is usually of the atactic form in which the phenyl group is arranged randomly about the carbon chain backbone as shown below.

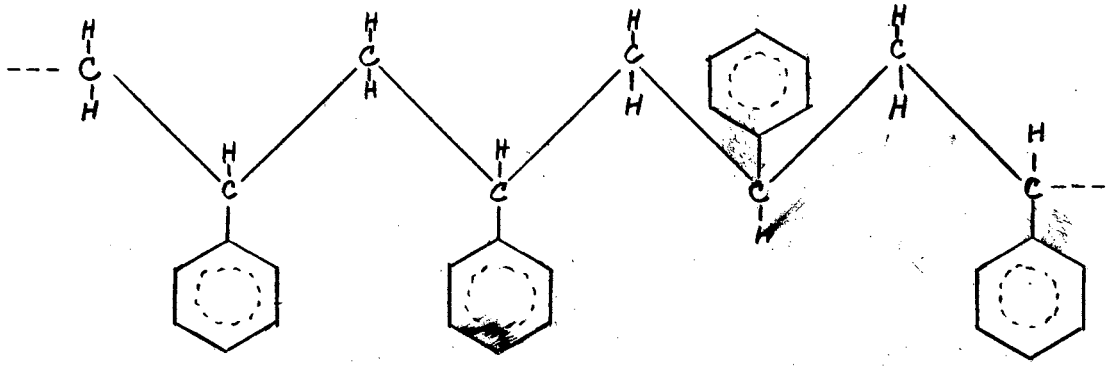

The distance between the centers of the carbon atoms of the chain backbone for a hydrocarbon of the form C_NH_{2N} have been determined as 1.55 Å (51, 84). From a compilation of light scattering, X-ray scattering and viscosity data, the distance between alternate carbon atoms in such a chain is thought to be 2.54 Å, and the valence bond angle to be 110 degrees (5, 84). Denbigh (23) gives values for the principal polarizabilities along and normal to a C-C bond as 18.8×10^{25} cm^3 and 0.2×10^{25} cm^3 respectively. The rotation about a carbon bond at the valence angle is hindered even for the relatively simple C_NH_{2N} hydrocarbons. There are three potential energy maxima and minima for one complete rotation, the potential energy difference between a maximum and a minimum being on the order of 3×10^3 calories per mole (84). Since polystyrene differs from the C_NH_{2N} hydrocarbons due to the large phenyl group extending in a direction normal to the backbone, and the width of the phenyl group is approximately 6 Å, the phenyl groups can be expected to interfere with each other sufficiently to further restrict the rotation of the C-C bonds in the chain backbone (28). Also, the close proximity of the phenyl groups may modify the distance between alternate carbon atoms in the chain backbone. The "diameter" of the atactic polystyrene chain has been estimated to be greater than 6 Å and less than 15 Å (5, 23). Typical values given for the valence bond angle for atactic polystyrene range from 110 degrees to 120 degrees (1, 28, 61, 85, 87). Dielectric measurements for solutions of atactic polystyrenes indicate that the polymer chain is fairly rigid, apparently due to the interference of the bulky phenyl side groups (21). Kuhn and Kuhn (55) calculated the difference between maximum potential energy values for rotation about a carbon bond as 1.14×10^4

calories per mole, a value almost 4 times that attributed to the C_NH_{2N} chain, again indicating that the chain is fairly stiff. Thus it would seem reasonable that several C-C bonds in the chain backbone of polystyrene would need to be incorporated in a Zimm subchain in order to approximate a random coil model for the chain. Atactic polystyrene in the solid form exhibits an index of refraction between 1.59 and 1.60 for the Sodium D line (5893 Å) and a density ρ = 1.06 gm/cc at 25°C (73).

An isotactic form of polystyrene has been obtained by Natta and co-workers by the addition of a special catalyst (64). The isotactic form is a more ordered chain in which the phenyl groups are oriented predominantly on one side of the chain as shown below.

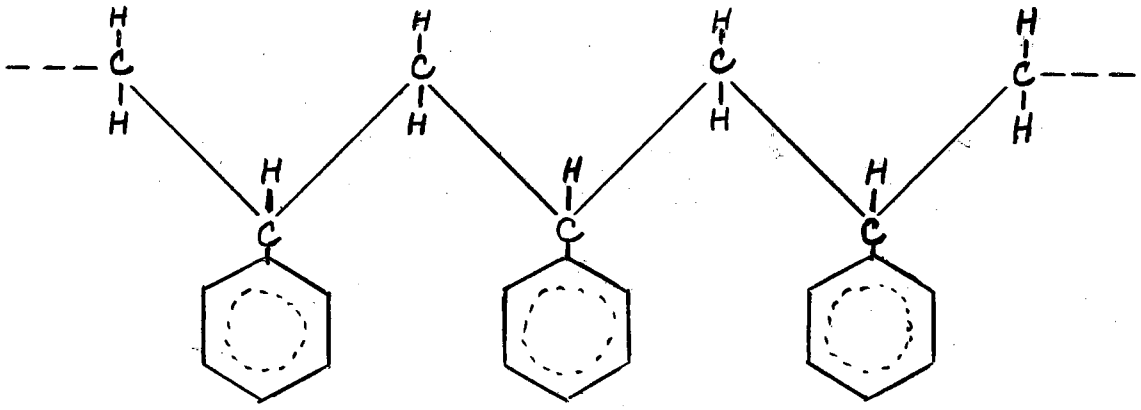

The isotactic form will form crystallites in the pure polymer state, while the atactic form will not, and it apparently forms a more rigid chain structure than that of the atactic form (1, 28, 61, 85, 87). The atactic form cannot be altered to the isotactic form by rotation of the chain carbon atoms (63, 64). The glass transition temperature for isotactic polystyrene is between 80 and 100°C (73).

Aroclor 1248 is listed by the manufacturer, Monsanto Chemical Company, as being a chlorinated polyphenyl having a molecular weight of approximately 292 (62). Other literature lists the Aroclor 1248

as an industrial grade chlorinated biphenyl (22, 29, 38, 72). Thus it would appear that the Aroclor 1248 is a biphenyl structure, having 4 chlorine atoms substituted for hydrogen atoms on the phenyl structures. Since the location of the chlorine atoms on the structure is unknown, and the material is an industrial grade product, it is difficult to speculate on the hindrance to rotation of the C-C bond joining the phenyl structures, as well as the orientation of the two structures relative to each other. One of several possible structures is shown below.

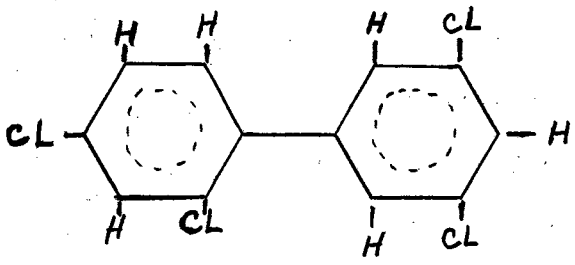

Such a structure would have a molecular weight of 292. It would appear that the dimensions of a styrene molecule are probably somewhat smaller than those of the Aroclor molecule.

The end-to-end length for dilute solutions of atactic polystyrene molecules in various solvents has been estimated from light and X-ray scattering data as well as from viscosity data. It would appear that for temperatures near room temperature, in nonflowing solutions using solvents such as cyclohexane, decalin or benzene, the S102 molecule ($\overline{M}_w \simeq 82{,}000$) could be expected to exhibit an end-to-end length of 2.1 to 2.7 x 10^2 Å, while the S13 molecule ($\overline{M}_w \simeq 968{,}000$) would exhibit a length of between 7.2 and 7.8 x 10^2 Å (73).

The optical polarizability $(\alpha_1 - \alpha_2)$ for one link of a Zimm subchain of the polystyrene chain has been evaluated by Tsvetkov for

polystyrene in bromoform (98). He found $(\alpha_1 - \alpha_2) = -1.45 \times 10^{-23}$ cm^3 for atactic and -2.24×10^{-23} cm^3 for isotactic polystyrene. Other experimenters have listed values for $(\alpha_1 - \alpha_2)$ in various solvents, but the values apparently were not corrected for the form birefringence contribution, which in most cases was large (50, 51, 54). Since the major contribution to the polarizability of the polystyrene in steady flow is that of the phenyl side group which has its largest principal polarizability in the direction of the C-C bond linking the phenyl group to the chain backbone, the sign of $(\alpha_1 - \alpha_2)$ will be negative. The larger value of $(\alpha_1 - \alpha_2)$ for the isotactic polystyrene is attributed to the higher degree of ordering of the phenyl groups (98). The phenyl side group is usually assumed to have an anisotropy of polarizability approximately equal to that of benzene, which is 60×10^{-25} cm^3. Since the chain backbone of the polystyrene chain should have a molecular polarizability near that of a C-C bond, 18.6×10^{-25} cm^3, the excess polarizability for a section of the polystyrene chain should be normal to the chain giving a negative value of $(\alpha_1 - \alpha_2)$ (23, 99). Also, since the value of $(\alpha_1 - \alpha_2)$ for the link of a Zimm subchain as given by Tsvetkov is so large, there must be several monomer units per link (99). From the polarizability values listed above, the number of monomers per link would appear to be greater than 3. Tsvetkov calculated the rotational freedom to be expected for various side groups of various polymer chains (98). He indicates that the phenyl group of the polystyrene molecule has less rotational freedom than side groups in many other polymers, the isotactic form having less freedom of rotation than the atactic form, and hence the largest values of $(\alpha_1 - \alpha_2)$. The value

of $(\alpha_1 - \alpha_2)$ has been found to be relatively independent of the solvent material for several polymer solute-solvent combinations. However, there are notable exceptions (98). For some polymeric systems, the change of intrinsic anisotropy with solvent is thought to be caused by a change in the interaction between the side groups and the solvent (98).

Tsvetkov has analyzed the form effect for solutions of polystyrene in butanone, dioxane, toluene, benzene and bromoform, as well as for polymethyl methacrylate in benzene and polybutadiene in benzene (97). From the measurements presented therein, it appears that the form birefringence is negligible when the difference between the solvent mean index of refraction and the mean polymer index of refraction is less than 0.1. For the polystyrene-Aroclor 1248 solutions studied herein the difference between polymer and solvent indices of refraction are as follows: -0.03 at 25°C, -0.01 at 65°C, and -0.1 at 0.0°C. So, except at temperatures near 0°C, the form effect should be insignificant, and even at 0°C the contribution should be small, probably less than 3 percent of the steady flow birefringence. Thus the form effect has been neglected for the work presented herein. It is possible, however, that at high frequencies where the polymer birefringence contribution will be small the form effect may be significant, especially at temperatures near 0°C.

There is considerable evidence indicating that polystyrene when in solution is a molecular dispersion of the solute and not some micellular dispersion. For example, the viscosity increment of solutions of polystyrene appears to be relatively independent of solvent and temperature (5). Further, measurements of the partial specific

volume in various solvents are essentially that of the pure polymer (82). Sedimentation velocity data also indicates that the polymer is unchanged by the solvent (83). Measurements of the factor $(\alpha_1 - \alpha_2)$ have been made for pure polystyrene using the theoretical treatment given by Kuhn and Grün for rubberlike materials subjected to simple elongation (50, 93). This treatment incorporates the same model for an individual polymer chain as was presented in Chapter II. That is, for small extensions,

$$\gamma_1 - \gamma_2 = \frac{3}{5}(\alpha_1 - \alpha_2)\frac{h^2}{h^2} \quad . \qquad \text{(IV-1)}$$

It is further assumed that there is a gaussian structural network containing N such chains whose end-to-end vectors in the unstrained state are randomly oriented so that no net birefringence is exhibited. When the material is deformed, it is assumed that the components of the end-to-end vectors for the chains are changed by the same ratio as the corresponding dimensions of the bulk material, giving rise to a net anisotropy. Summing the contributions of all of the chains in the network gives the total polarizability of the whole network. If β_1 and β_2 are the principal polarizabilities along and normal to the direction of extension respectively, they obtain:

$$\beta_1 - \beta_2 = N(\alpha_1 - \alpha_2) \cdot \frac{1}{5} \cdot \frac{h^2}{h^2}\left(\lambda^2 - \frac{1}{\lambda}\right) \qquad \text{(IV-2)}$$

where λ is the extension ratio for the material. The stress in the gaussian network is given as

$$\tau = NkT\left(\lambda^2 - \frac{1}{\lambda}\right). \qquad \text{(IV-3)}$$

Thus

$$(n_1 - n_2) = C\tau, \qquad \text{(IV-4)}$$

where C is the stress optic coefficient given by

$$C = \frac{2\pi}{45kT} \cdot \frac{(\bar{n}^2+2)^2}{\bar{n}} \cdot (\alpha_1 - \alpha_2) \qquad \text{(IV-5)}$$

and $\bar{n}$ is the mean index of refraction of the material. Applying equations (IV-4) and (IV-5) to measured values of birefringence and stress, Tsvetkov obtained for atactic polystyrene $(\alpha_1 - \alpha_2)$ $= -1.22 \times 10^{-23}$ cm^3, a value within 15 percent of the value of $(\alpha_1 - \alpha_2)$ obtained from solution measurements (97). Assuming that the theoretical treatment is applicable, it would appear that the polymer chain is not modified appreciably, as far as optical properties of the link of the chain are concerned, by putting it in solution.

The Aroclor 1248 used as the solvent for the polystyrene solutions studied exhibits a significant amount of flow birefringence. However, the large viscosity exhibited by the Aroclor 1248 is needed to obtain coverage of the relaxing region of the oscillatory flow birefringence in view of the frequency capabilities of the equipment as presented in Chapter III. Thus the use of the Aroclor as solvent was considered essential in spite of the birefringence complication. As was noted in connection with equations (II-259) and (II-260), the optical properties of the solutions must be corrected for the solvent birefringence in

order to examine the optical properties of the polystyrene chain. Further, the nature of the correction to be applied is subject to some question. However, for the work contained herein the vector subtraction method of equations (II-259) and (II-260) will be applied. Thus for the oscillatory flow birefringence measurements in which the extinction angle χ for the solution as well as for the pure Aroclor did not deviate appreciably from 45 degrees, the correction for the solvent birefringence is given by

$$S^*_{SOLUTE} = S^*_{SOLUTION} - S^*_{SOLVENT} \qquad \text{(IV-6)}$$

Measurement of S^* versus f for the Aroclor 1248 shows that for temperatures above $-8°C$ and frequencies below 1000 cps θ is zero degrees and S_M is independent of frequency and equal to S_{MO}. Since the S^* versus f measurements do not show any deviation from the steady flow value S_o, the Aroclor viscosity for similar temperature and frequency conditions is probably equal to the steady flow viscosity. It is assumed in the following analysis of the oscillatory flow birefringence measurements that both S^* and η^* for the Aroclor 1248 are equal to the values obtained from steady flow measurements.

2. Measurements

Figures 16 through 21 present measured values of S_M and θ versus f obtained at various temperatures for the S102, S111 and S13 polystyrene solutions respectively. The measurements were obtained using the closely spaced oscillating plane and reflector system discussed in Chapter II. All measurements were made at sufficiently

Figure 16. S_M Versus f for the 4% Solution of Polystyrene S102 in Aroclor 1248 at Various Temperatures, for an Optical Wavelength of 5790 Å.

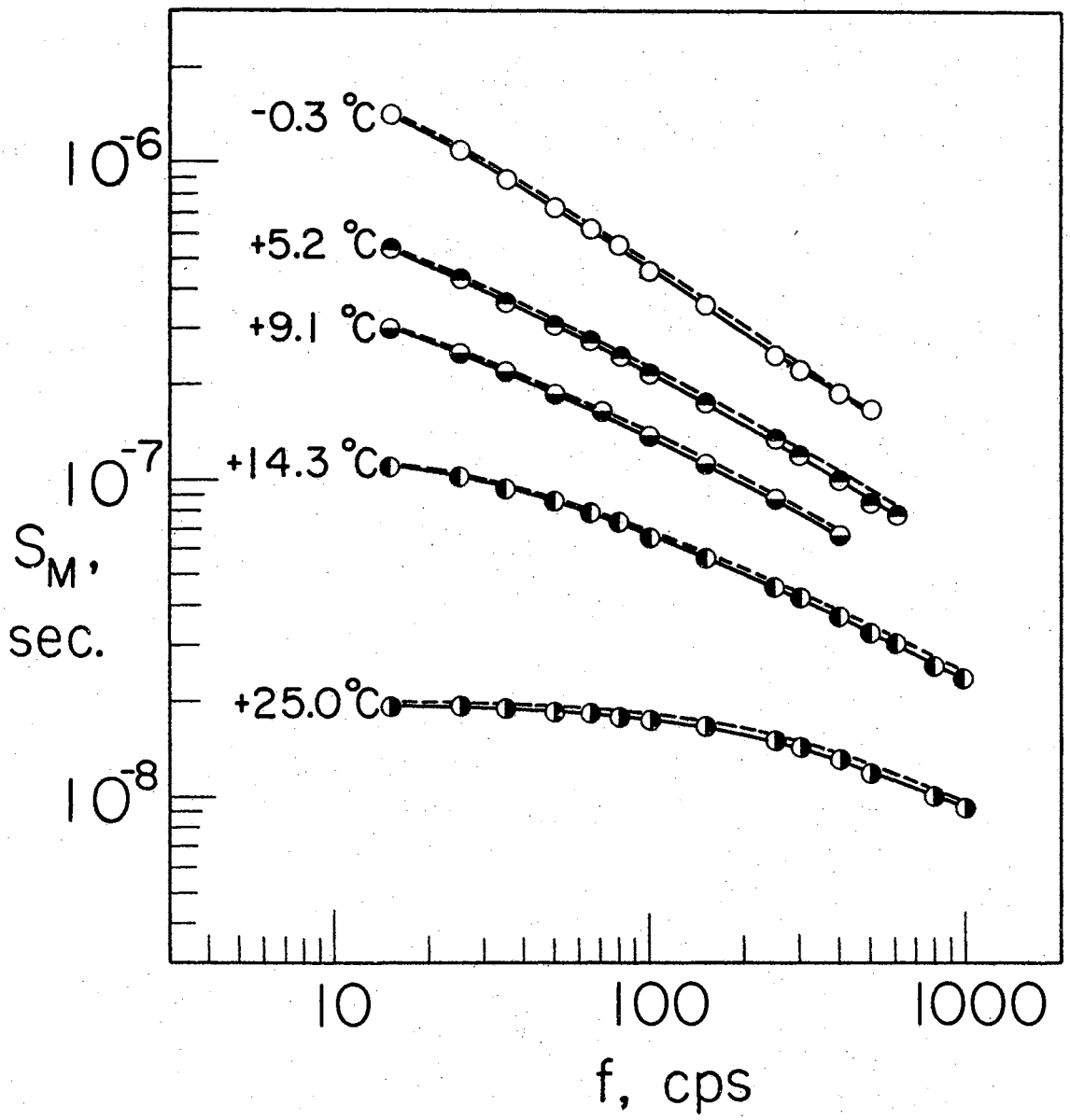
-0.3 °C
+5.2 °C
+9.1 °C
+14.3 °C
+25.0°C
10^{-6}
10^{-7}
10^{-8}
S_M, sec.
10
100
1000
f, cps

Figure 17. θ Versus f for the 4% Solution of Polystyrene S102 in Aroclor 1248 at Various Temperatures, for an Optical Wavelength of 5790 Å.

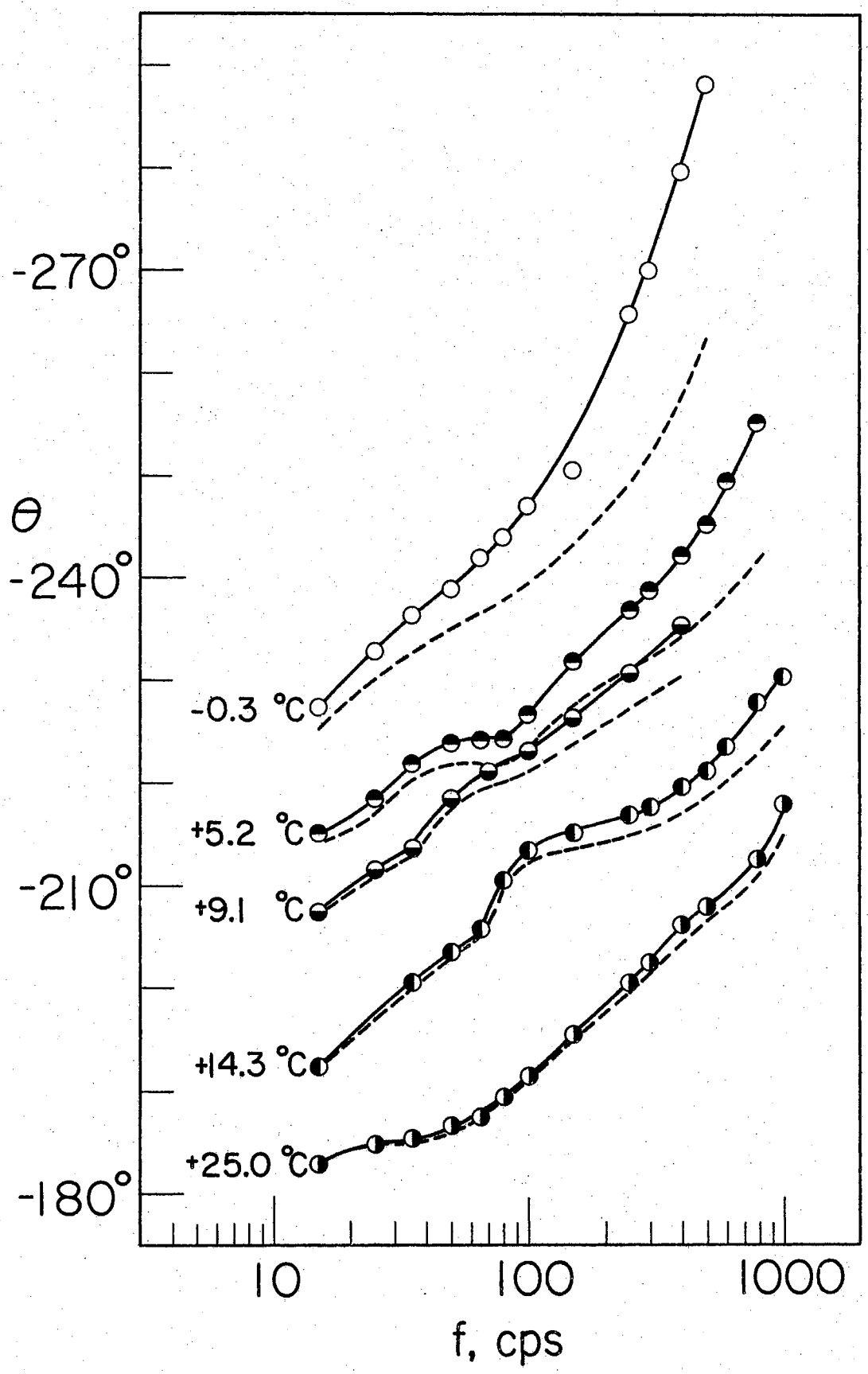
-270°
θ
-240°
-210°
-180°
-0.3 °C
+5.2 °C
+9.1 °C
+14.3 °C
+25.0 °C
10
100
1000
f, cps

Figure 18. S_M Versus f for the 2% Solution of Polystyrene S111 in Aroclor 1248 at Various Temperatures, for an Optical Wavelength of 5790 Å.

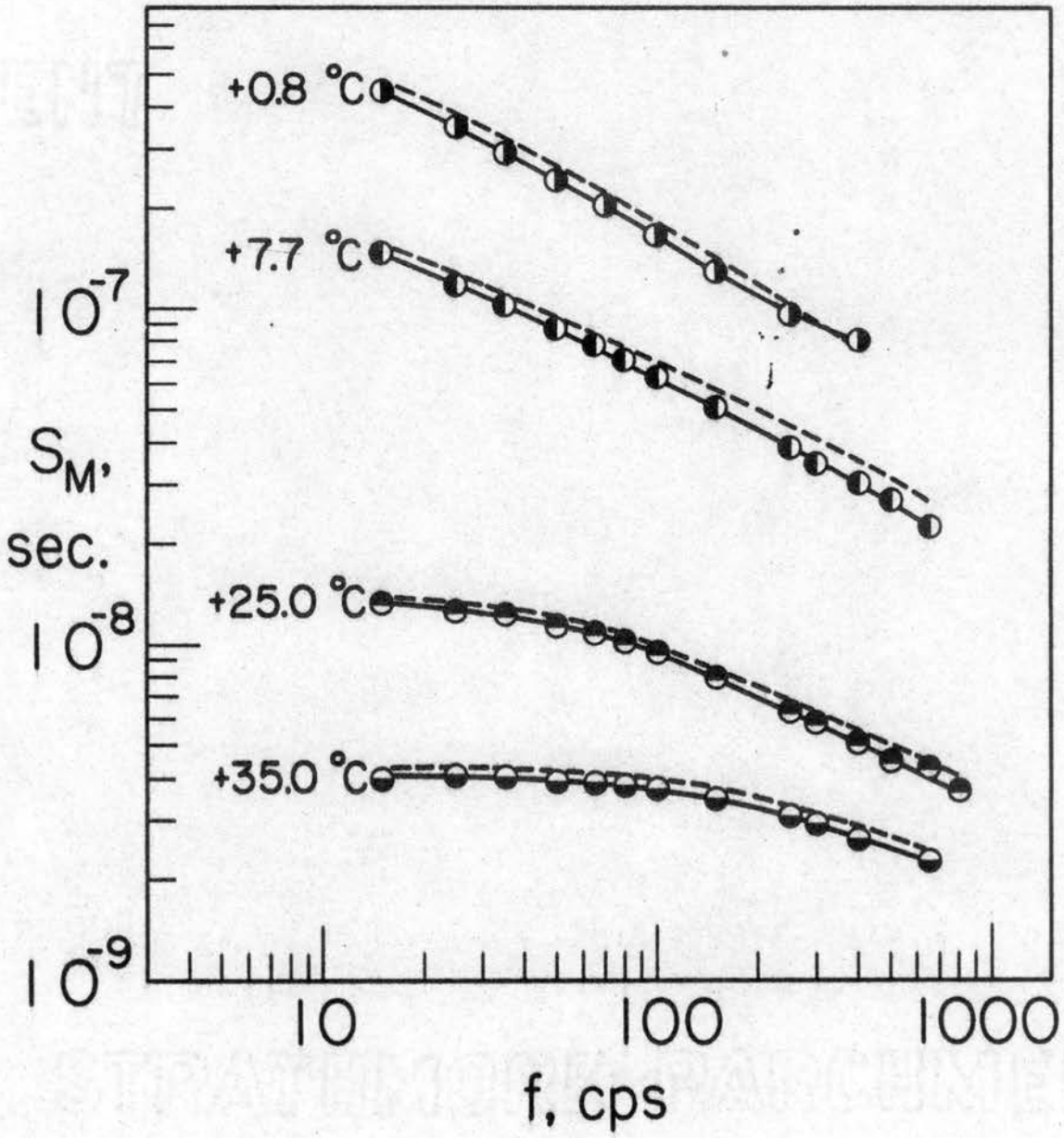
+0.8 °C
+7.7 °C
+25.0 °C
+35.0 °C
10^{-7}
S_M, sec.
10^{-8}
10^{-9}
10
100
1000
f, cps

Figure 19. θ Versus f for the 2% Solution of Polystyrene S111 in Aroclor 1248 at Various Temperatures, for an Optical Wavelength of 5790 Å.

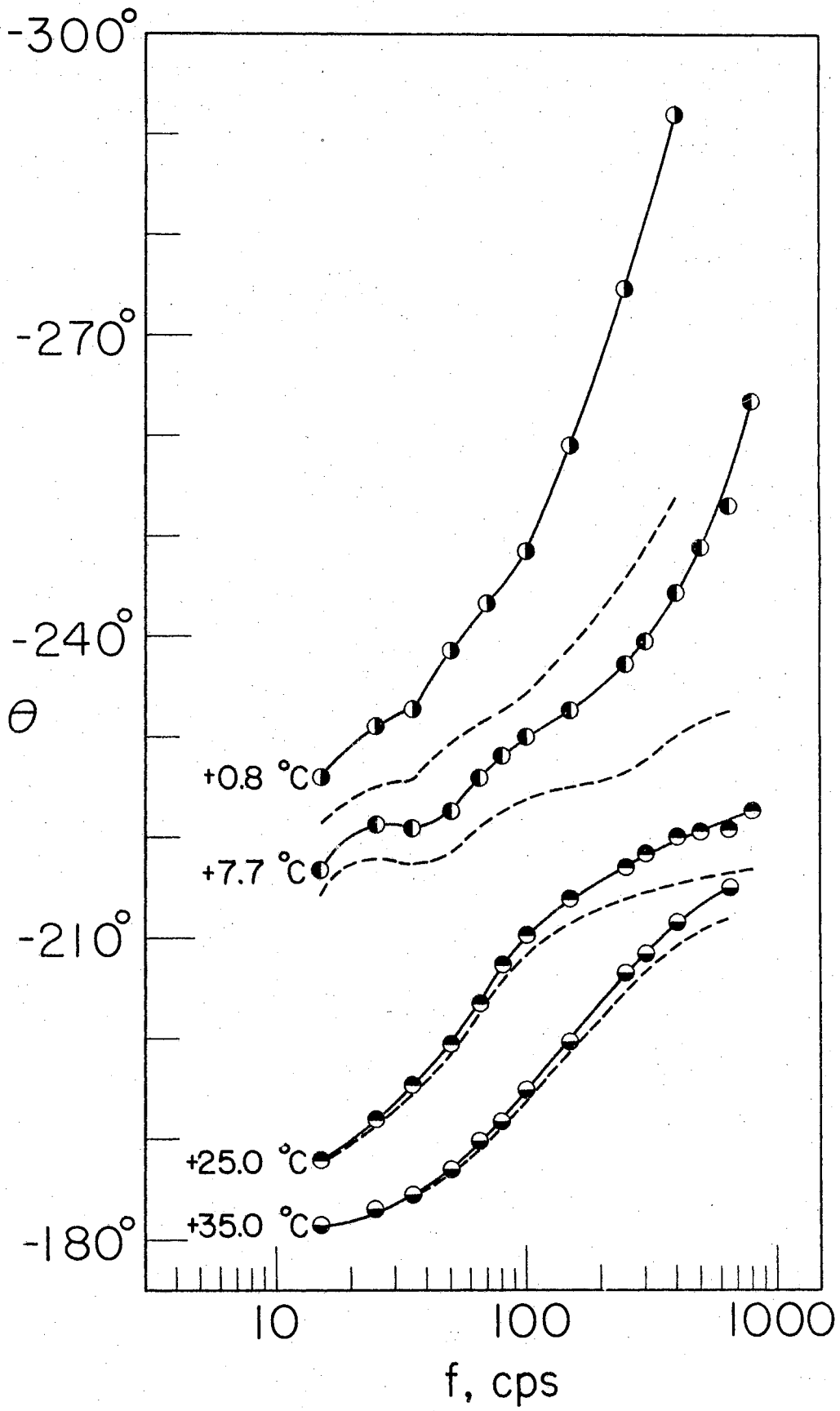
-300°
-270°
-240°
-210°
-180°
θ
+0.8 °C
+7.7 °C
+25.0 °C
+35.0 °C
10
100
1000
f, cps

Figure 20. S_M Versus f for the 1% Solution of Polystyrene S13 in Aroclor 1248 at Various Temperatures, for an Optical Wavelength of 5790 Å.

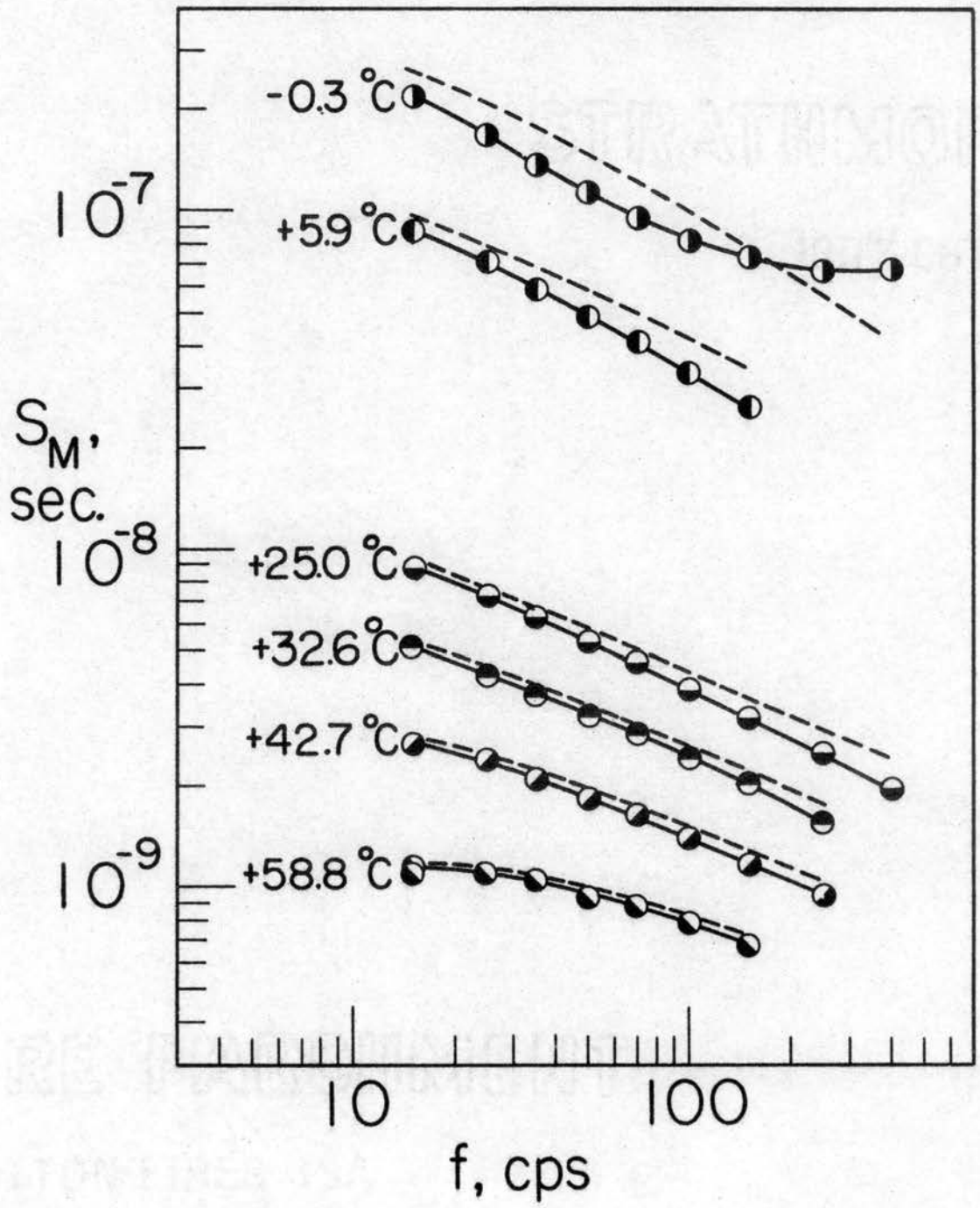
-0.3 °C
+5.9 °C
+25.0 °C
+32.6 °C
+42.7 °C
+58.8 °C
10^{-7}
10^{-8}
10^{-9}
S_M, sec.
10
100
f, cps

Figure 21. θ Versus f for the 1% Solution of Polystyrene S13 in Aroclor 1248 at Various Temperatures, for an Optical Wavelength of 5790 Å.

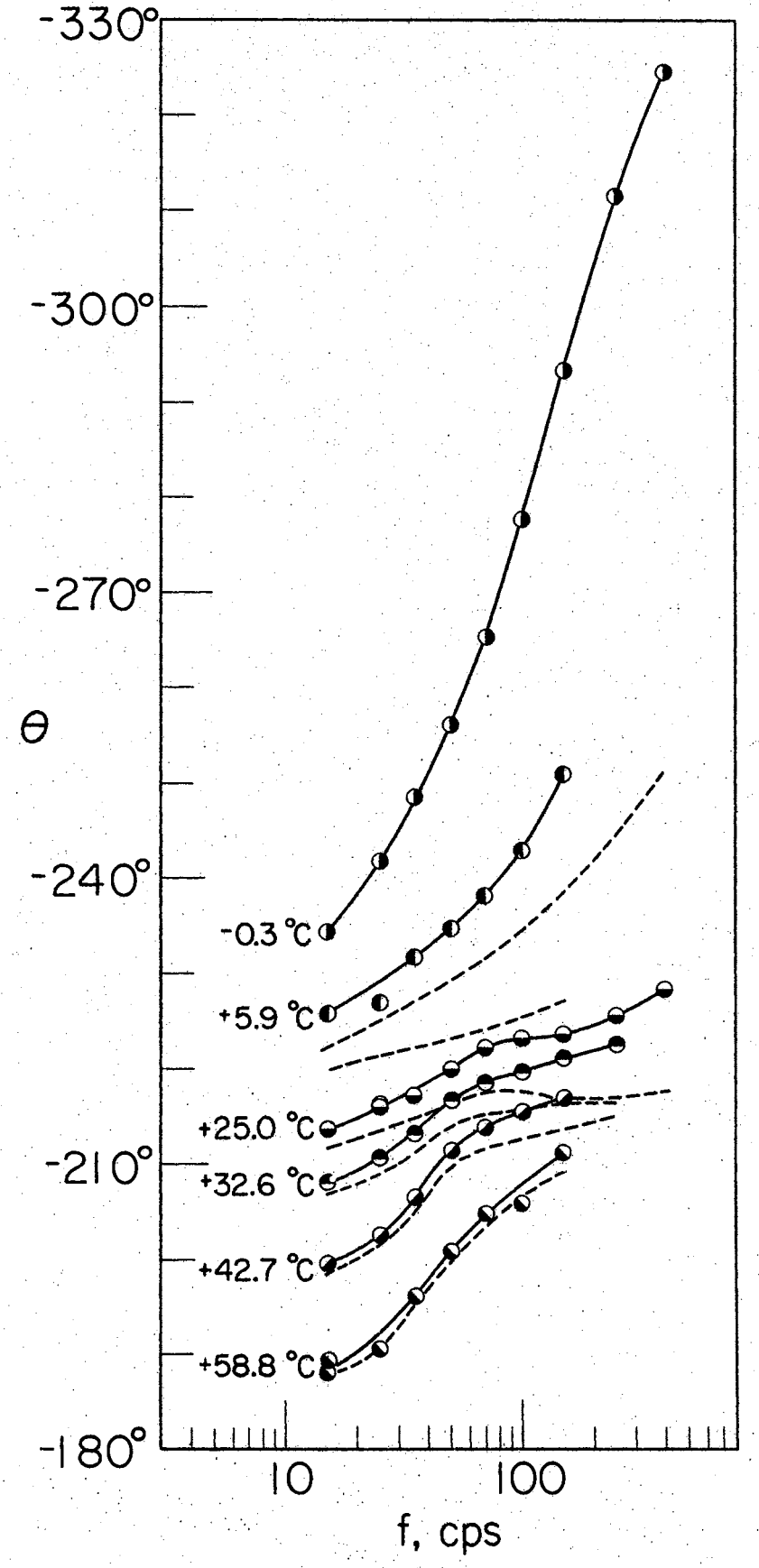
-330°
-300°
-270°
θ
-240°
-210°
-180°
-0.3 °C
+5.9 °C
+25.0 °C
+32.6 °C
+42.7 °C
+58.8 °C
10
100
f, cps

small velocity gradients that no deviation of the extinction angle from 45 degrees could be detected. The maximum gradients used for the measurements contained herein were less than 80 $sec.^{-1}$. Extinction angle modulation was detectable at increasingly lower velocity gradients as the molecular weight was increased. The data points shown in the figures are the measured values of S_M and θ before any correction for the solvent birefringence was performed. The dashed lines indicate the values of S_M and θ calculated for the polymer molecules only by performing the correction for the solvent birefringence contribution to the measured birefringence given by equation (IV-6). Since except at the highest frequencies the real part of S^* measured for the solution is of opposite sign to that of Aroclor 1248, the values of S_M obtained by correction for the solvent birefringence are for the most part larger than the uncorrected values. The correction is especially significant at high frequencies and low temperatures where the measured values of S_M for the solution are decreasing rapidly, so that the constant value S_0 for the solvent used in the correction is becoming more and more significant. For the S13 sample, the highest frequencies at which measurements could be performed for T = -0.3°C yielded values of S_M for the solution of the same order of magnitude as the solvent S_0. Thus in view of the uncertainty as to applicability of the correction procedure applied as noted in the discussion of equations (II-259) and (II-260), the corrected values of S_M and θ may not be characteristic of the chain only, and hence may not represent accurately the dynamics of the polymer chain, especially for high frequencies and low temperatures. However, the correction appears to be in the right

direction since, for example, the measured phase angles for S13 of Figure 21 exceed -320 degrees before correction, and are reduced to less than the theoretical limit of -270 degrees after correction. Also, from Figure 20, the corrected S_M curve corresponding to measurements of S^* versus f at -0.3°C corresponds more closely to the theoretical curves than does the uncorrected curve. The significance of the correction for the solvent birefringence was one of the primary reasons for not using more dilute solutions.

Figure 22 presents values of S_o versus temperature for the solvent Aroclor 1248, lot KD-507. The measurements were made on the coaxial cylinder system discussed in Chapter III. These values of were used to obtain the corrected S_M and θ curves (dashed lines) of Figures 16 through 21. Figure 23 presents corresponding values of η_o versus temperature for Aroclor 1248 obtained on the same coaxial cylinder system. Figure 24 presents values of (S_o/S_{or}) which have been corrected for the Aroclor birefringence contribution, obtained from measurements of S_o versus temperature using the coaxial cylinder system. S_{or} is the value of S_o at the reference temperature T_r = 25.0°C. From equation (II-248) it is seen that from the dilute solution theory (S_o/S_{or}) is equal to a_T if q' and c are not temperature dependent. For the work contained herein all values of a_T were obtained from equation (II-248) assuming q' and c to be essentially temperature independent. The following section indicates that the assumption regarding q' is reasonably accurate. And, since the concentration variation is proportional to the density, (c/c_r) is less than 1.01 for temperatures between 0°C and 50°C (62). The corrected S_{or} values

Figure 22. S_o Versus Temperature for Aroclor 1248, lot KD-507, for an Optical Wavelength of 5800 Å.

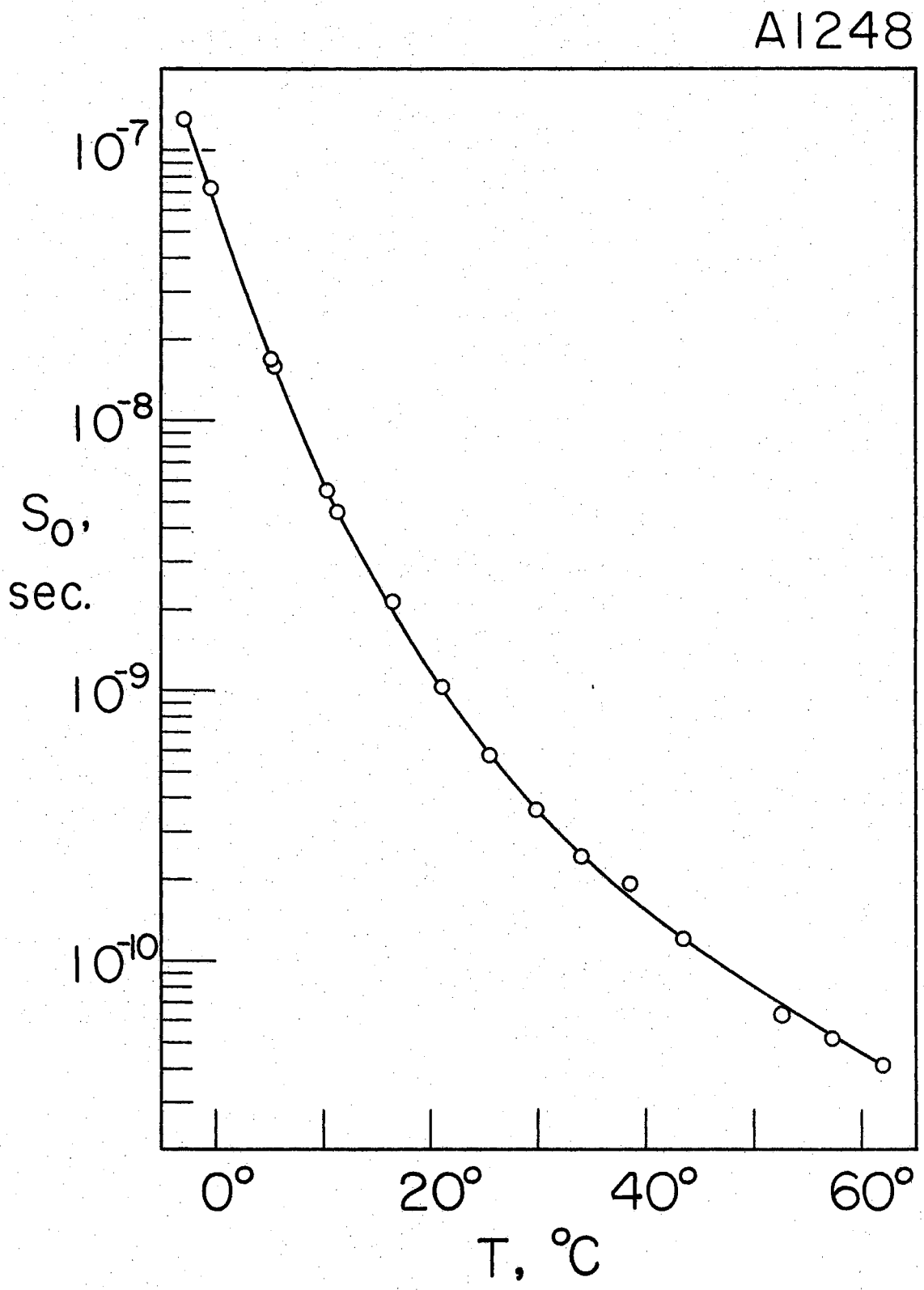
A1248
10^{-7}
10^{-8}
10^{-9}
10^{-10}
S_0, sec.
0°
20°
40°
60°
T, °C

Figure 23. η_0 Versus Temperature for Aroclor 1248, lot KD-507.

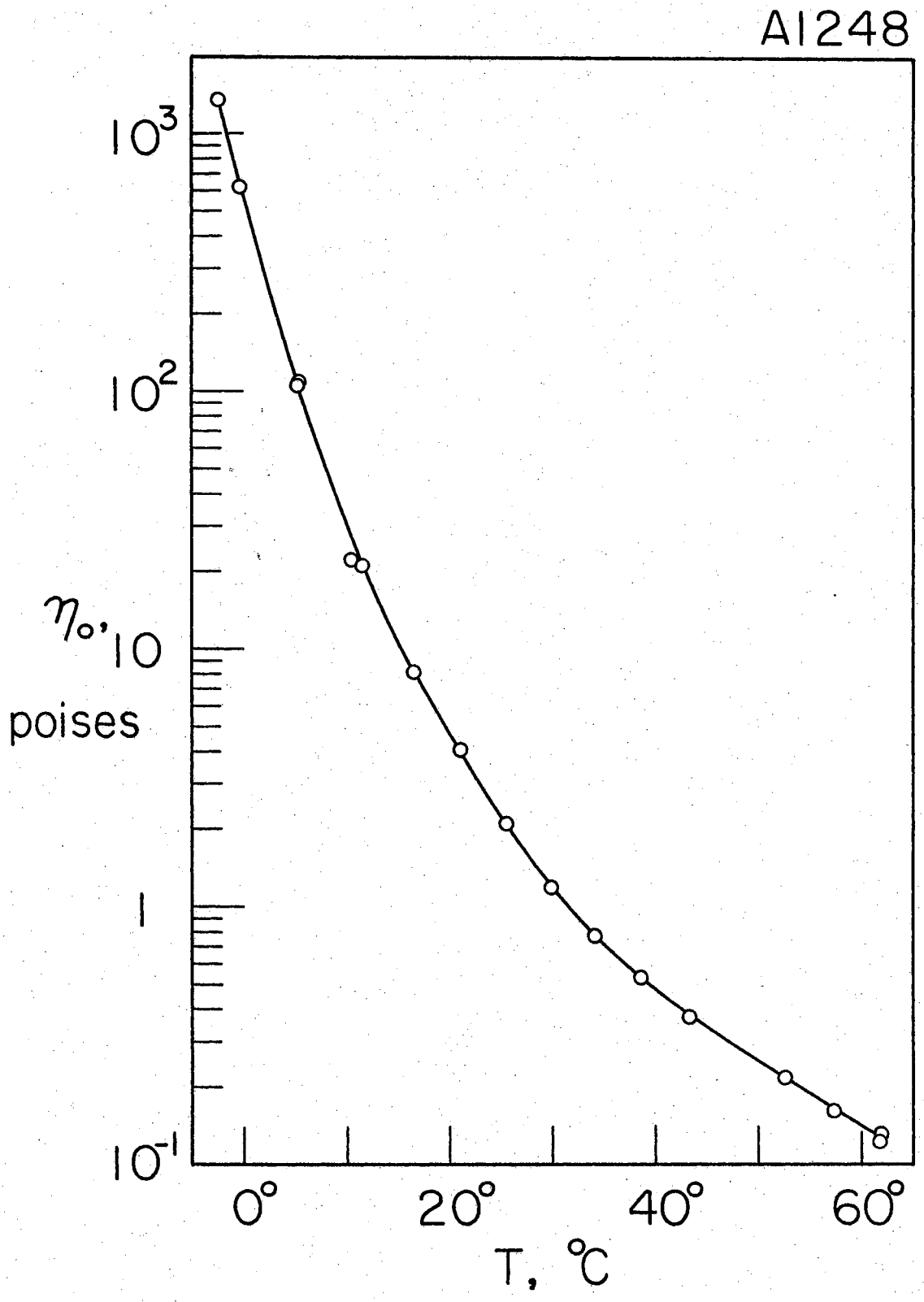
A1248
10^3
10^2
η_o, 10
poises
1
10^{-1}
0°
20°
40°
60°
T, °C

Figure 24. (S_o / S_{or}) Versus Temperature for the Solutions of Polystyrene S102 (4%), S111 (2%), and S13 (1%) in Aroclor 1248, and $(\eta_s T_r / \eta_{sr} T)$ Versus Temperature for Aroclor 1248.

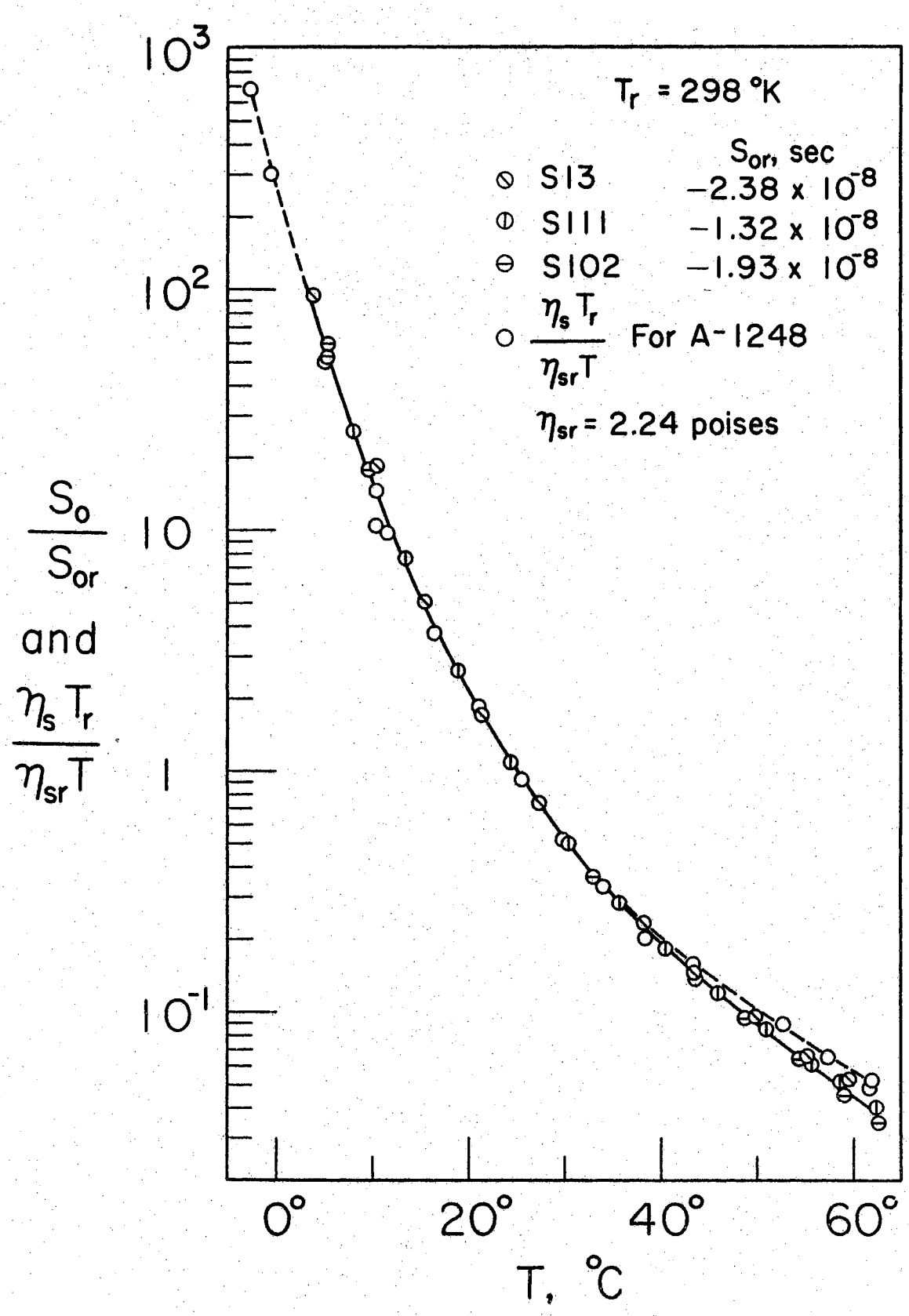
10^3
10^2
10
1
10^{-1}
$\frac{S_o}{S_{or}}$ and $\frac{\eta_s T_r}{\eta_{sr} T}$
T_r = 298 °K
S_{or}, sec
S13 -2.38×10^{-8}
S111 -1.32×10^{-8}
S102 -1.93×10^{-8}
$\frac{\eta_s T_r}{\eta_{sr} T}$ For A-1248
η_{sr} = 2.24 poises
0°
20°
40°
60°
T, °C

in Figure 24 are as follows: $S_{or} = -1.93 \times 10^{-8}$ sec. for the S102 solution, $S_{or} = -1.32 \times 10^{-8}$ sec. for the S111 solution and $S_{or} = -2.38 \times 10^{-8}$ sec. for the S13 solution. Also shown on Figure 24 is a plot of $(\eta_s T_r / \eta_{sr} T)$ versus T, which, according to the dilute solution theory will be equal to a_T if the assumed temperature dependence of the friction factor from equations (II-217) and (II-222) is valid. Figure 25 presents measured values of η_o versus temperature for the S102, S111 and S13 solutions. The measurements were made on the concentric cylinder apparatus using velocity gradients comparable to those used for the S_o measurements where possible.

Figures 26 through 31 present curves of (S_M / a_T) versus $f a_T$ and θ versus $f a_T$ for the S102, S111 and S13 solutions, obtained from the values of a_T given by (S_o / S_{or}) from Figure 24 and values of S_M and θ versus f from Figures 16 through 21. The values of a_T used for the various temperatures and solutions are noted on the corresponding (S_M / a_T) curves. Note that this shifting of data is the reduction scheme discussed in connection with equations (II-245) and (II-246). Bracketing theoretical curves for dilute solutions of non-free-draining molecules (see Figures 7 and 8) are also shown on Figures 26 through 31. The free-draining theoretical curves did not match any of the data. Theoretical non-free-draining curves were fitted to the experimental data weighting the lower frequencies more heavily since, as has been noted, the solvent birefringence correction is probably more likely to be in error for large values of $f a_T$, and the experimental θ versus $f a_T$ curves do appear to have too great a slope for the largest values of $f a_T$. Lines are drawn through each set of (S_M / a_T) and

Figure 25. η_o Versus Temperature for the Solutions of Polystyrene S102 (4%), S111 (2%) and S13 (1%) in Aroclor 1248.

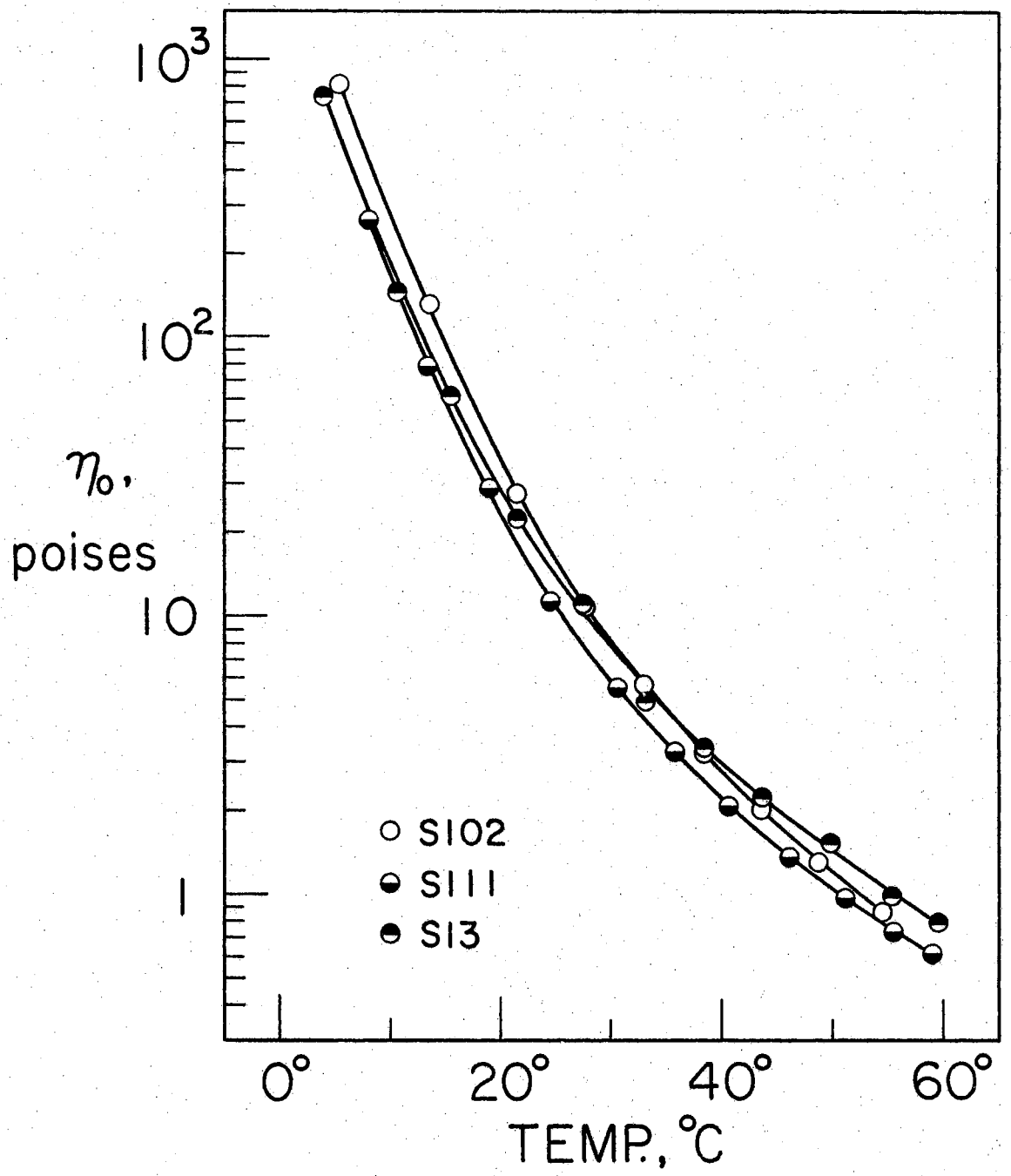
10^3
10^2
η_0,
poises
10
1
SI02
SI11
SI3
0°
20°
40°
60°
TEMP., °C

Figure 26. (S_M/a_T) Versus fa_T for the 4% Solution of Polystyrene S102 in Aroclor 1248. The Theoretical Curves Shown for Non-free-draining Model Chains Having Values of N of 10 and 40 were Obtained Using $\gamma_{1r} = 5.85 \times 10^{-4}$ sec. and $S_{or} = -2.01 \times 10^{-8}$ sec. The Reference Temperature is 25.0°C.

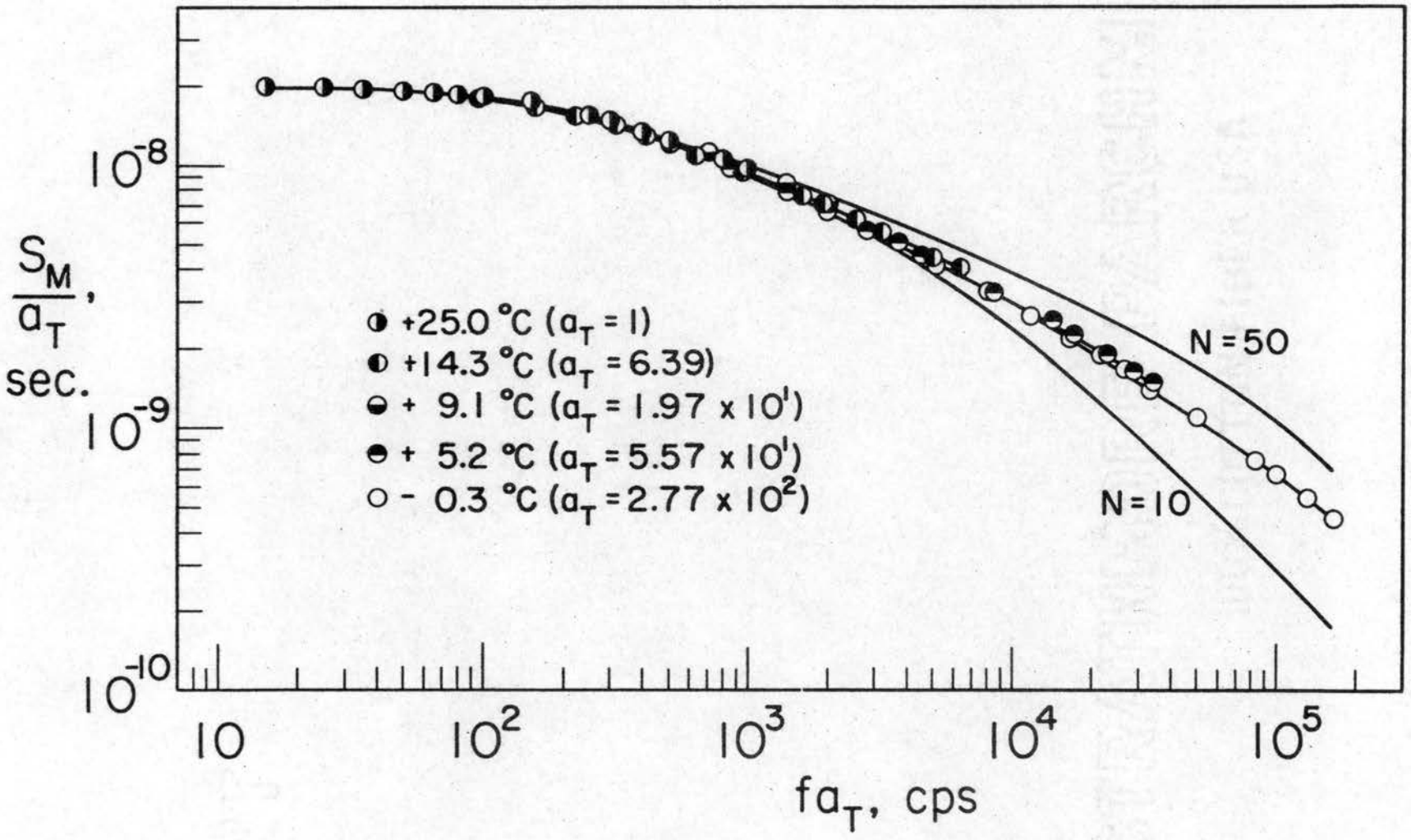
10^{-8}
10^{-9}
10^{-10}
$\frac{S_M}{a_T}$, sec.
+25.0 °C (a_T = 1)
+14.3 °C (a_T = 6.39)
+ 9.1 °C (a_T = 1.97 x 10¹)
+ 5.2 °C (a_T = 5.57 x 10¹)
- 0.3 °C (a_T = 2.77 x 10²)
N = 50
N = 10
10
10^2
10^3
10^4
10^5
fa_T, cps

Figure 27. θ Versus $f a_T$ for the 4% Solution of Polystyrene S102 in Aroclor 1248. Theoretical Curves Shown for Non-free-draining Model Chains Having Values of N of 10 and 40 Were Obtained Using τ_{1r} = 5.85×10^{-4} sec. and θ_o = -180 degrees. The Reference Temperature is 25.0°C.

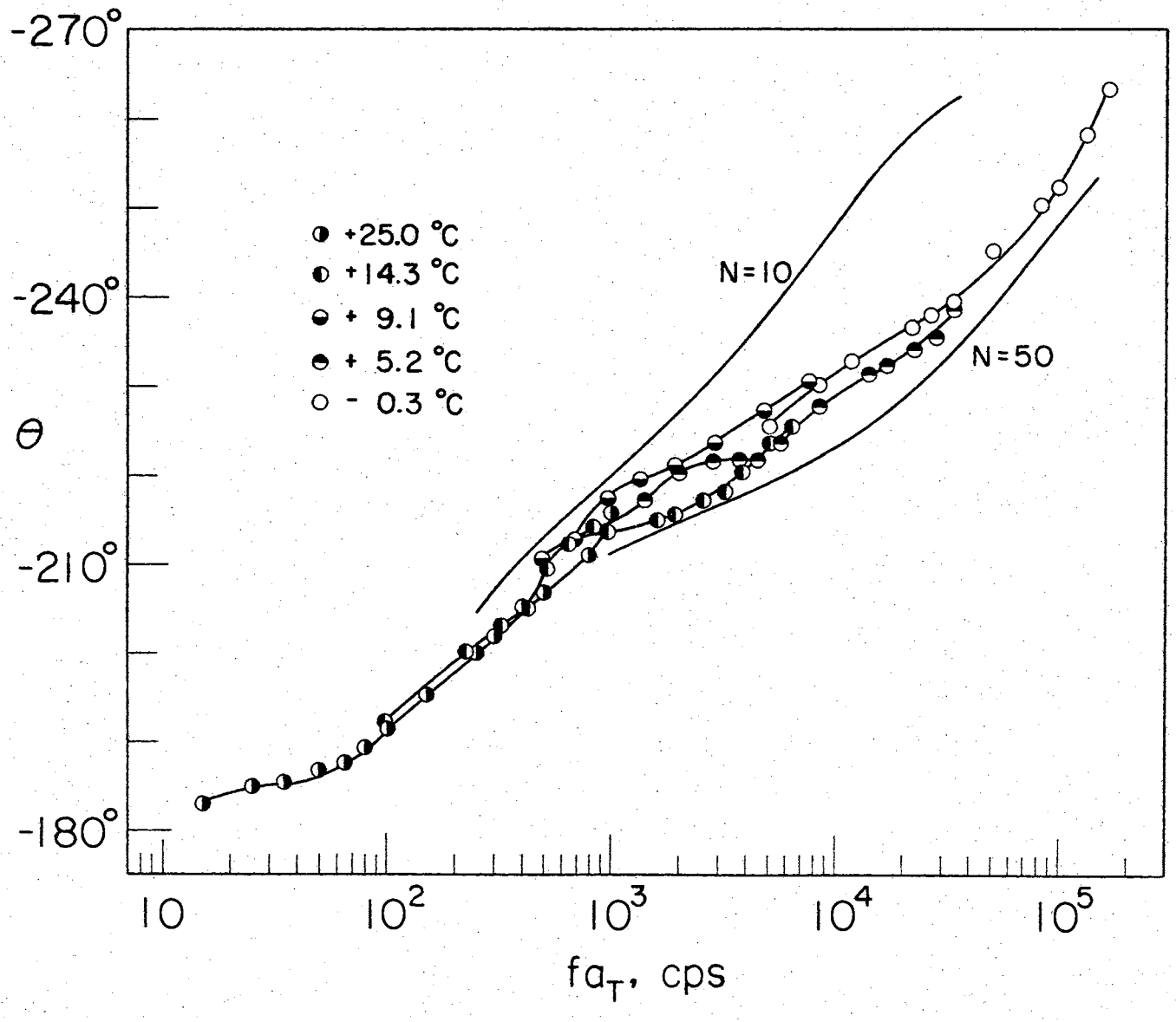
-270°
-240°
-210°
-180°
θ
+25.0 °C
+14.3 °C
+ 9.1 °C
+ 5.2 °C
- 0.3 °C
N=10
N=50
10
10^2
10^3
10^4
10^5
fa_T, cps

Figure 28. (S_M/a_T) Versus fa_T for the 2% Solution of Polystyrene S111 in Aroclor 1248. The Theoretical Curves Shown for Non-free-draining Model Chains Having Values of N of 30 and 100 Were Obtained Using $\tau_{1r} = 2.65 \times 10^{-3}$ sec. and $S_{or} = -1.40 \times 10^{-8}$ sec. The Reference Temperature is 25.0°C.

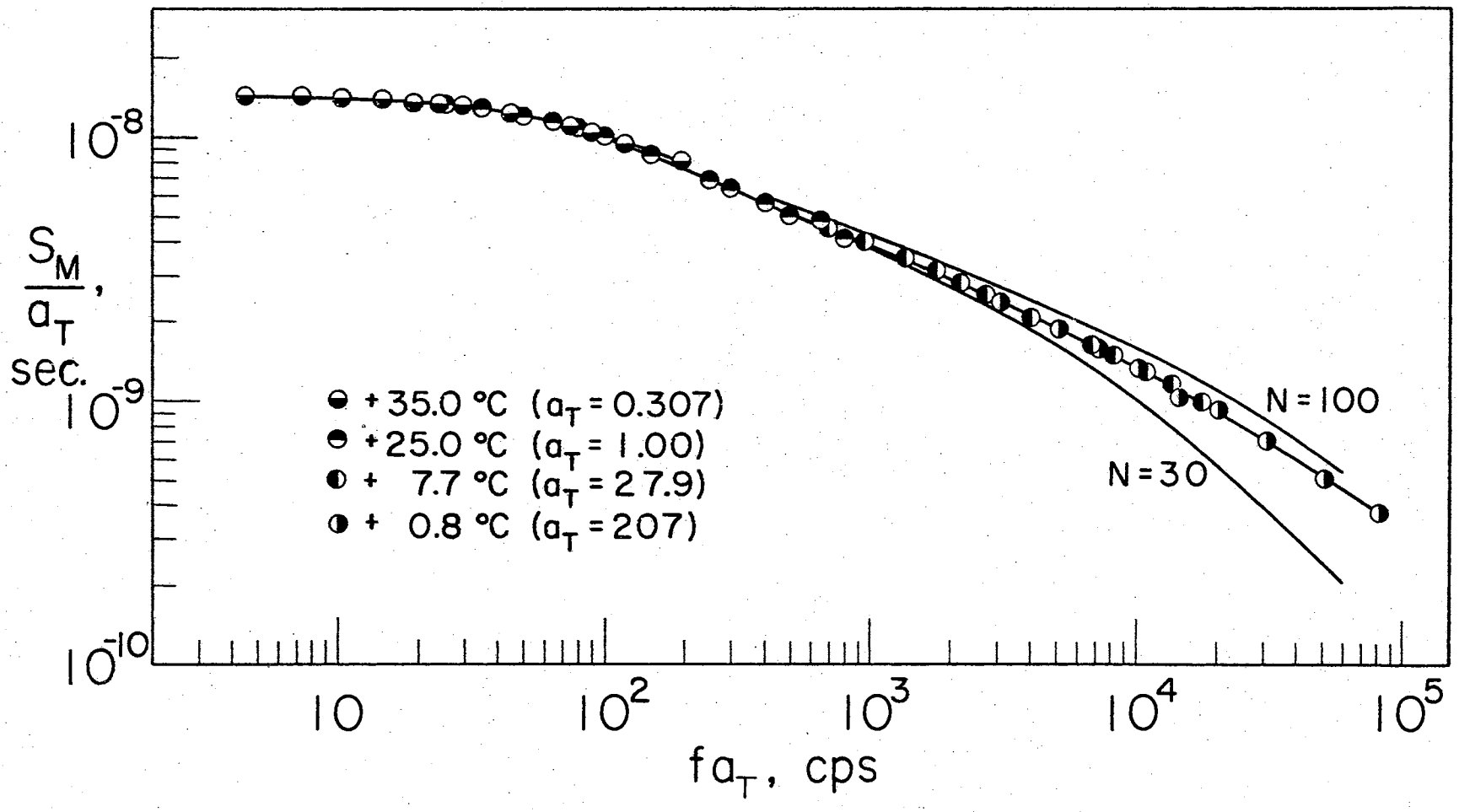
10^{-8}
$\frac{S_M}{a_T}$, sec.
10^{-9}
10^{-10}
+35.0 °C (a_T = 0.307)
+25.0 °C (a_T = 1.00)
+ 7.7 °C (a_T = 27.9)
+ 0.8 °C (a_T = 207)
N = 100
N = 30
10
10^2
10^3
10^4
10^5
fa_T, cps

Figure 29. θ Versus $f a_T$ for the 2% Solution of Polystyrene S111 in Aroclor 1248. The Theoretical Curves Shown for Non-free-draining Model Chains Having Values of N of 30 and 100 Were Obtained Using $\tau_r = 2.65 \times 10^{-3}$ sec. and $\theta_0 = -180$ degrees. The Reference Temperature is 25.0°C.

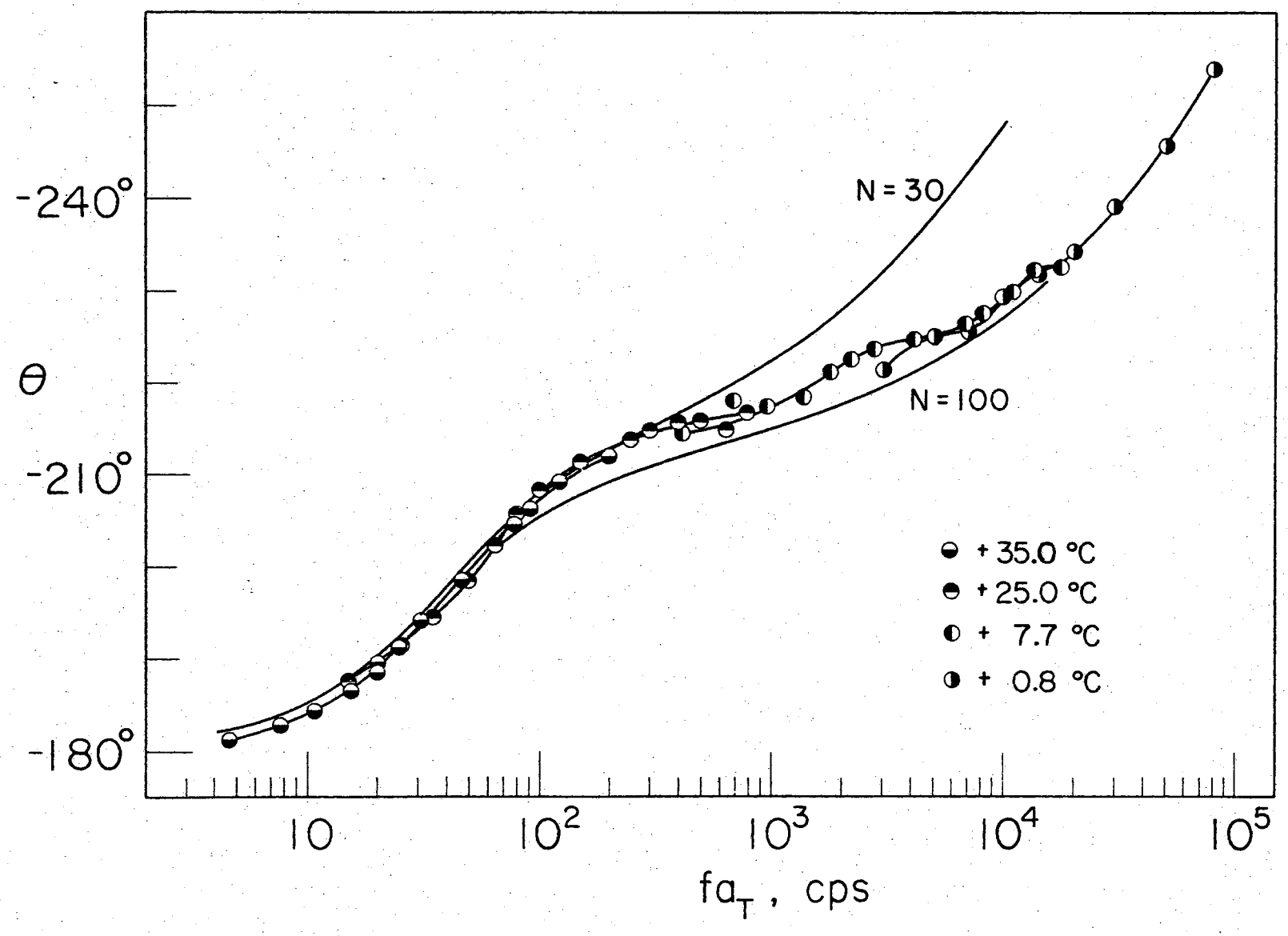
-240°
θ
-210°
-180°
N = 30
N = 100
+ 35.0 °C
+ 25.0 °C
+ 7.7 °C
+ 0.8 °C
10
10²
10³
10⁴
10⁵
fa_T , cps

Figure 30. (S_M/a_T) Versus $f a_T$ for the 1% Solution of Polystyrene S13 in Aroclor 1248. The Theoretical Curves Shown for Non-free-draining Model Chains Having Values of N of 50 and 400 Were Obtained Using $\tau_{1r} = 5.85 \times 10^{-2}$ sec. and $S_{or} = -2.17 \times 10^{-8}$ sec. The Reference Temperature is 25.0°C.

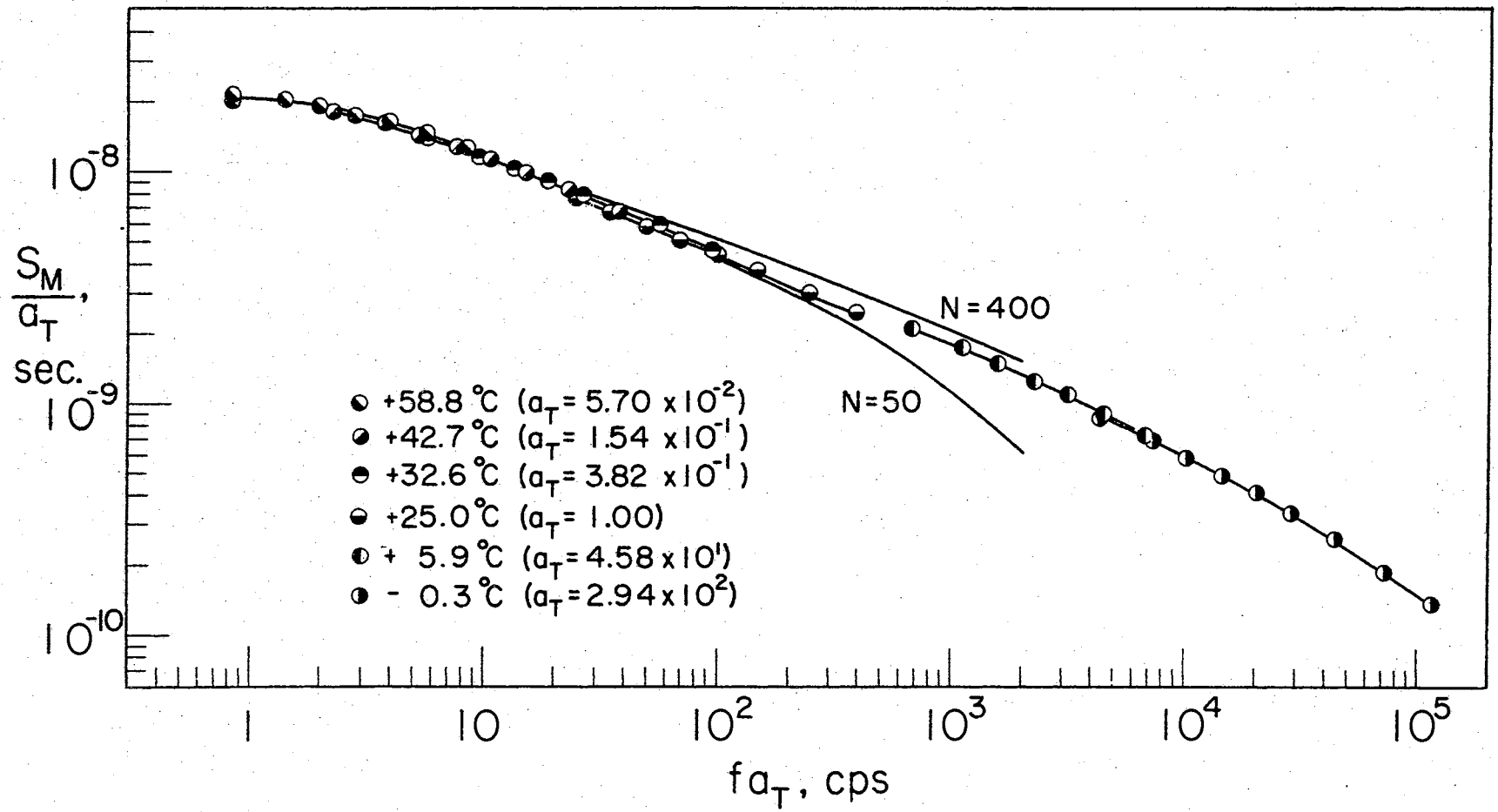
10^{-8}
$\frac{S_M}{a_T}$, sec.
10^{-9}
10^{-10}
N=400
N=50
+58.8 °C (a_T= 5.70 x 10^{-2})
+42.7 °C (a_T= 1.54 x 10^{-1})
+32.6 °C (a_T= 3.82 x 10^{-1})
+25.0 °C (a_T= 1.00)
+ 5.9 °C (a_T= 4.58 x 10^{1})
- 0.3 °C (a_T= 2.94 x 10^{2})
1
10
10^2
10^3
10^4
10^5
fa_T, cps

Figure 31. θ Versus $f a_T$ for the 1% Solution of Polystyrene S13 in Aroclor 1248. The Theoretical Curves Shown for Non-free-draining Model Chains Having Values of N of 50 and 400 Were Obtained Using $\tau_{1r} = 5.85 \times 10^{-2}$ sec. and $\theta_o = -180°$. The Reference Temperature is 25.0°C.

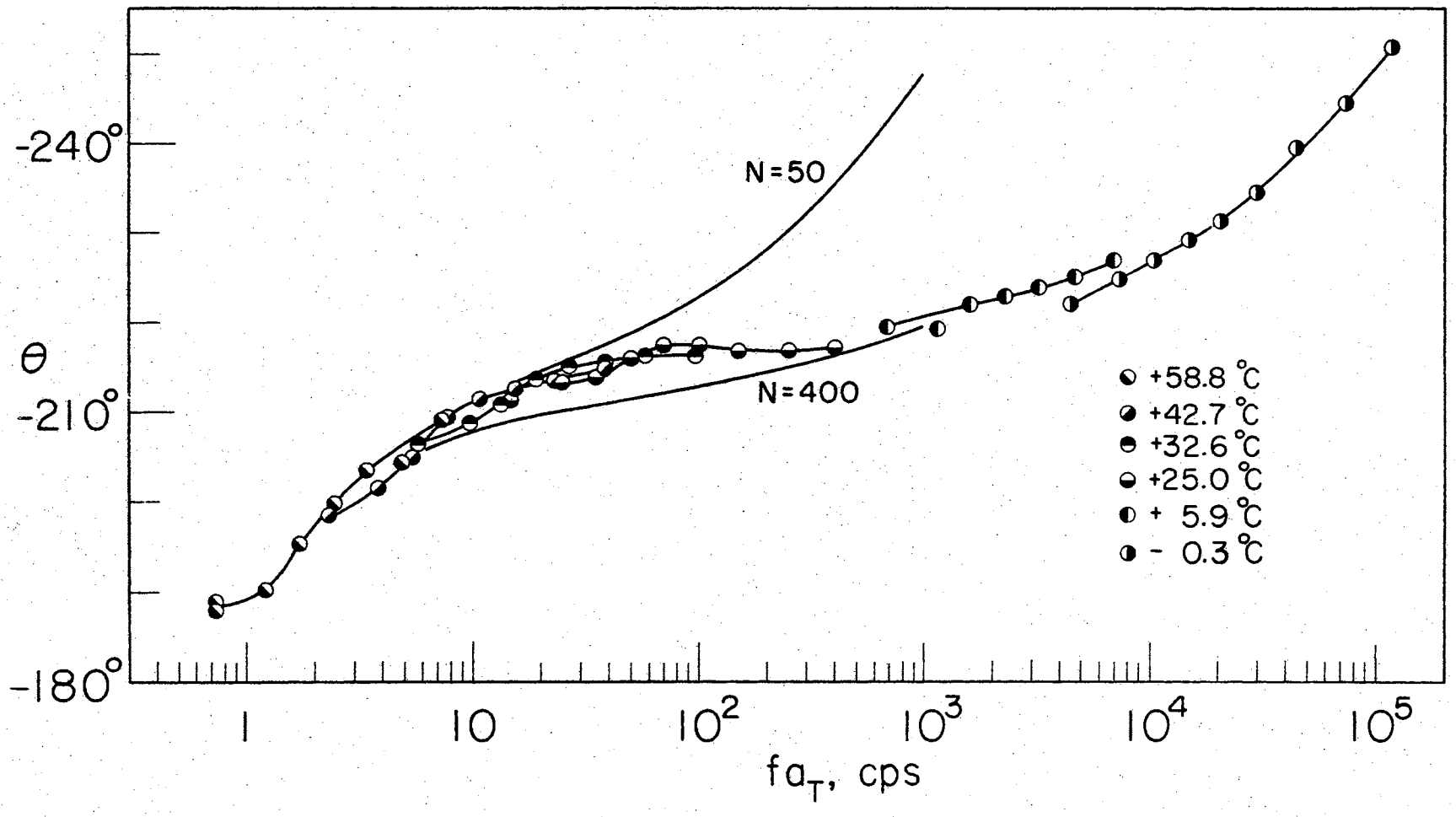
-240°
-210°
-180°
θ
N=50
N=400
+58.8 °C
+42.7 °C
+32.6 °C
+25.0 °C
+ 5.9 °C
- 0.3 °C
1
10
10²
10³
10⁴
10⁵
fa_T, cps

θ versus fa_T data points corresponding to a single temperature to illustrate the degree of matching among the various curves upon reduction. From Figures 26 and 27 for the 4 percent polystyrene S102 solution it is seen that from the comparison of the theoretical and experimental curves the number of subchains N for the 4 percent S102 solution lies between 10 and 50. A best fit value of N for values of $fa_T < 5 \times 10^3$ cps is $N \simeq 20$ using $\tau_{1r} = 5.85 \times 10^{-4}$ sec., $\theta_o = -180$ degrees and $S_{or} = -2.01 \times 10^{-8}$ sec. In view of the possible experimental phase error of ± 3 degrees associated with each set of data, the reduction of the θ versus fa_T data for S102 as shown in Figure 27 appears to be satisfactory. The corresponding (S_M/a_T) data also appears to reduce satisfactorily although each set of data for a given temperature seems to show a slight upturn at the high frequency end of the curve.

Figures 28 and 29 present (S_M/a_T) and θ versus fa_T curves obtained for the 2 percent polystyrene S111 solution. Again, a comparison with the theoretical curves of Figures 5 through 8 indicates that (S_M/a_T) and θ for the 2 percent S111 solution correspond most nearly to the theoretical non-free-draining curves. Bracketing theoretical curves for $N = 30$ and $N = 100$ are shown. For fa_T less than 2×10^3 cps the best fit value for N is $N \simeq 60$, using $\tau_{1r} = 2.65 \times 10^{-3}$ sec., $\theta_o = -180$ degrees and $S_{or} = -1.40 \times 10^{-8}$ sec. The (S_M/a_T) and θ versus fa_T data appears to follow the reduction scheme. However, the experimental curves for large fa_T do not follow the indicated theoretical curves, but appear to tend toward theoretical curves for larger N.

Figures 30 and 31 present the (S_M/a_T) and θ versus fa_T

curves obtained for the 1 percent polystyrene S13 solution. Comparison of the theoretical curves and the experimental data indicates that the measured values of (S_M/a_T) and θ for the S13 solution do not fit the theoretical dilute solution curves for either non-free-draining or free-draining chains, but may correspond to curves characteristic of some intermediate degree of hydrodynamic interaction. The theoretical non-free-draining curves come nearest to fitting the experimental data. Thus from a comparison of the theoretical and experimental curves of (S_M/a_T) and θ versus fa_T N lies between 100 and 400, as indicated by the bracketing theoretical non-free-draining curves, with an approximate best fit for $N \simeq 100$ using $\tau_{1r} = 5.85 \times 10^{-2}$ sec., $\theta_0 = -180$ degrees and $S_{or} = -2.17 \times 10^{-8}$ sec. The reduction procedure appears to be applicable. Again, the experimental curves in the region of large fa_T tend toward theoretical curves for larger values of N than are indicated by the small fa_T end of these curves.

Figure 32 presents measured values of the index of refraction for Aroclor 1248, lot KD-507, determined for an optical wavelength corresponding to the sodium D line (5,890 Å) using an Abbe refractometer. The probable error in the absolute magnitude of the measured values of the index of refraction is ± 0.0015. Thus from Figure 32, extrapolating n to 0°C, the factor $[(n_s^2+2)^2/n_s]$ of equation (II-214) does not vary from $[(n_s^2+2)^2/n_s]_r$ by more than 0.03 for temperatures from 0°C to 50°C.

3. Discussion of Results

In the previous section the measured values of flow birefringence for the solutions of S102, S111 and S13 in Aroclor 1248 were matched

Figure 32. Index of Refraction n Versus Temperature for Aroclor 1248, lot KD-507 for an optical wavelength corresponding to the sodium D line (5890 Å).

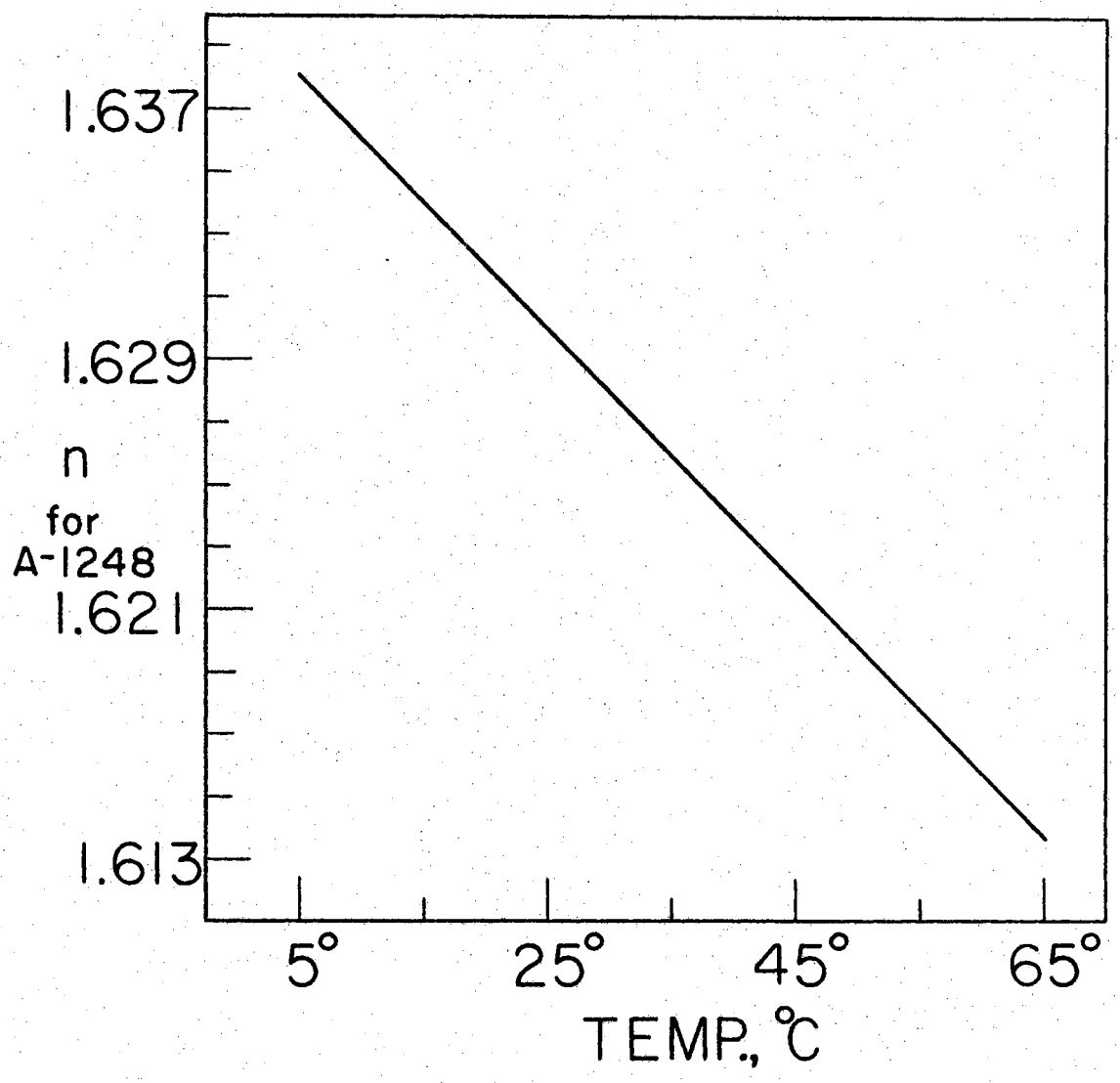
1.637
1.629
n
for
A-1248
1.621
1.613
5°
25°
45°
65°
TEMP., °C

to the theoretical curves of flow birefringence versus frequency obtained for dilute solutions of the model chains for which C is approaching zero. The polystyrene solutions on which measurements were made cannot be considered to be dilute. However as is seen from Figures 26 through 31 the character of the experimental curves does correspond to that of the theoretical curves. Corresponding measurements of the viscoelastic properties of polystyrene solutions have been made at various concentrations. The measured frequency dependence of the viscosity when compared with a modified Zimm theory, in which intermediate degrees of hydrodynamic interaction can be incorporated for infinite N , has shown that the longest relaxation time τ_{1r} is shifted to larger values as the concentration is increased. Also, for a given molecular weight, the hydrodynamic interaction seems to decrease with increasing concentration (29, 38). Peterlin (67, 98) has proposed a theory treating the concentration dependence of flow birefringence and viscosity for small velocity gradients in which the hydrodynamic forces acting on the chain molecule are assumed to increase with increasing concentration to the same extent as does the reduced viscosity $[\eta]_{RED.}$ defined by

$$[\eta]_{RED.} = \frac{\eta - \eta_s}{\eta_s C} \cdot \qquad \text{(IV-7)}$$

Thus the ratio of S_0 to $(\eta_0 - \eta_s)$ is given by

$$\frac{S_0}{(\eta_0 - \eta_s)} = \frac{4\pi}{45kT} \cdot \frac{(n_s^2+2)^2}{n_s} \cdot (\alpha_1 - \alpha_2) \qquad \text{(IV-8)}$$

for $\chi \simeq$ 45 degrees, which is the same result as is obtained

from equations (II-227), (II-229) and (II-214) for dilute solutions. Experimental verification of relation (IV-8) has been obtained by Tsvetkov (98) for both atactic and isotactic polystyrenes of various molecular weights and concentrations in bromoform. Thus although no exact description of the effects of finite concentration on the flow birefringence and viscosity is available, it appears that the calculated optical factor $(\alpha_1 - \alpha_2)$ as obtained from concentrated solution measurements may equal the difference in principal polarizabilities for the subchain link. Further, the shapes of the (S_M/a_T) and θ versus $f a_T$ curves will probably vary as concentration is varied. The variation of the value of τ_{1r} with concentration has been observed in oscillatory flow birefringence measurements made in this laboratory. In view of the above, the experimental measurements contained herein will be analyzed in terms of the dilute solution Zimm theory since adequate experimental and theoretical information concerning concentration dependence is not available.

Figure 33 presents plots of $(\eta_0 - \eta_s)/(\eta_0 - \eta_s)_r$ versus temperature for the S102, S111 and S13 solutions as well as a plot of (η_s/η_{sr}) versus temperature for Aroclor 1248, lot KD-507. From equations (II-233) and (II-222)

$$\frac{(\eta_0 - \eta_s)}{(\eta_0 - \eta_s)_r} = \frac{J}{J_r} , \qquad \text{(IV-9)}$$

and from the assumed relation between the friction factor and the solvent viscosity given by equations (II-217) and (II-223)

$$\frac{\eta_s}{\eta_{sr}} = \frac{J}{J_r} . \qquad \text{(IV-10)}$$

Figure 33. $(\eta_0-\eta_s)/(\eta_0-\eta_s)r$ Versus Temperature for the Solutions of Polystyrene S102 (4%), S111 (2%) and S13 (1%) in Aroclor 1248, and (η_s/η_{sr}) Versus Temperature for Aroclor 1248.

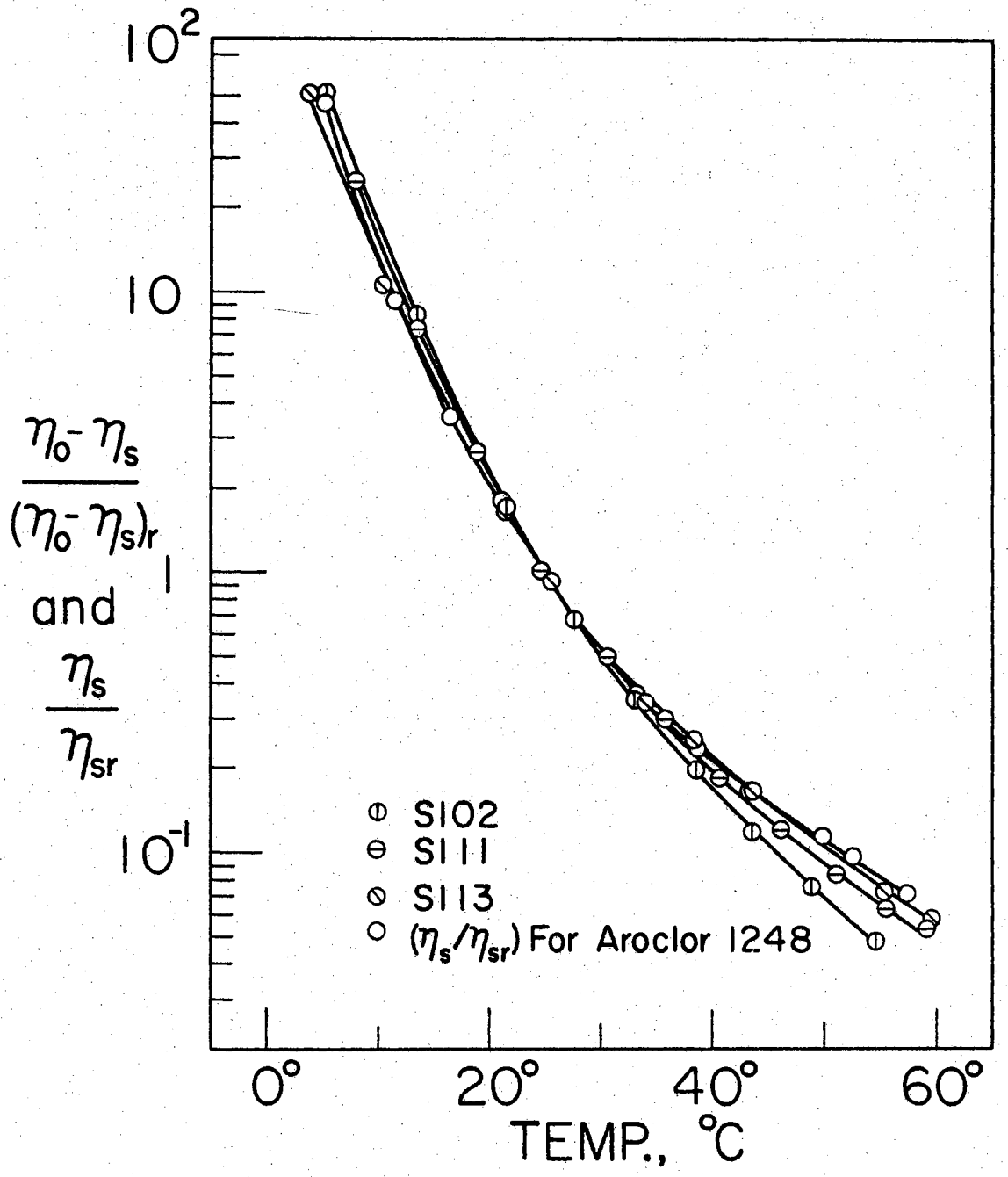
10^2
10
1
10^{-1}
$\frac{\eta_0 - \eta_s}{(\eta_0 - \eta_s)_r}$ and $\frac{\eta_s}{\eta_{sr}}$
S102
S111
S113
(η_s/η_{sr}) For Aroclor 1248
0°
20°
40°
60°
TEMP., °C

Thus from equations (IV-9) and (IV-10) and Figure 33 it is seen that the assumed temperature dependence relation between J and η_s given by equation (II-217) is valid for the polystyrene solutions studied for temperatures below about 35°C. Above 35°C the curves deviate appreciably. The deviation may be due to the finite concentration of the solutions or to the internal viscosity of the polymer molecule.

Figure 34 presents a plot of the longest relaxation time τ_{1r} versus weight average molecular weight $\overline{M_w}$ for values of τ_{1r} determined from the matching of experimental and theoretical S^* versus $f a_T$ curves as shown in Figures 26 through 31, as well as values obtained from steady flow viscosity measurements. From equations (II-227) and (II-160) τ_{1r} is given by

$$\tau_{1r} = \frac{M(\eta_0 - \eta_s)r}{cN_a kT \sum_{p=1}^{N} (\tau_p/\tau_1)} \quad . \tag{IV-11}$$

Values of N obtained from the theoretical and experimental curve fitting of Figures 26 through 31 were used together with the (τ_p/τ_1) ratios for the non-free-draining molecule given by equations (II-220), (II-170) and Table I to obtain τ_{1r} from the η_0 and η_s values of Figures 23 and 25. As is seen from the figure, the values of τ_{1r} obtained from the steady flow viscosity measurements are consistently lower than the values obtained from the S^* measurements. The reason for such a discrepancy is not apparent, although it is possible that finite concentration affects the entire relaxation time spectrum in a different manner than it affects some of the

Figure 34. The Longest Relaxation Time τ_{1r} Versus Weight Average Molecular Weight M_w. Also Shown are Lines Representing the Theoretical Slopes Representing the Variation of τ_{1r} With M for Free-draining and Non-free-draining Model Chains. The Reference Temperature is 25.0°C.

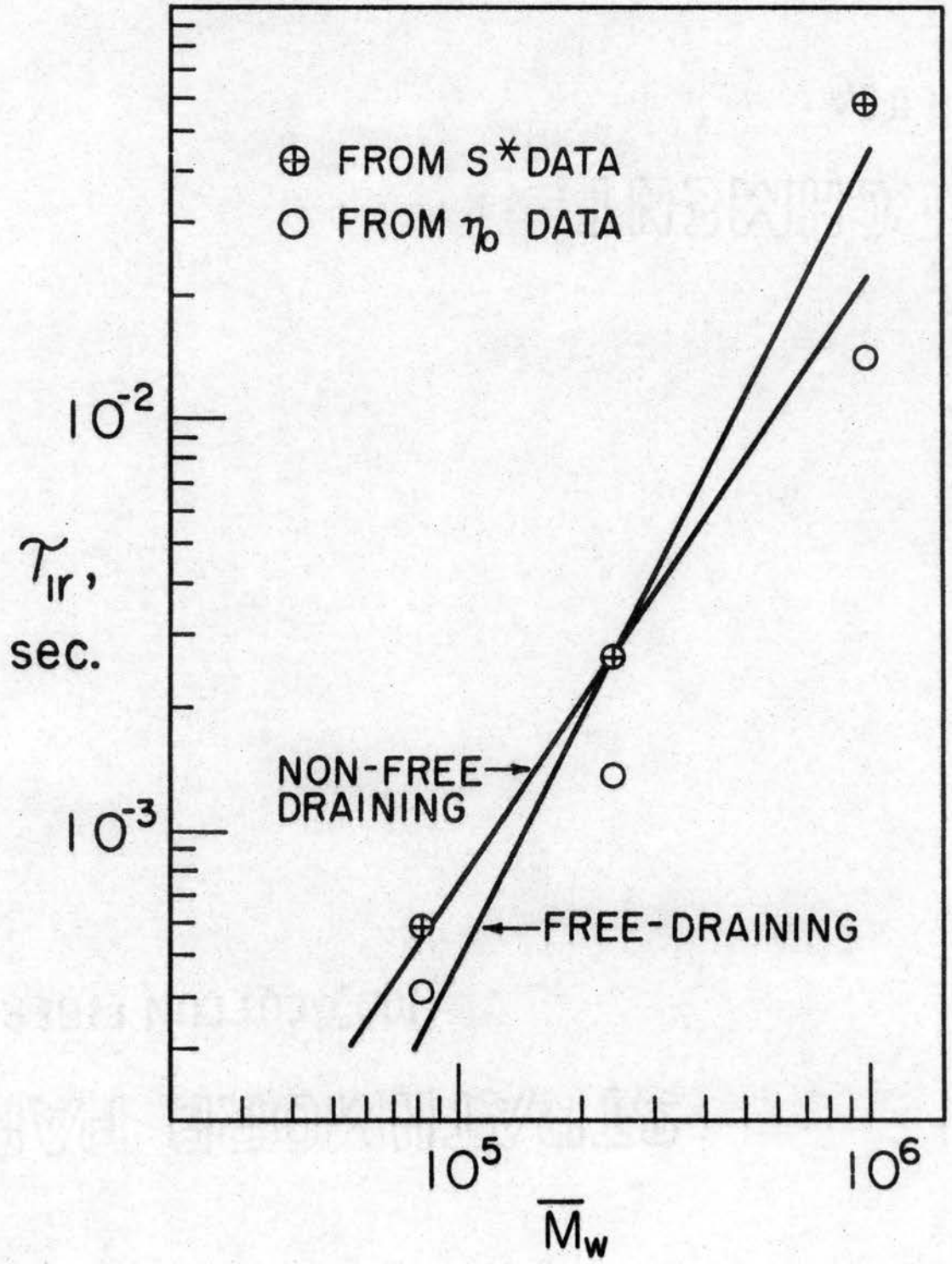
⊕ FROM S* DATA
○ FROM η_0 DATA
10^{-2}
10^{-3}
τ_{ir}, sec.
NON-FREE DRAINING
FREE-DRAINING
10^5
10^6
$\overline{M}_w$

oscillatory flow relaxation times. However, the same trends are noted for both sets of τ_{1r}. Assuming that b^2 and $\mathcal{J}$ are not functions of the molecular weight for the samples being considered, it is seen from equation (II-160), (II-168) and (II-169) that τ_1 will increase with molecular weight such that

$$\tau_1 \propto N^2 \propto M^2, \quad h \ll 1, \tag{IV-12}$$

and

$$\tau_1 \propto N^{3/2} \propto M^{3/2}, \quad h \gg 1. \tag{IV-13}$$

Lines corresponding to these limiting slopes are shown on Figure 34. From the figure it appears that the values of τ_{1r} obtained for the S102 and S111 solutions correspond to the non-free-draining slope, while the values obtained for the S13 solution seem to indicate that it may be more nearly free-draining. This tendency was noted previously in connection with the shape of the θ versus $f a_T$ curve of Figure 31. A similar tendency has been noted in the viscoelastic properties of the comparable polystyrene samples of identical concentration by Ferry and co-workers (29). Table II presents the values of τ_{1r} and h obtained by Ferry and co-workers from the measured viscoelastic properties of solutions of S102 and S111, as well as the values obtained herein. The values of τ_{1r} and h obtained by them for a 1 percent solution of a polystyrene in Aroclor 1248 having $\overline{M}_w \simeq 10^6$ is also listed for comparison with the values obtained herein for the S13 solution. The viscoelastic measurements and the oscillatory flow birefringence measurements appear to be in

TABLE II

A SUMMARY OF FACTORS DERIVED BY THE APPLICATION OF THE ZIMM THEORY TO THE FLOW BIREFRINGENCE AND VISCOSITY DATA FOR SOLUTIONS OF POLYSTYRENE S102, S111 AND S13 IN AROCLOR 1248

Solution Designation	M_w	c_w at 25°C (wt, %)	c at 25°C (gm/cc)	τ_{ir} from S^* Data (sec.)	τ_{ir} from η_o Data (sec.)	τ_{ir} from Ref. 29 (sec.)
S102	82,000	4.00%	5.70×10^{-2}	5.85×10^{-4}	4.03×10^{-4}	5.89×10^{-4}
S111	239,000	2.00%	2.86×10^{-2}	2.65×10^{-3}	1.37×10^{-3}	2.32×10^{-3}
S13	968,000	1.00%	1.43×10^{-2}	5.8×10^{-2}	1.40×10^{-2}	
MDP-2 Data from Ref. 29	1,000,000	1.0%	1.44×10^{-2}			5.01×10^{-2}

TABLE II (continued)

Solution Designation	N	$(q' b^2)_r$ (cm^3)	$(\alpha_1-\alpha_2)_r$ (cm^3)	Draining Condition	No. of Monomers Per Zimm Subchain
S102	$\simeq$ 20 (between 10 and 50)	-5.67×10^{-23}	-1.53×10^{-23}	$h \gg 1$ ($h \simeq \infty$)*	39
S111	$\simeq$ 60 (between 30 and 100)	-6.18×10^{-23}	-1.66×10^{-23}	$h \gg 1$ ($h \simeq 100$)*	38
S13	$\simeq$ 100 (between 50 and 400)	-8.63×10^{-23}	-2.33×10^{-23}	Intermediate, but nearer to $h \gg 1$	93
MDP-2 Data from Ref. 29				($h \simeq 15$)*	

* See Reference 29

agreement as to the value of τ_{1r} and the trend of the hydrodynamic interaction factor h .

The optical factors $(\alpha_1-\alpha_2)$ and $q'b^2$ may be evaluated from the S_o , η_o and η_s measurements of Figures 23, 24, and 25. From equations (II-227), (II-241) and (II-214),

$$q'b^2 = \frac{S_o}{(\eta_o-\eta_s)} \cdot kT \qquad \text{(IV-14)}$$

and

$$(\alpha_1-\alpha_2) = q'b^2 \cdot \frac{n_s}{(n_s^2+2)^2} \cdot \frac{45}{4\pi} , \qquad \text{(IV-15)}$$

assuming that there is no appreciable form birefringence. Table II lists the values of $(q'b^2)_r$ and $(\alpha_1-\alpha_2)_r$ calculated by inserting the measured values of S_{or} , η_{or} and η_{sr} in equations (IV-14) and (IV-15). Note that the values obtained for $(\alpha_1-\alpha_2)_r$ for the solutions of S102 and S111 correspond fairly well to the value given by Tsvetkov ($(\alpha_1-\alpha_2) = -1.45 \times 10^{-23}$ cm^3) for atactic polystyrenes in bromoform. However, the $(\alpha_1-\alpha_2)_r$ for the S13 solution agrees more nearly with the value listed by Tsvetkov for the isotactic form of polystyrene ($(\alpha_1-\alpha_2) = -2.24 \times 10^{-23}$ cm^3) (98). Also, the values of $(\alpha_1-\alpha_2)_r$ obtained for the S102 and S111 solutions are not identical although the small difference could be due to experimental error. Thus it is possible that either the factor $(\alpha_1-\alpha_2)_r$ for polystyrene in Aroclor 1248 may not follow the simple concentration dependence followed by polystyrene in bromoform or the polystyrene S13 may be an isotactic

polystyrene and the S102 and S111 samples atactic polystyrene (98). The form birefringence which has been neglected in the Zimm treatment of flow birefringence apparently would not account for the increased value of $(\alpha_1 - \alpha_2)_r$ for the S13 solution since although the form birefringence should increase with molecular weight it should be a positive quantity (19, 98).

Table III lists values of $(\alpha_1 - \alpha_2)$ for three temperatures, 10°C, 25°C and 40°C, for the three polystyrene samples, to demonstrate the temperature dependence of the subchain segment anisotropy $(\alpha_1 - \alpha_2)$. The variation of $(\alpha_1 - \alpha_2)$ for S102 and S111 is sufficiently small that to within experimental error the (S_0/S_{0r}) ratios of Figure 24 are equal to a_T as has been assumed herein. The S13 data indicates that this assumption is valid for it also, except perhaps at the lowest temperatures. However, this solution was quite viscous at low temperature, so that heating effects in the gap of the concentric cylinder apparatus might have given a value for η_0 that is too small.

The conclusion that the (S_0/S_{0r}) ratio should give adequate values of a_T is supported by the curve of $[(\eta_s/\eta_{sr})(T_r/T)]$ of Figure 24. Since (η_s/η_{sr}) was shown to exhibit the same temperature dependence as $\frac{(\eta_0 - \eta_s)}{(\eta_0 - \eta_s)_r}$ for temperatures below 35°C in Figure 33, $(\eta_s/\eta_{sr})(T_r/T)$ should be equal to a_T below $T = 35$°C. From Figure 24 it is seen that (S_0/S_{0r}) does match $(\eta_s/\eta_{sr})(T_r/T)$ below 35°C for all three polymer solutions, so that (S_0/S_{0r}) should be equal to a_T, and the temperature dependences of q' and C are apparently negligible for all three solutions.

TABLE III

THE VARIATION OF $S_o/(\eta_o-\eta_s)$ AND $(\alpha_1-\alpha_2)$ WITH TEMPERATURE FOR SOLUTIONS OF POLYSTYRENES S102, S111 AND S13 IN AROCLOR 1248

T (°C)	$\frac{S_o}{(\eta_o-\eta_s)}$ (sec./poise)	$(\alpha_1-\alpha_2)$ (cm^3)	Polystyrene Sample
10	-1.32×10^{-9}	-1.38×10^{-23}	S102
	-1.56×10^{-9}	-1.64×10^{-23}	S111
	-2.87×10^{-9}	-3.01×10^{23}	S13
25	-1.38×10^{-9}	-1.53×10^{-23}	S102
	-1.50×10^{-9}	-1.66×10^{-23}	S111
	-2.11×10^{-9}	-2.33×10^{-23}	S13
40	-1.27×10^{-9}	-1.49×10^{-23}	S102
	-1.47×10^{-9}	-1.72×10^{-23}	S111
	-1.92×10^{-9}	-2.24×10^{-23}	S13

Table II presents a summary of the data obtained from the birefringence and steady flow viscosity measurements for the polystyrene solutions. The table also lists values of τ_{1r} and h obtained by Ferry and co-workers from viscoelastic measurements (29). Also shown is the number of monomers per subchain computed from the best fit values of N obtained from the oscillatory flow birefringence measurements. The value obtained for the S13 solution would indicate that the S13 molecule is more rigid than the S102 and S111 molecules, the value of N obtained is too small by a factor of two, polydispersity effects are significantly altering the shapes of the curves, or the effects of finite concentration are more pronounced for this sample. If the S13 sample is an isotactic sample, the chain could be more rigid (61, 85). However, the value of N may be incorrect, since no adequate match between the theoretical and experimental curves could be obtained for this solution. It should be noted that the $(\overline{M_W}/\overline{M_N})$ value for S13 is larger than for S102 or S111, indicating that the polydispersity of the S13 sample is greater.

CHAPTER V

CONCLUSIONS AND SUGGESTIONS FOR FURTHER STUDY

1. Conclusions

The oscillatory flow birefringence exhibited by a solution containing polymer molecules in suspension is a sensitive indicator of the dynamics of the motions of such molecules in an oscillatory flow field. The data obtained for the polystyrene S102, S111 and S13 solutions studied indicates that there is a definite spectrum of relaxation times associated with the oscillatory flow birefringence of the polystyrene molecule. Thus any model used as the foundation for a theoretical treatment of the birefringence must exhibit such a spectrum of relaxation times. Models such as the elastic dumbbell (51, 52) and the deformable sphere (31, 48, 97, 98, 100) would not be adequate. The elastic sphere treatment by Cerf (13) does, however, predict such a spectrum of relaxation times. The bead and spring models of Rouse (75), Cerf (12, 13, 14) and Zimm (103, 104) appear to be particularly amenable to the treatment of oscillatory flow birefringence from the standpoint of the relaxation time spectrum predicted by the normal vibrational modes of the chain.

The measured frequency and temperature dependence of the oscillatory flow birefringence of the S102, S111 and S13 polystyrene solutions does exhibit the general character of the theoretical flow birefringence predictions of the Zimm theory as presented herein, although the

theory incorporates assumptions that may well be violated, such as small forces being exerted on the model chain by the fluid and by the chain on the fluid, quasi-static force conditions and equilibrium chain configurations for the treatment of the hydrodynamic interaction within the model chain, subchains obeying random walk (gaussian) statistics, a Stokes law type of interaction between the solvent and the subchain acting on the end points (beads) of the subchains only, no internal energy losses in the chain (internal viscosity), no optical interaction between the subchains, and a solution sufficiently dilute that there will be no mechanical or optical interaction among the chains in solution.

Since most polymer molecules exhibit some type of hindrance to rotation at the valence bond angle in the polymer chain, and such bonds may have several different potential energy maxima and minima, the rotation from one minimum to another can mean an apparent dissipation of energy in the chain so that an effective internal viscosity will appear for the chain (1, 28, 61, 63, 85). Cerf (12, 13, 14) states that the internal viscosity may play a more important role than the hydrodynamic interaction between segments in the chain. Thus the assumption of no internal viscosity seems questionable. The assumption of no optical interaction between segments may be an approximation to the physical situation, since neighboring segments which are separated by small distances may influence the local electric field acting on each other (39). The bead and spring model of Zimm assumes a Stokes law type of hydrodynamic interaction between the model beads and a continuous solvent. Since the Aroclor solvent molecules are of a size comparable to the styrene monomer units contained in the whole

polystyrene molecule it is surprising that the oscillatory flow birefringence predictions based on the Zimm model correspond to the observed birefringence for the polystyrene solutions (28).

Tha analysis of the oscillatory flow birefringence data for the polystyrene solutions in terms of the dilute solution Zimm theory shows that the reduction procedure discussed in connection with equations (II-246) and (II-247) may be used effectively to examine experimentally relaxation processes corresponding to frequencies not directly attainable because of the frequency limitations of the equipment. Also, the correction of the birefringence data for the contribution of the birefringent Aroclor solvent used appears to be proper except possibly for the highest frequencies and lowest temperatures at which measurements could be made, since the corrected data appears to have the proper frequency dependence, the reduction procedure works adequately and the values of $(\alpha_1 - \alpha_2)$ seem reasonable. The high frequency-low temperature discrepancy may be due to a decreasing contribution of the large phenyl side groups of the polystyrene chain with increasing frequency, since these large groups may have some freedom of movement about the chain backbone (102) and hence may not be following the chain motions at high frequency, resulting in a smaller value of anisotropy $(\alpha_1 - \alpha_2)$ associated with a link of the subchain. Or, the discrepancy may be due to a small form birefringence which is undetectable at lower frequencies, but which introduces a small positive value of optical anisotropy that is significant at high frequency. Another possible source of the high frequency discrepancy is the presence of a small amount of some contaminating material in the solution that exhibits a positive anisotropy. The applicability of the

reduction procedure indicates that the value of a_T given by the (S_0/S_{0r}) ratio is adequate and that b^2 and N are at most weakly dependent on temperature. N also appears to be essentially independent of fa_T for the range of frequencies covered, although as the high frequency end of the relaxation curve is approached motions within the subchain itself would be expected to become significant, thus altering the value of N .

The steady flow viscosity versus temperature measurements for the polystyrene solutions and the Aroclor solvent indicate that the temperature dependence of the friction factor ζ associated with the hydrodynamic interaction between the model bead and the solvent does follow the temperature dependence of the solvent viscosity for temperatures less than 35°C, as would be predicted by a Stokes law type of interaction between the bead and the solvent, in spite of the comparable dimensions of the Aroclor molecules and the monomeric units of the polystyrene chain. Above 35°C the temperature dependence of the friction factor apparently increases, an effect that may be due to either the internal viscosity of the polymer or the finite concentration of the solution.

The steady flow viscosity and birefringence measurements indicate that the optical factor q' is a weak function of temperature and the oscillatory birefringence measurements indicate no appreciable dependence of q' on frequency, although for sufficiently high frequencies where motions within the subchain should become significant q' would probably exhibit a dependence on frequency. The values of $(\alpha_1 - \alpha_2)_r$ obtained herein for the S102 and S111 polystyrene samples in Aroclor 1248 agree with the values obtained by

Tsvetkov (97, 98) for various atactic polystyrenes in bromoform and show a reasonable agreement as well with solid polystyrene $(\alpha_1 - \alpha_2)$ values. The value of $(\alpha_1 - \alpha_2)_r$ obtained for the S13 sample agrees well with the value given by Tsvetkov for isotactic polystyrenes in bromoform. The agreement between the values of $(\alpha_1 - \alpha_2)_r$ obtained herein and those of Tsvetkov which are corrected for form birefringence indicates that the form birefringence is probably negligible for these solutions as was assumed, except possibly for the data corresponding to large values of fa_T. The larger value of $(\alpha_1 - \alpha_2)_r$ obtained for the S13 sample probably is not due to form birefringence, since apparently form birefringence always exhibits a positive anisotropy (19, 20, 97, 98). The values of $(\alpha_1 - \alpha_2)_r$ obtained herein are as follows: $(\alpha_1 - \alpha_2)_r = -1.53 \times 10^{-23}$ cm^3 for polystyrene S102, $(\alpha_1 - \alpha_2)_r = -1.66 \times 10^{-23}$ cm^3 for polystyrene S111, and $(\alpha_1 - \alpha_2)_r = -2.33 \times 10^{-23}$ cm^3 for polystyrene S13. The treatment of the optical anisotropy of the polymer chain given by Kuhn and Grün (50) which is used in the Zimm theory appears to be adequate for the polystyrene-Aroclor solutions in view of the agreement between the theoretical and experimental S^* versus fa_T curves.

A comparison of the theoretical free-draining and non-free-draining oscillatory birefringence curves of Figures 5 through 8 indicates that for values of N between 20 and 100 the variation of $(\theta - \theta_0)$ with N is as large as the variation with limiting hydrodynamic interaction condition. Thus a good description of the birefringence properties of the chain model will involve a treatment in terms of a variable hydrodynamic interaction parameter h as well as a variable

number of chain segments N . Also, the random coil subchain concept applied to polymer chains to obtain the bead and Hookean spring model will break down for sufficiently low molecular weights since the polymer chain will not be sufficiently long to approximate a random coil, but will have a sufficient number of bonds of limited flexibility to combine characteristics of both flexible and rigid molecules.

From a best fit matching of the theoretical dilute solution oscillatory birefringence curves of Figures 5 through 8 and the experimental oscillatory birefringence curves of Figures 26 through 31 it is seen that the experimental curves do not correspond to the theoretical free-draining curves for any of the polystyrene samples. A best fit matching of the theoretical non-free-draining curves and the experimental data yields the following: For the 4 percent solution of polystyrene S102, N is between 10 and 50, with a best fit value of $N \simeq 20$; for the 2 percent solution of polystyrene S111, N is between 30 and 100, with a best fit value of $N \simeq 60$; for the 1 percent solution of polystyrene S13, N is between 50 and 400, with a best fit value of $N \simeq 100$. The number of monomer units per Zimm subchain given by the weight average molecular weight divided by the best fit value of the number of subchains N times the monomeric molecular weight are 38 monomer units, 39 monomer units and 93 monomer units for the S102, S111 and S13 samples respectively. The large number of monomer units obtained for the S13 polymer may indicate a more rigid chain structure, an incorrect value of N due to the inadequate match between theoretical and experimental curves for this sample, or some effect of the relatively high solution concentration.

Values of the longest relaxation time τ_{1r} at $T = 25.0°C$

obtained by the best fit matching of the theoretical curves and the experimental data are as follows: $\tau_{1r} = 5.85 \times 10^{-4}$ sec. for the S102 solution, $\tau_{1r} = 6.25 \times 10^{-3}$ sec. for the S111 solution, and $\tau_{1r} = 5.8 \times 10^{-2}$ sec. for the S13 solution. These values of show a tendency toward a more nearly free-draining hydrodynamic interaction condition with increasing molecular weight. A similar tendency has been noted from viscoelastic measurements, and the values of τ_{1r} obtained are in good agreement with those obtained herein (29). Values of τ_{1r} computed from the steady flow viscosity data for these solutions are consistently smaller. The trend toward a more nearly free-draining condition with increasing molecular weight is also indicated by the θ versus fa_T curve for S13 (Figure 31), which exhibits a curve shape intermediate to those of the theoretical free-draining and non-free-draining chains.

The large value of the number of monomer units per subchain and the larger value for $(\alpha_1 - \alpha_2)_r$ obtained for the S13 polymer might indicate that this sample is an isotactic polystyrene, whereas the S102 and S111 samples are probably atactic polystyrenes. However, since the effects of finite concentration are not known, the observed values of $(\alpha_1 - \alpha_2)_r$ and N for the S13 solution may be due to finite concentration effects instead.

2. Suggestions for Further Study

The need for consideration of both the number of subchains and the hydrodynamic interaction condition demonstrated by the present study points to the need for an extension of the Zimm theory to intermediate degrees of hydrodynamic interaction for a finite number of segments N. Such an extension has been performed by Tschoegl (94) for the case of

an infinite number of subchains. Also, adequate theoretical treatment of the concentration dependence of the oscillatory flow birefringence, and companion measurements demonstrating the influence of finite concentration are needed.

An extension of the frequency capabilities of the apparatus to higher frequencies to permit an experimental examination of the upper end of the oscillatory birefringence relaxation curve, a region that as of yet is not defined, is needed. Calculation of values of λ_p for finite N for the non-free-draining case when combined with the λ_p for finite N given by Rouse for the free-draining case would help resolve the theoretical predictions of the Zimm theory for the same region for small N (70, 75).

The use of a viscous but nonbirefringent solvent for polystyrene solutions having a viscosity comparable to that of the Aroclor 1248 used herein would be helpful in determining the role of the solvent birefringence in these measurements and the validity of the solvent birefringence correction procedure employed herein. Measurements of the oscillatory flow birefringence for sufficiently low molecular weights of polystyrene that the chain size approaches the size of the gaussian subchain noted herein would clarify the applicability of the subchain concept to real macromolecules.

The effects of polydispersity should be studied both experimentally and theoretically, since the presence of widely different molecular weight polymer molecules can alter the shapes of the experimental birefringence curves appreciably. Also, the study of other flexible macromolecules to broaden the experimental study of the oscillatory flow birefringence exhibited by flexible macromolecules would be useful.

In particular, naturally occurring polymer molecules which tend to be more monodisperse than molecules prepared by chemical synthesis might help to resolve the effect of polydispersity (98).

REFERENCES

1. O. A. Battista, Fundamentals of High Polymers, Reinhold Publishing Corp., New York (1958)

2. P. Boeder, Z. Physik 75, 258 (1932)

3. V. Bloomfield and B. H. Zimm, J. Chem. Phys. 44, 315 (1966)

4. M. Born and E. Wolf, Principles of Optics, MacMillan Company, New York (1964)

5. J. M. Burgers, Second Report on Viscosity and Plasticity of the Amsterdam Academy of Sciences, Koninklijke Nederlandse Akademie Van Wetenschappen, Verhanddingen afd. Naturkunde, section 1, 16 (1938)

6. R. Cerf, Compt. Rend. 226, 1586 (1948)

7. R. Cerf, Compt. Rend. 227, 1221 (1948)

8. R. Cerf, Compt. Rend. 227, 1352 (1948)

9. R. Cerf, J. Chim. Phys. 48, 59 (1951)

10. R. Cerf, Compt. Rend. 238, 1403 (1954)

11. R. Cerf, J. Chim. Phys. 52, 53 (1955)

12. R. Cerf, Compt. Rend. 241, 496 (1955)

13. R. Cerf, J. Poly. Sci. 23, 125 (1957)

14. R. Cerf, J. Phys. Radium, 19, 122 (1958)

15. R. Cerf and H. Scheraga, Chem. Rev. 51, 185 (1952)

16. R. Cerf and G. B. Thurston, J. Chim. Phys. 61, 1457 (1964)

17. S. Chandrasekhar, Rev. Mod. Phys. 15, 1(1943)

18. J.S.R. Chisholm and R. M. Morris, Mathematical Methods in Physics, W. B. Saunders Co., Philadelphia (1965)

19. M. Copic, J. Chem. Phys. 26, 1382 (1957)

20. M. Copic, Tech. Report #411, Nuclear Institute "J. Stefan," Ljubljana, Yugoslavia (1963)

21. A. J. Curtis, Progress in Dielectrics, Vol. 2 edited by J. Birks and J. Schulman, J. Wiley and Sons, Inc., New York (1960)

22. R. B. DeMallie, M. H. Birnboim, J. E. Frederick, N. W. Tschoegl and J. D. Ferry, J. Phys. Chem. 66, 536 (1962)

23. K. G. Denbigh, Trans. Far. Soc. 36, 936 (1940)

24. J. T. Edsall, Adv. Coll. Sci. 1, 269 (1942)

25. F. I. Federov and T. L. Katyash, Opt. Spectry,. (USSR) 12, 162 (1962)

26. J. D. Ferry, Viscoelastic Properties of Polymers, John Wiley and Sons, Inc., New York (1961)

27. J. D. Ferry, J. Poly. Sci. Part C, No. 15, 307 (1966)

28. P. J. Flory, Principles of Polymer Chemistry, Cornell University Press, Ithaca, New York (1953)

29. J. E. Frederick, N. W. Tschoegl and J. D. Ferry, J. Phys. Chem. 68, 1974(1964)

30. L. D. Grandine and J. D. Ferry, J. Appl. Phys. 24, 679 (1953)

31. W. Haller, Kolloid Z. 61, 26 (1932)

32. E. Hatschek, The Viscosity of Liquids, D. Van Nostrand Co., Inc., New York (1928)

33. J. J. Hermans, Physica 10, 777 (1943)

34. J. J. Hermans, Rec. Trav. Chim. 63, 219 (1944)

35. J. J. Hermans, Rec. Trav. Chim. 63, 205 (1944)

36. F. B. Hildebrand, Methods of Applied Mathematics, Prentice-Hall, Inc., Englewood Cliffs, N. J. (1963)

37. T. L. Hill, An Introduction to Statistical Thermodynamics, Addison-Wesley Publishing Company, Inc., Reading, Mass. (1960)

38. L. A. Holmes, K. Ninomiya and J. D. Ferry, J. Phys. Chem. 70, 2714 (1966)

39. J. D. Jackson, "Classical Electrodynamics," John Wiley and Sons, Inc., New York (1962)

40. H. G. Jerrard, J. O. S. A. 38, 35 (1948)

41. H. G. Jerrard, Chem. Rev. 59, 345 (1959)

42. A. Katchalsky, O. Kunzle and W. Kuhn, J. Poly. Sci. V, 283 (1950)

43. J. G. Kirkwood, J. Chem. Phys. 4, 592 (1936)

44. J. G. Kirkwood, Rec. Trav. Chim. 68, 649 (1949)

45. J. G. Kirkwood, J. Poly. Sci. 12, 1 (1954)

46. J. G. Kirkwood and J. Riseman, J. Chem. Phys. 16, 565 (1948)

47. H. A. Kramers, J. Chem. Phys. 14, 415 (1946)

48. W. Kuhn, Kolloid Z. 62, 269 (1933)

49. W. Kuhn, Kolloid Z 68, 2 (1934)

50. W. Kuhn and F. Grün, Kolloid Z. 101, 248 (1942)

51. W. Kuhn and H. Kuhn, Helv. Chim. Acta 26, 1394 (1943)

52. W. Kuhn and H. Kuhn, Helv. Chim. Acta 28, 1533 (1945)

53. W. Kuhn and H. Kuhn, Helv. Chim. Acta 29, 609 (1946)

54. W. Kuhn and H. Kuhn, Helv. Chim. Acta 29, 609 (1946)

55. W. Kuhn and H. Kuhn, J. Coll. Sci. 3, 11 (1948)

56. A. Kundt, Pogg. Ann. 153, 1 (1874)

57. J. Lamb and A. Matheson, Proc. Roy. Soc. A, 281, 207 (1964)

58. M. E. Mach, Optisch-Akustisch Versuche., Calve, Prague (1873)

59. J. C. Maxwell, Proc. Roy. Soc. (London) A, 22, 46 (1873)

60. J. C. Maxwell, Scientific Papers, Vol. II, 379, Cambridge Univ. Press, London (1890)

61. M. L. Miller, The Structure of Polymers, Reinhold Publishing Corporation, New York (1966)

62. Monsanto Chemical Company, Organic Chemical Division, St. Louis, Mo., Product Information Literature.

63. R. T. Morrison and R. N. Boyd, Organic Chemistry, Allyn and Bacon, Inc., Boston (1961)

64. Natta et al., J. Am. Chem. Soc. 77, 1708 (1955)

65. A. Peterlin, Z. Physik 111, 232 (1938)

66. A. Peterlin, Proc. 2nd Intern. Congr. Rheol., edited by V.G.W. Harrison, Butterworths Scientific Publications, London (1954)

67. A. Peterlin, J. Poly. Sci. 12, 45 (1954)

68. A. Peterlin and H. A. Stuart, Z. Physik 112, 1, 129 (1939)

69. W. L. Peticolas, Rubber Chem. Tech. 36, 1422 (1963)

70. W. Philippoff, Trans. Soc. Rheol. 4, 159 (1960)

71. W. Philippoff, International Congress of Rheology Proceedings, Providence, Rhode Island, p. 343 (1963)

72. W. Philippoff, Trans. Soc. Rheol. 8, 117 (1964)

73. Polymer Handbook, edited by J. Brandrup and E. Immergut, Inter science Publishers, Inc., New York (1966)

74. C. V. Raman and K. S. Krishnan, Phil. Mag. 5, 769 (1928)

75. P. E. Rouse, Jr., J. Chem. Phys. 21, 1272 (1953)

76. C. Sadron, J. Phys. Radium 9, 381 (1936)

77. C. Sadron and H. Mosimann, J. Phys. Radium 9, 384 (1936)

78. C. Sadron, J. Phys. Radium 9, 381 (1938)

79. H. A. Scheraga, J. T. Edsall and J. O. Gadd, Jr., J. Chem. Phys. 19, 1101 (1951)

80. J. L. Schrag, J. F. Guess and G. B. Thurston, J. Appl. Phys. 36, 1996 (1965)

81. F. W. Schremp, J. D. Ferry and W. W. Evans, J. Appl. Phys. 22, 711 (1951)

82. R. Signer and H. Gross, Helv. Chim. Acta 17, 75 (1934)

83. R. Signer and H. Gross, Helv. Chim. Acta 17, 59, 355, 726 (1934)

84. R. S. Stein, J. Chem. Phys. 21, 1193 (1953)

85. J. K. Stille, Introduction to Polymer Chemistry, J. Wiley and Sons, Inc., New York (1962)

86. C. Tanford, Physical Chemistry of Macromolecules, John Wiley and Sons, Inc., New York (1965)

87. W. C. Teach and G. C. Kiessling, Polystyrene, Reinhold Publishing Corp., New York (1960)

88. G. B. Thurston, Appl. Opt. 3, 755 (1964)

89. G. B. Thurston and L. E. Hargrove, Jr., Optical Birefringence Induced by Shear Wave Propagation in Aqueous Milling Yellow Solutions, Technical Report #4 under contract #DA-23-072-ORD-283, Stillwater, Oklahoma, Research Foundation of Oklahoma Agricultural and Mechanical College (1957).

90. G. B. Thurston and J. L. Schrag, Trans. Soc. Rheol. 4, 325 (1962)

91. G. B. Thurston and J. L. Schrag, J. Appl. Phys. 35, 144 (1964)

92. G. B. Thurston and J. L. Schrag, J. Chem. Phys. 45, 3373 (1966)

93. L.R.G. Treloar, The Physics of Rubber Elasticity, Oxford Univ. Press, London (1958)

94. N. W. Tschoegl, J. Chem. Phys. 39, 149 (1963)

95. N. W. Tschoegl, J. Chem. Phys. 40, 473 (1964)

96. V. N. Tsvetkov, Doklady Acad. Nauk. S.S.S.R. 78, 465 (1951)

97. V. N. Tsvetkov, J. Poly. Sci. 23, 151 (1957)

98. V. N. Tsvetkov, Polymer Reviews, Vol. 6, edited by B. Ke, Interscience Publishers, New York (1964)

99. V. N. Tsvetkov and A. Petrova, Rubber Chem. and Tech. 19, 360 (1946)

100. V. N. Tsvetkov and S. M. Savoon, J. Tech. Phys. U.S.S.R. 26, 348 (1956); translated in Soviet Physics (Technical Physics) 1, 342 (1956)

101. M. V. Volkenstein, Configurational Statistics of Polymeric Chains, Interscience Publishers, New York, Chapter 7 (1963)

102. M. C. Wang and G. E. Uhlenbeck, Rev. Mod. Phys. 17, 323 (1945)

103. B. H. Zimm, J. Chem. Phys. 24, 269 (1956)

104. B. H. Zimm, Rheology, Chapter 1, edited by F. R. Eirich, Academic Press, New York (1960)

105. B. H. Zimm, G. M. Roe and L. F. Epstein, J. Chem. Phys. 24, 279 (1956)

VITA

John Lindblad Schrag

Candidate for the Degree of

Doctor of Philosophy

Thesis: MEASUREMENT OF THE OSCILLATORY FLOW BIREFRINGENCE OF POLYSTYRENE SOLUTIONS

Major Field: Physics

Biographical:

Personal Data: Born in Siloam Springs, Arkansas, April 14, 1937, the son of Verna and John Schrag; married to Beverly Harwick Schrag, August 6, 1960; father of one son, John Jeffrey, born August 31, 1962.

Education: Attended grade school in Siloam Springs, Arkansas, and in Omaha, Nebraska; was graduated from Central High School in Omaha, Nebraska, in 1955; received the Bachelor of Arts degree from the University of Omaha, with majors in Physics and Mathematics, in August, 1959; received the Master of Science degree from Oklahoma State University in August, 1961; completed the requirements for the Doctor of Philosophy degree in May, 1967.

Professional and Honorary Organizations: Acoustical Society of America; Sigma Pi Sigma; Phi Kappa Phi.